UNIVERSIDAD NACIONAL AUTÓNOMA DE MÉXICO

PROGRAMA DE MAESTRÍA Y DOCTORADO EN INGENIERÍA
INGENIERÍA CIVIL – HIDRÁULICA

OLEAJE EXTREMO Y CAMBIO CLIMATICO EN EL GOLFO DE MEXICO

EXTREME WAVES AND CLIMATE CHANGE IN THE GULF OF MEXICO

TESIS
QUE PARA OPTAR POR EL GRADO DE:
DOCTOR EN INGENIERÍA

PRESENTA:
CHRISTIAN MARIO APPENDINI ALBRECHTSEN

TUTOR PRINCIPAL
Dr. ADRIAN PEDROZO ACUÑA
COORDINACION DE HIDRAULICA
INSTITUTO DE INGENIERIA

MEXICO, D.F. FEBRERO 2017

JURADO ASIGNADO

Presidente:	Dr. JOSÉ ANTONIO SALINAS PRIETO
Secretario:	Dr. RUTH CEREZO MOTA
Vocal:	Dr. ADRIÁN PEDROZO ACUÑA
1er. Suplente:	Dr. CARLOS GAY Y GARCÍA
2do. Suplente:	Dr. KERRY ANDREW EMANUEL

Lugar o lugares donde se realizó la tesis: Sisal, Yucatán, México

TUTOR DE TESIS:

Dr. Pedrozo Acuña Adrián

FIRMA

“It is fatal to know too much at the outset. Boredom comes as quickly to the ***scientist who is certain of its results*** *as the novelist who is over-certain of his plot.” – Paul Thoreau (****modified****)*

Resumen

La caracterización del oleaje extremo es imprescindible para una eficiente planeación de operaciones marítimas, regulación de actividades en la costa y el diseño de estructuras e instalaciones marítimas y costeras. En el Golfo de México el oleaje extremo es resultado de ciclones tropicales y sistemas anticiclónicos conocidos como *Nortes*. Si bien el oleaje generado por ciclones tropicales puede tener consecuencias devastadoras, su ocurrencia es bajo, mientras que los *Nortes* son frecuentes durante los meses de otoño/invierno y generan olas que interrumpen las actividades marítimas. La planificación actual de las operaciones marítimas y el diseño de las estructuras se basan en datos históricos, sin embargo, es probable que el calentamiento global modifique las condiciones actuales durante los próximos años. Así, en este trabajo se analiza el efecto del cambio climático sobre el oleaje generado por ciclones tropicales y *Nortes*.

El oleaje generado por ciclones tropicales se caracterizó en base a eventos sintéticos que permiten una estimación estadística robusta tanto para el clima actual como para el futuro bajo los escenarios RCP 4.5 y RCP 8.5. Lo eventos utilizados se derivaron del reanálisis NCEP y los modelos HadGEM2-ES y NOAA/GFDL CM3 del CMIP5. Los resultados sugieren un aumento en la actividad de oleaje en el clima futuro, aunque también se espera una reducción en la energía de oleaje en algunas áreas. Las implicaciones sobre el diseño de estructuras se ejemplifica por medio de la ola de diseño de 100 años, donde el uso del clima actual resulta en una sobre/sub diseño de las estructuras al considerar que la vida útil incluye el periodo considerado como clima futuro.

En cuanto al oleaje generados por *Nortes*, se desarrolló la metodología para identificar y clasificar eventos según su efecto sobre el estado del mar. Para la identificación de *Nortes* se utiliza un nuevo índice que incluye las condiciones sobre el mar. En base a la energía de oleaje de cada *Norte* identificado en el reanálisis CFSR y el modelo CMIP5 CNRM-M5 (clima actual y escenario RCP 8.5) se realizó un análisis de componentes principales y una clasificación por medio de k-means. Se identificaron 5 tipos de *Nortes* y se analizó su ocurrencia bajo el clima actual y futuro. Se concluyó que el calentamiento global resultará en menos eventos intensos y un mayor número de los eventos menos intensos.

Esto puede proporcionar un alivio para las operaciones marítimas, en relación con los tiempos de parada debido a las condiciones extremas de oleaje.

En conclusión, podemos esperar que el clima extremo de oleaje en el Golfo de México a consecuencia del calentamiento global, este caracterizado por una intensificación del oleaje generado por ciclones tropicales, una menor ocurrencia de eventos intensos de *Nortes* y una mayor ocurrencia de *Nortes* de menor intensidad. De esta manera, el diseño de estructuras marítimas deberá considerar una intensificación en el oleaje de diseño, como resultado de ciclones tropicales, y una menor frecuencia de eventos extremos para el diseño operacional de instalaciones marítimas, como resultado de *Nortes*.

Palabras clave: Oleaje; Ciclones tropicales; Nortes; Golfo de México; Calentamiento global, Cambio climático; Oleaje extremal

Abstract

The characterization of extreme ocean waves allows for better planning of maritime operations, regulation of coastal activities, and the design of coastal and offshore structures and facilities. In the Gulf of Mexico, extreme ocean waves result from the incidence of tropical cyclones and anticyclone systems known as *Nortes*. Waves derived from tropical cyclones have devastating consequences but have a low probability of occurrence, whereas *Nortes* are a frequent phenomenon producing disruptions of maritime activities during autumn/winter months. While current planning of maritime operations and the design of structures is based on historical data, global warming will likely affect such conditions during the coming years and into the 22nd century. Therefore, this investigation is an analysis of the expected waves induced from tropical cyclones and *Nortes*, considering the influence that climate change has modifying both the frequency and intensity of these extreme weather events.

In the case of waves induced by tropical cyclones, synthetic events were used to provide a robust statistical estimate for both the present and future wave climates under the RCP 4.5 and RCP 8.5 scenarios. The events used were derived using the NCEP reanalysis and the CMIP5 models HADGEM2-ES and NOAA/GFDL CM3. The results suggest an increase in wave activity for the future climate, particularly for the less biased GFDL model, although in some areas a decrease in wave energy is also found. Since the lifespan of a structure includes the future wave climate period, it is expected that these changes will have implications on the design of maritime structures and their secure operation. In particular, the modification of the 100-year design wave could result in an under/over design of structures when not considering climate change effects.

On the other hand, for the waves generated by *Nortes*, a methodology was developed to identify these events and classify them according to their effect over the sea state. For this, a new index is proposed to identify events, providing good results when compared to other studies. In this case, a wave model was run for each of the events identified in the CFSR reanalysis and the CMIP5 model CNRM-M5 under the RCP 8.5 scenario. In order to classify the events into 5 types, the methodology incorporated both a principal

component analysis applied to the computed wave power, and a cluster analysis by k-means. The occurrence of the different types of *Nortes* under the influence of present and future climates indicate that climate change will result in less frequent events of higher intensity and more frequent mild events. This may provide a relief for coastal and marine operations, in relation to downtimes due to extreme wave conditions.

In conclusion, this study shows that the extreme wave climate in the Gulf of Mexico due to the effect of global warming is expected to be characterized by an intensification of the waves generated by tropical cyclones, a lower occurrence of intense events generated by *Nortes*, and an increased occurrence of mild *Norte* events. As such, the design of maritime structures should considered an intensification of the design waves, as a result of tropical cyclones, and the operational design maritime structures should consider a lower occurrence of extreme events as a result of *Nortes*.

Keywords: Ocean waves; Tropical cyclones; Nortes; Gulf of Mexico; Global warming; Climate change; Extreme waves

Dedicatoria

Para Gabriela, Amaranta y Cosimo…

Agradecimientos

Quisiera agradecer el apoyo otorgado por el Programa de Apoyos para la Superación del Personal Académico de la UNAM, así como al apoyo del Instituto de Ingeniería por el apoyo otorgado a través del Proyecto Interno No. 5358/4340, y a su Consejo Interno por permitirme emprender el Doctorado.

Quisiera agradecer a Graciela Binimelis de Raga por invitarme a participar en el proyecto financiado por el InterAmerican Institute for Global Change Research (IAI, Grant CRN II 2048), ya que me permitió adentrar en el mundo de ciclones tropicales y hacer las redes necesarias para trabajar con estos temas.

I am in debt with Professor Kerry Emanuel for his unconditional support and constant supply of synthetic events used in this study and several others.

Agradezco profundamente el apoyo otorgado por el Dr. Adrián Pedrozo Acuña por proveerme de los medios necesarios para llevar a cabo este Doctorado. También agradezco el apoyo otorgado por el resto del comité sinodal: Dra. Ruth Cerezo Mota, Dr. Antonio Salinas Prieta y Carlos Gay y García.

Quisiera dar una mención especial a Rafael Meza Padilla por el apoyo en varios estudios realizados en paralelo a este trabajo, esperando que dicha colaboración siga creciendo.

También quisiera agradecer el apoyo de Jaime Lasheras Hernández y a Gonzalo Uriel Martin por el apoyo necesario para echar a andar este estudio.

Agradezco a todos mis colegas del trabajo, en particular los del LIPC y sus cátedras CONACYT.

Finalmente el agradecimiento más importante va a mi familia por siempre estar ahí, aunque no estuvieran no hubiera terminado antes, así que los quiero igual o más!

Artículos relacionados con este trabajo

Appendini, C.M., R. Meza-Padilla, A. Pedrozo-Acuña y A. Torres-Freyermuth. En revisión. **On the role of climate change on wind waves generated by tropical cyclones in the Gulf of Mexico**. Coastal Engineering Journal.

Appendini, C.M., M. Rosengaus., R. Meza-Padilla and V. Camacho-Magaña. Aceptado. (2017). **Rapid wave and storm surge warning system for tropical cyclones in Mexico**. Bulletin of the American Meteorological Society, 98(3), doi:10.1175/BAMS-D-15-00170.1.

Appendini, C.M., V. Magaña-Camacho, J.A. Breña-Naranjo. 2016. **ALTWAVE: Toolbox for use of satellite L2P altimeter data for wave model validation**, Advances in Space Research, 57(6), pp 1426-1439, doi:10.1016/j.asr.2015.12.015.

Indice

Indice de Tablas

Indice de Figuras

List de acrónimos

API	American Petroleum Institute
CFSR	Climate Forecast System Reanalysis
CMIP	Coupled Model Intercomparison Project
CMIP3	CMIP Phase 3
CMIP5	CMIP Phase 5
CNRM	Centre National de Recherches Météorologiques (National Centre for Meteorological Research)
FF	Far Future
GCM	Global Circulation Model
GFDL	Geophysical Fluid Dynamics Laboratory
GFDL-CM3	GDFL Climate Model 3
GOES	Geostationary Operational Environmental Satellite
GoM	Gulf of Mexico
HADGEM	UK Met Office Hadley Centre Global Environmental Model
HADGEM2-ES	UK Met Office Hadley Global Environmental Model 2 – Earth System
HURDAT	North American Hurricane Database
INEGI	Instituto Nacional de Geografía, Geografía e Informática
IPCC	Intergovernmental Panel on Climate Change
MDR	Main Development Region
MSLP	Mean Sea Level Pressure
MWD	Mean Wave Direction
NCAR	National Center for Atmospheric Research
NCEP	National Centers for Environmental Prediction
NDBC	National Data Buoy Center
NF	Near Future
NOAA	National Oceanic and Atmospheric Administration
PC	Present Climate
PC	Principal Component
PCA	Principal Component Analysis

PWP	Peak Wave Period
RCP	Representative Concentration Pathways
SRES	Special Report Emissions Scenarios
SW	Spectral Wave
SWH	Significant Wave Height
TC	Tropical Cyclones
UK	United Kingdom
US	United States
USD	US Dollars
WP	Wave Power

Chapter 1.

Introduction

Understanding ocean waves has been critical for humans since the early days of civilization. Ocean waves have influenced maritime transport, modified coastlines, affected trade and restrained or allowed colonization of new land. Nowadays, ocean waves continue to have an important impact of human activities, which are boosted by population growth and associated infrastructure in coastal areas, the increased demand in marine natural resources (e.g. oil and gas, fishing, renewable energies) and maritime shipping in a globalized world. Ocean waves give no truce, they are always there, but the extreme ocean waves are the ones with more consequences. They stall operations of marine facilities, they halt marine trade and activities such as fishing and tourism, they damage offshore and onshore structures, they flood and erode coastal areas, and ultimately they dictate how we shall design structures and improve operations in the marine environment.

Mexico, with 2/3 of its territory as ocean and more than 11,000 km of coastline, is not an outsider to the effect of ocean waves. For Mexico, an important part of the economy is dependent on marine activities and affected by ocean waves. Particularly oil/gas extraction and beach tourism represent an important contribution to the gross national product, and are severely affected by extreme ocean waves. This makes ocean wave activity a main factor to be considered in strategic planning for most coastal and ocean activities as well as design of onshore and offshore structures. There is also the increased population growth of the coastal areas, leading to infrastructure development of the coast, and thus increasing the vulnerability to marine hazards, including ocean waves. Thus, the characterization of extreme events is essential for the country’s economic development and strategic planning.

The main oil and gas production areas in Mexico are located in the Gulf of Mexico (GoM), while the main beach tourism destination, Cancun, is located south of the western limit of the Gulf. Both activities, along with fisheries and shipping, are affected by extreme ocean waves associated to the passage of Central American Cold Surges (*Nortes*) during fall-winter, and due to tropical cyclones (TC) during summer-fall (Appendini et al. 2014). While the *Nortes*-derived waves are more frequent, TC generated waves are more energetic and usually have catastrophic consequences. For instance, mean annual losses due to hurricanes in the US has been estimated to be 10 billion USD with single events (i.e. Great Miami Storm) being able to reach up to 157 billion USD (Pielke et al. 2008). Nevertheless, *Nortes* can still generate significant damage, for instance in 2007 the cold front crossing the GoM at the end of November damaged oil rigs in the Campeche Sound by an estimated amount of $2.5 billion USD[1] (López-Méndez 2009).

While *Nortes* are more frequent events in the GoM, with a mean of 22 annual events (Ramírez-Elías 2007), TCs are more intense, although showing a low occurrence with a mean density per square degree of 0.13 events in the Mexican Gulf and 0.24 events in the Mexican Caribbean Sea (Rosengaus-Moshinsky et al. 2002), as a result of approximately 3.7 TCs per year in the GoM and 4 events in the Caribbean Sea. Both events modulate the extreme wave climate in the GoM as shown by Appendini et al. (2014). In regards to TCs, there are several studies related the generated ocean waves, whether studying an specific event (Hope et al. 2013; Olume et al. 2011; Powell et al. 2010; Wang and Oey 2008; Dietrich et al. 2011), or by modeling tropical cyclone generated waves (Tolman and Alves 2005; Dietrich et al. 2011; Chao et al. 2005; Liu et al. 2007), or deriving wave climate from TCs (Meza-Padilla et al. 2015; Panchang et al. 2013). On the other hand there are few studies related to *Norte* generated waves, with few studies describing the wave climate of the GoM where *Norte*-derived waves are identified as extreme events (Appendini et al. 2014).

Besides the importance of characterizing extreme waves in the GoM due to its relevance on design and planning of structures and activities, it is important to evaluate

[1]Calculated with the 2009 exchange rate of 12.5 MXN to USD.

the effect that global warming can have on the extreme waves of the GoM. This phenomena is critical considering that extreme waves are an important design parameter for maritime structures, where the return period for the design depends on the structure itself but could be anything from a 10 years return period to more than 1000 years. While the present climate is used to design a structure today, global warming may change the design wave conditions even by half of the 21st century. This means that the probability of the design wave to occur in a particular time frame could increase (or diminish) as a result of climate change. In case of a decrease of the future climate design wave, the use of the present climate is mainly translated to a higher than required economical cost, but in the opposite scenario, it could lead to unaccounted damages during the expected structure lifespan. Thus, characterizing the effect of climate change on GoM extreme waves has important engineering implications and is already a necessity.

1.1. Motivation

1.1.1. Scientific

Since the work of Keeling et al. (1976) in the 70s, the CO_2 concentrations in the atmosphere had been reportedly rising and linked to industrial emissions. Even a decade earlier, Manabe and Wetherald (1967) determined that doubling the concentration of CO_2 in the atmosphere will lead to a 2°C, which in fact was predicted more than 70 years earlier by Arrhenius (1896). It comes with no surprise, nowadays, that the IPCC (2014a) states that the “human influence on the climate system is clear” (p. 2) and that the “warming of the climate system is unequivocal” (p. 2). The increase in greenhouse gas concentration in the atmosphere and the subsequent global warming is expected to generate changes in the climate, modifying existing risks differently among regions (IPCC 2014a). Considering the impacts of global warming in the climate system, the winds and consequent ocean waves are likely to suffer changes. In the ocean, the impacts and vulnerability report of the IPCC (2014b) mentions a knowledge gap regarding surface ocean waves, with a low confidence in the understanding of the changes expected for

significant wave height (SWH). The scientific motivation of this study is to bridge this gap in relation to extreme waves.

The study of the GoM presents an opportunity to better understand the effect of global warming and extreme ocean waves derived from high vorticity (TC) and synoptic scale (*Nortes*) events. In relation to TCs, the scientific motivation is to present a new method to determine the extreme wave climate based on synthetic events. Such events allow to address the low resolution of wind fields from TC and their low occurrence in global models, in order to provide more accurate estimates of derived ocean waves. Synthetic events have been successfully used to derive extreme wind estimates and storm surges, being this study the first one using such events to characterize the extreme wave climate derived from TCs under climate change. With regards to *Nortes*, this study is the first one to characterize ocean waves associated with *Nortes* and the effect of climate change. Hence, it will provide a new understanding of both *Nortes* events as they cross the GoM, and the derived ocean waves, under a warming climate.

Thus, the scientific motivation of this work is to pave the road towards a better understanding of the effects of climate change on extreme waves in the GoM. This includes a better assessment of the impact of climate change on the wave climate generated by TCs; and the characterization of large scale atmospheric systems that have an impact on extreme waves under climate change scenarios.

1.1.2. Engineering

Determining the wave climate is one of the basic steps for the design of maritime structures. While the mean wave climate is needed to determine the functional design, the extreme wave climate is required for the structural design. Designing a structure with a permanent lifetime between 30 to 100 years requires a design wave with a return period of 100 years in order to have a low probability of occurrence of such an event (CIRIA et al. 2007). Thus 100-year design waves are commonly used for structures in ports, coastal protection and offshore platforms.

The design wave is usually derived from long term wave measurements or wave hindcasts based on present climate conditions, but on the other hand, the time frame for global warming scenarios is 100 years in advance or even less (2040-2070 is many times considered as a mid-term time frame in climate change studies). If global warming assessments are done for time frames less than 100 years, we should expect that physical parameters affected by climate change will experience changes by the end of the 21st century. Such a time frame could even be shorter than the expected lifetime of maritime structures and facilities, and the probability of the design wave to occur in the lifespan of a structure could be increased/decreased by the effect of a warming climate.

Therefore, the acknowledgement of a warming climate creates the next question: Can we expect that a structure designed under the present climate will withstand the future climate conditions expected by the end of the century or even by mid-century? The non-stationary assumption in climate parameters for the design of engineering structures is no longer valid. If extreme waves are increased by global warming, as some studies have suggested for some areas, then it is likely that structures designed under the present climate will suffer damage before the end of their expected lifespan.

Considering the above, the engineering motivation for this study is focused on the GoM, and area where the design of structures for ports, oil and gas, and coastal facilities constantly takes place, and where global warming should be incorporated in the designing criteria.

1.1.3. Societal

The GoM is an important economic asset for Mexico and the US due to the extraction of oil and gas, fisheries, shipping and tourism (Adams et al. 2004). The coastal zone of the GoM is also an important area for human settlements, with approximately 50% of the total population in the US and Mexico living in coastal states. In Mexico, activities related to the coast represent 80% of the economic activity for the coastal states: it is where most of the oil and gas production takes place, shipping and maritime transport accounts for 75% of all maritime transport in Mexico when considering tonnage, and

fishing activities are an important income for coastal settlers (Sanchez-Gil et al. 2004). If both the US and Mexico oil and gas industry are considered, the GoM is one of the most productive areas in the world (Kaiser el at., 2015).

Due to the importance of offshore and onshore activities in the GoM, the sea state is a key driver determining the exploitation of the natural resources and thus for the region's economy. In this regard, ocean waves are a main factor in the planning and regulation of coastal activities, where extreme waves usually stall operations: offshore platforms are evacuated, maritime transport and fishing are interrupted, and tourism avoided in these locations. As such, wave climate studies are critical for successful planning and management. Such studies should incorporate the effects of global warming, due to the relevance of the GoM for the local settlements, the regional environment and the global economy.

1.2. Review of existing research

There are several studies assessing wave tendencies based on observations (e.g. Gulev et al. 2003; Gulev and Grigorieva 2004), buoy data (e.g. Allan and Komar 2006; Menéndez et al. 2008; Ruggiero et al. 2010), satellite data (e.g. Woolf et al. 2002; Young et al. 2011), model results for the present climate (e.g. Sterl and Caires 2005; Semedo et al. 2011; Dodet et al. 2010; Appendini et al. 2014; Weisse et al. 2009), and model results under different climate change scenarios (Semedo et al. 2013; Hemer et al. 2013a; Fan et al. 2014; Mori et al. 2010; Caires et al. 2006; Wang et al. 2004; Lionello et al. 2008; Fan et al. 2013).

Despite the lack of specific studies for the GoM, global studies provide results that could be used as a first step to determine the effect of climate change on waves in the GoM. Table 1 shows a list of the different global wave studies discuss herein, listing the scenarios and Global Circulation Models (GCMs) used in each study. Semedo et al. (2013) determine that the annual wave climate of the GoM will remain stable, although they found a decrease in SWH and mean wave period during the winter months and an

increase in the summer months, where some localized areas show significant trends. Similar conclusions are found by Fan et al. (2013); Hemer et al. (2013b) and Mori et al. (2010), however, Fan et al. (2013) showed an opposite trend in this regard. To give an example, their study reported an increase in 10% of extreme wave height during the winter along the northeast coast of Yucatan and the Mexican Caribbean, with up to a 15% increase in Cabo Catoche, as well as a slight increase along Tamaulipas and northern Veracruz; while for the summer season they report an expected decrease of about 10% in wave energy along Veracruz and Tamaulipas.

Table 1. Climate change scenarios and Global Circulation Models used in different global wave studies

REFERENCE	CLIMATE CHANGE SCENARIO	GCMS
Hemer et al. (2013a)	Analyzes multiple datasets based on SRES scenarios and multiple CMIP3 models	
Hemer et al. (2013b)	A2	ECHAM5, CSIRO Mk3.5
Fan et al. (2013)	A1B	CMIP3 Ensemble (18 models), GFDL CM2.1, HadCM3, ECHAM5
Semedo et al. (2013)	A1B	ECHAM5
Mori et al. (2010)	A1B	MRI-JMA
Wang and Swail (2006)	A2, A1B	HadCM3, ECHAM4/OPYC3, CGCM2

Considering that the extreme waves in the GoM during winter are a result of *Nortes* (Appendini et al. 2013), the work from Fan et al. (2013) suggests that there will be an intensification of the wind speeds from *Nortes*, leading to more energetic extreme waves during winter. This conclusion is also supported by the work of Hemer et al. (2013a), who also showed a decrease in the SWH and the mean wave period in the GoM during the summer, in contrast to an expected increase in both parameters of between 1% and 3%

during winter. This indicates a possible effect of climate change on the intensity of *Norte* winds, as well as a possible rotation of the winds from the north to the northeast were a longer fetch will lead to an increase of the mean wave period during winter. The increase of intensity of the winds from *Nortes* is also reported by Pérez et al. (2014), who found that climate change will lead to more intense events, but of shorter duration, based on the TL959L60 model from the Meteorological Research Institute of Japan under the A1B scenario. In contrast to those studies, Vanem et al. (2012) did not find any tendencies for the wave climate in the GoM using a Bayesian hierarchical space-time model to do wave climate projections based on CO_2 emission scenarios A1B, A2, B1 and B2.

Other studies have based their analysis on historical data, such as Reguero et al. (2013) who reported in the area of Tamaulipas and northern Veracruz, an expected decline of ~0.2 cm/year in the mean wave height value. In contrast, for the region between southern Veracruz and western Yucatan, they do not report any foreseeable change in future wave climate. Moreover, in the northern region of Yucatan a positive trend of ~0.2 cm/year is reported, while a negative trend of ~0.2 cm/yr is expected along the Mexican Caribbean Sea. With regards to the extreme wave climate, a negative trend of ~6.0 cm/yr is generally reported to be expected, with the exception of the northern coast of Tamaulipas (near the US-Mexico border) and the Yucatan Peninsula, with both areas reporting an expected positive trend of ~0.3 cm/year, and ~1.2 cm/year near Cabo Catoche, respectively.

Appendini et al. (2014) determine that the mean wave climate only shows slight negative trends in the eastern part of the GoM, with some months showing positive trends on the order of 2 cm/year, particularly in October. With regards to extreme wave climate, they do not find significant annual trends, but they find positive trends for the months between April and October (except September). While these finding do not support the hypothesis from the studies derived from climate change scenarios, Appendini et al. (2014) do find that October has the highest positive trend for the extreme waves, precisely in southern Veracruz, where there is a high incidence of *Norte* events and low incidence of tropical storms particularly in October (only hurricane Stan in 2005 has affected that area since 1949). Considering this, we could infer that the theory of intensification of the

Norte-generated waves due to climate change is supported by the tendencies in the last 30 years.

From the literature review, the prediction of the extreme waves in the GoM is either based on historical trends, or derived from global wave models with a coarse resolution to define the GoM. It is then clear that there is a lack of studies of extreme waves and climate change for the GoM and that further research is required to overcome the limitation of previous studies.

1.3. Objectives

1.3.1. Main objective

This work aims at determining the effect of global warming on the extreme waves of the GoM, that is, the waves generated by TCs and *Nortes*.

1.3.2. Specific goals

In order to accomplish the main objective of this study, the following specific goals are addressed.

1. Determine the effect of global warming on TC-derived ocean waves.
    a. Establish a tropical cyclone climatology in the GoM for the present and future climates.
    b. Determine the wave climate for TCs in the GoM for the present and future climates.
2. Determine the effect of global warming on the ocean waves derived from *Norte* events.
    a. Identify *Norte* events in the present and future climates
    b. Determine the wave power generated by each *Norte* event in the present and future climates.
    c. Classify the *Norte* events based on the derived wave power.
    d. Assess the effect of global warming on the different *Norte* types.

1.4. Thesis structure

The thesis has been divided in two major sections. Chapter 2 is related to the extreme waves derived from TCs and Chapter 3 to the extreme waves derived from *Nortes*. Each chapter is composed of an introductory review of previous studies, followed by a description of the methodology used, the results and discussion and final conclusions. Chapter 4 presents the major conclusions of the thesis as well as the foreseen future work.

Chapter 2.

Extreme ocean waves from TCs

2.1. Introduction

Ocean waves generated by TCs may directly affect diverse activities in coastal and offshore areas, including tourism, shipping and the offshore oil and gas industry. Therefore, risk imposed by hurricanes has encouraged the American Petroleum Institute (API) to provide TC guidance on wind, waves, currents and storms surge. Since the 1990s, a simultaneous increase in both the risk due to more infrastructure exposure and more energetic hurricane seasons have been reported (Klotzbach et al. 2015). In 2005, hurricanes Rita and Katrina damaged the largest number of platforms and pipelines ever reported in the GoM (Cruz and Krausmann 2008). Only three years later, in 2008, hurricanes Gustav and Ike produced less damage but the oil and gas reserves at risk were much higher (Kaiser and Yu 2010). As a result of the 2004 and 2005 hurricane seasons, the API presented an updated document for guidance on hurricane conditions (American Petroleum Institute 2007). The updated document was a response to the highest ever SWH reported by the National Data Buoy Center (NDBC), generated by hurricane Ivan in 2004 (Panchang and Li 2006; Wang et al. 2005), as well as the record peak SWH set by Hurricane Katrina in 2005 (Wang and Oey 2008). Both records were measured in the GoM at buoy 42040, where maximum SWHs registered during the incidence of hurricane Ivan were 15.96 m and 16.91 m for Hurricane Katrina. The maximum registered SWH at this buoy before Ivan and Katrina was 10.88 m during hurricane Georges in 1998. This buoy shows an approximately mean SWH of 1 m between 1995 and 2012.

Following this report, Panchang et al. (2013) performed a 51-year wave hindcast (1951-2008) to revise the values from API (2007). They found that the SWH for the 100-year return period in the GoM increases when including the 2004-2008 hurricane season, as well as the increasing trends for the eastern part of the GoM. Despite these findings, a trend analysis based on measurements (Komar and Allan 2008) and wave hindcast

information (Appendini et al. 2014) found no significant trends for extreme waves in the GoM. Therefore, the sensitivity of the 100-year SWH to specific hurricane seasons in Panchang et al. (2013) and the discrepancy in the tendencies from the other studies can be related to the limited length of wave records generated by TCs, which do not allow the implementation of a robust statistical analysis to characterize present climate and trends.

On the other hand, previous studies have focused on characterizing future wave climates based on the special report on emission scenarios (SRES) (Nakicenovic and Swart 2000) from the Intergovernmental Panel on Climate Change (IPCC) and/or the representative concentration pathways (RCPs) based on the work by Moss et al. (2010). Such studies use wave models forced by winds fields from the Coupled Model Intercomparison Project (CMIP) phases 3 (CMIP3) and 5 (CMIP5) or downscaled winds from higher resolution models. As an example of such studies, Hemer et al. (2013a) performed a multi-model ensemble analysis of the future wave climate from other works, including dynamic projections from Mori et al. (2010), Hemer et al. (2013b), Fan et al. (2013) and Semedo et al. (2013), and statistical projections from Wang and Swail (2006). While the aim was to characterize waves at a global level, the authors discuss the results for areas strongly affected by TCs. For instance, Fan et al. (2013) found that TCs are an important factor determining the extreme wave climate in areas such as the North Atlantic and the North Pacific. The study found a decrease in mean SWH in the GoM during the hurricane season in the future climate as a result of less hurricanes entering the GoM. On the other hand, Mori et al. (2010) concluded that the extreme waves south of Japan in the Pacific Ocean will increase due to TCs, but they acknowledge that the 25 years of data used is not enough for robust statistics of TC- derived waves. The use of GCMs for characterizing TC-generated waves will then present two major drawbacks. First, the GCMs underestimate the maximum wind speeds from TCs (Emanuel 2010; Hill and Lackmann 2011); secondly, TC activity is underestimated in GCMs (Camargo 2013) and the number of TCs is not enough for performing robust statistics, as is the case with historical data.

The use of a limited amount of historical data, wind reanalyses, and GCMs imposes a limitation when characterizing TC winds and hence the derived storm surge

and waves. Therefore, the use of synthetic TCs had been favored by several authors to overcome the limitation given by short records of historical events (which is further reduced when considering the data reliable since advent of satellite imagery in the mid 60's (Landsea 2007). This strategy employs site specific statistics of TCs, through which several authors create synthetic events to estimate design parameters and assess hurricane risk, as summarized by Vickery et al. (2000). More recently, Emanuel et al. (2006) employed a deterministic model based on the statistical properties of the genesis areas of TCs to derive synthetic events. The statistical part of the process is removed in the work by Emanuel et al. (2008), where the genesis locations are not prescribed and the synthetic events are randomly seeded in the ocean in order to be able to produce synthetic events for future climates. The intensity component of the model then determines which seeds survive. Synthetic events derived from Emanuel et al. (2006) and the successive improvements of the technique (Emanuel et al. 2008; Emanuel 2013, 2015), have allowed studies to determine hurricane wind speed return periods (Emanuel and Jagger 2010), as well as storms surge risk assessments in areas with low probability of TCs (Lin et al. 2010). In addition, the technique has also helped to establish trends in TCs for long historical time periods (Reed et al. 2015), and to determine damage from TCs under climate change scenarios (Emanuel 2011; Mendelsohn et al. 2012; Hallegatte 2007). Moreover, it has also been used to determine the occurrence of plausible extreme TCs that have not been recorded in history (Lin and Emanuel 2015). The method used to derived synthetic events (Emanuel et al. 2008; Emanuel 2013, 2015), allows the characterization of TCs for the present climate and for future climate based on different scenarios. It has also been shown that considering the present climate, the information from the synthetic events can also be utilized to generate wind fields, which are then employed as forcing conditions in numerical models to numerically derive waves and storm surges due to these events (Meza-Padilla et al. (2015).

Following the study by Meza-Padilla et al. (2015), this chapter employs this methodology and expands it to determine the conditions given not only by the present climate but also future climates and their effect in TCs. This is done to characterize ocean waves generated by TCs in the GoM and to provide an assessment of the effects of

climate change with emphasis on the implication for design criteria (e.g., 100-year return period).

2.2. Methodology

Synthetic TCs and derived wind fields were used to force a third generation wave model. The synthetic events include present and future climate events, which allow the characterization of the TC-derived waves correspondingly. The wave projections were based on: (i) the NOAA/GFDL Climate Model 3 (CM3) (Griffies et al. 2011) and (ii) the UK Met Office Hadley Global Environmental Model 2 – Earth System (HADGEM2-ES) (Jones et al. 2011), under both the RCP 4.5 and 8.5 scenarios from the IPCC. Figure 1 summarizes the method and data employed.

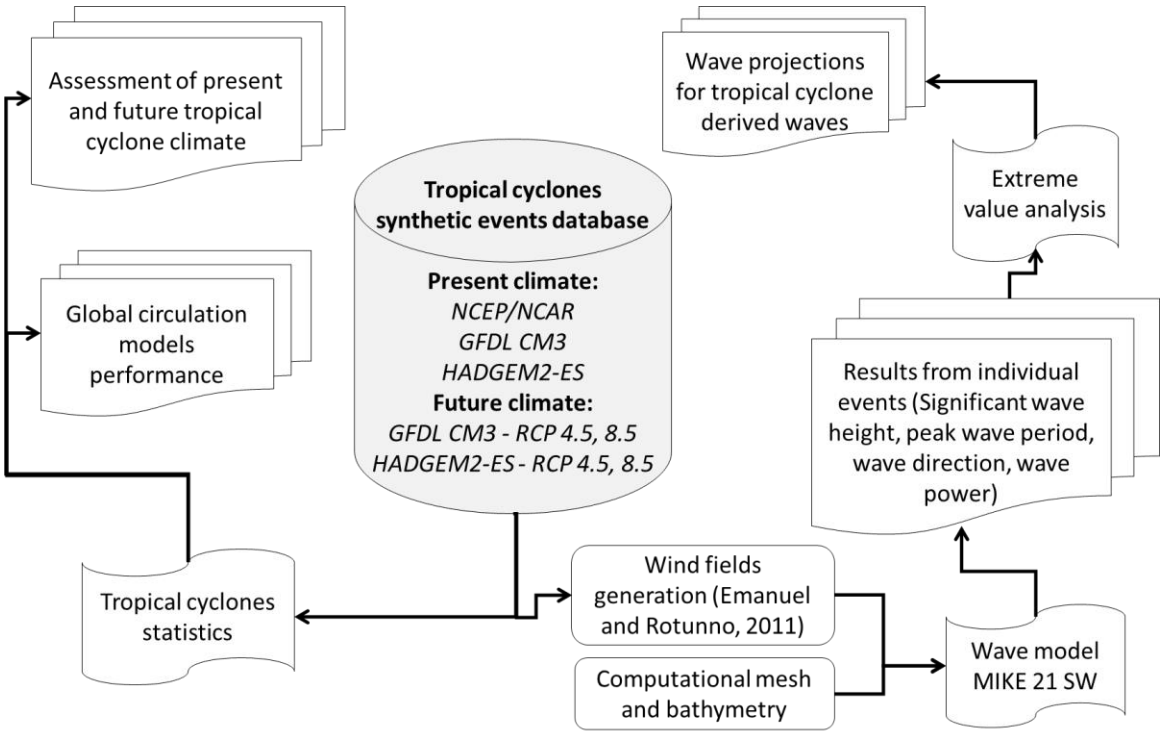

Figure 1. Flux diagram for the assessment of tropical cyclone derived waves and effect of global warming.

2.2.1. Synthetic TCs

The generation of synthetic events was based on the methodology presented by Emanuel et al. (2006, 2008), which comprises the random seeding of warm core vortices across the ocean. The vortices have peak wind speeds of 12 m/s and can either develop or decay according to how favorable the large-scale oceanic and atmospheric environment is. The vortices that develop are steered by a beta-advection model driven by large-scale wind fields. In order to consider present climate conditions, these wind fields are obtained from an atmospheric reanalysis, while for the future climate conditions outputs from the GCMs are utilized. The seeded vortices are considered TCs only if they develop wind speeds of at least 21 m/s. For this study, only the synthetic events entering the numerical model domain were included in the analysis.

In particular, with regards to the present climate, the synthetic events derived using the NCEP/NCAR wind reanalysis (referred hereafter as NCEP) (Kalnay et al. 1996), and the events derived from the GCMs: the NOAA/GFDL CM3 (referred hereafter as GFDL) and the UK Met Office HADGEM2-ES (referred hereafter as HADGEM) are employed. The future climate conditions were considered through the incorporation of the outputs of the GFDL and HADGEM models under the RCP 4.5 and RCP 8.5 scenarios. The HADGEM model has shown to properly capture some of the main features of the Mexican climate features on the present day, whereas the GDFL tends to rank in the middle among all the CMIP5 models (Sheffield et al. 2013a), therefore a larger representation of all the possible outcomes is considered by using these two models.

The present climate encompassed the period 1975-2005, while the future climate includes the period 2070-2100. The present climate database is comprised of 1550 events, while the future climate considers 1612 events for GFDL and 1560 for HADGEM (table 1).

Table 2. Synthetic event databases

Stirring wind fields	Climate (scenario)	Period	Number of events
NCEP/NCAR	Present	1975-2005	1550
GFDL	Present	1975-2005	1550
HADGEM	Present	1975-2005	1550
GFDL	Future (RCP 4.5)	2070-2100	1612
HADGEM	Future (RCP 4.5)	2070-2100	1560
GFDL	Future (RCP 8.5)	2070-2100	1612
HADGEM	Future (RCP 8.5)	2070-2100	1560

2.2.2. Parametric wind model

For each synthetic event track there are two hourly data including date (year, month, day, hour), position (latitude, longitude), maximum wind speed, radius of maximum wind speed, atmospheric pressure in the hurricane eye, and neutral atmospheric pressure. This information was used to derived the wind fields for each event, by means of the parametric model of Emanuel and Rotunno (2011), given by,

Equation 1

$$V_r = \frac{2r\left(R_{mw}V_m + \frac{1}{2}fR_{mw}^2\right)}{R_{mw}^2 + r^2} - \frac{fr}{2}$$

where R_{mw} is the radius of maximum winds, V_m is the maximum wind speed, r is the radial distance from the eye of the hurricane to any given point surrounding it, f is the Coriolis parameter, and V_r is the wind speed of the hurricane at radius r. To provide more realistic winds, the asymmetry generated by the effect of the surface background winds

was included using a reduction factor of 0.55 for the storm translation velocity and a counter clockwise rotation of 20° (Lin and Chavas 2012).

The choice of the parametric model was based on previous studies evaluating the accuracy of different parametric wind models, either directly by winds (Lin and Chavas 2012; Ruiz-Salcines 2013) or indirectly by storm surge (Lin and Chavas 2012) and waves (Ruiz-Salcines 2013). Both studies found that Emanuel and Rotunno (2011) profile provides the most accurate results. Jeong et al. (2012) proposed another parametric model for the GoM, although there is no evidence that this model produces better results than the model from Emanuel and Rotunno (2011). On the other hand, Lin and Chavas (2012) provide an exhaustive wind accuracy assessment using all observed surface wind fields from the Hurricane Research Division H*Wind (Powell et al. 1998) between 1998–2009 in the Atlantic basin.

2.2.3. Wave modeling

The wind fields generated for each synthetic event forced the third-generation wave model MIKE 21 SW (Sørensen et al. 2004) to create the TC-derived ocean waves. The MIKE 21 SW model is based on the wave action equation used to simulate the growth, decay, and transformation of wind-generated waves and swells in coastal and offshore regions. The model is formulated in terms of mean wave direction, θ, and the relative angular frequency, σ, where the action density, N(σ, θ), is related to the energy density, E(σ, θ), by

Equation 2

$$N(\sigma,\theta) = \frac{\mathrm{E}(\sigma,\theta)}{\sigma}$$

For this study, the wave action balance equation was formulated in spherical coordinates, where the evolution of the wave spectrum in the position given by latitude (∅), and longitude (λ) at a particular time (*t*), as given by

Equation 3

$$\frac{\delta N}{\delta t} + \frac{\delta}{\delta \emptyset} c_{\emptyset} N + \frac{\delta}{\delta \lambda} c_{\lambda} N + \frac{\delta}{\delta \sigma} c_{\sigma} N + \frac{\delta}{\delta \theta} c_{\theta} N = \frac{S}{\sigma}$$

where the energy source term *S* represents a superposition of energy source/sink functions that describe the multiple physical phenomena during wave generation and transformation as given by Eq. (4).

Equation 4

$$S = S_{in} + S_{nl} + S_{ds} + S_{bot} + S_{surf}$$

where S_{in} represents the wind energy input given by a linear and a non-linear growth rate (Janssen 1989, 1991; Janssen et al. 1989); S_{nl} represents the non-linear wave-wave interaction, such as quadruplet-wave interactions (Hasselmann and Hasselmann 1985; Hasselmann et al. 1985; Komen et al. 1994), and triad-wave interactions (Eldeberky; Battjes 1995, 1996); S_{ds} is the energy dissipation due to whitecapping (Komen et al. 1994), S_{bot} is the energy dissipation due to bottom friction (Johnson and Kofoed-Hansen 2000); and S_{surf} is the energy dissipation due to depth induced wave breaking (Battjes and Janssen 1978; Eldeberky and Battjes 1996). The spatial discretization of the equations is based on a centered finite volumes method over unstructured meshes. Readers are referred to Sørensen et al. (2004) for details regarding source terms, discretization of the governing equation, time integration, and model parameters.

The computational domain for this study was constructed with an approximate resolution of 10 km and included boundaries along longitude 80°W, so that there is a boundary at the Florida Strait and another at the Caribbean Sea between Central America and Cuba. Bathymetry data included ETOPO 1 data (Amante and Eakins 2009) and local surveys of selected areas along the Mexican coast. Based on sensitivity tests for events occurring outside the model domain, we assumed that the swell generated in the North Atlantic and the central/eastern Caribbean Sea has negligible influence in the GoM.

The model setup was determined following the work presented by Ruiz-Salcines (2013), who calibrated the model to simulate historical hurricane events and compared numerical results against field measurements obtained by different NOAA buoys deployed in the GoM. The final setup was created on the fully spectral and non-stationary time formulation, with a directional discretization for 360° divided in 18 directions and a logarithmic spectral discretization with a minimum frequency of 0.05 Hz, 17 frequencies, and a frequency factor of 1.1. The time step was based on a multisequence integration step, with a minimum value of 0.01 s and a maximum value of 10800 s. Quadruplet-wave interactions were included for energy transfer. We used a wave-breaking factor with a constant gamma value of 0.80 and an alpha value of 1.0. Bottom friction was included with a constant value of 0.04 m based on the Nikuradse roughness. Whitecapping was assigned the dissipation coefficients Cdis and Deltadis with values of 3.5 and 0.6 correspondingly. A JONSWAP fetch growth expression with shape parameters *a* and *b* of 0.07 and 0.09 respectively, was used as initial condition, together with a peakness parameter is 3.3. The offshore boundaries at the Caribbean Sea and the Florida Strait were considered closed, where no waves enter the model domain and the outgoing waves are fully absorbed (e.g., Appendini et al. 2013, 2014).

The directional discretization in the model is too coarse for the study of individual events, since the dispersion of the bin of energy away from the hurricane center (i.e. garden sprinkler effect) has an important effect on the wave propagation as it departs from the tropical cyclone (Young 1999). While it is acknowledged that a finer resolution would reduce its effect, the consequent increment in computational time due to this solution makes the simulation of 10,994 TC too computationally expensive to implement it. Nevertheless, this study focuses on the maximum values generated by each individual event during its entire lifetime to obtain the extreme value statistics from all events. The garden sprinkler effect becomes more important away from the TC center in the areas where most wave decay occurs. Since the present study focuses in the maximum waves achieved by all the synthetic events, and there are TC tracks covering the whole domain, we do not expect to have a bias due to the garden sprinkler effect for the SWH. However, this may not hold true with regards to numerical results related to wave period, which may be overestimated far from the generation source due to the garden sprinkler effect.

The numerical results comprise wave fields at each time step for each synthetic event, including SWH, peak wave period (PWP), mean wave direction (MWD), and wave power (WP). The results were processed to obtain maps of maximum values for each of the parameters during the entire lifetime of each individual event. To do so, the maximum value from the time series at each grid point was stored for every individual event and maximum value envelopes were created. From this results it was possible to characterize the mean maximum SWH and associated PWP, mean maximum PWP, the 99%-ile of the maximum SWH and associated PWP, and the 99%-ile PWP.

The use of historical events to assess the performance of GCMs to generate synthetic events may be misleading due to the short historical record. Nevertheless, results from past events (based on HURDAT2 data from 1975-2005) were compared against the NCEP and GCM results to provide a sense of accuracy for the most general parameters such as wind speeds and annual cycle. In order to revise the results from the GCMs considering present wave climate, we utilized the NCEP events. The bias of the GCMs to reproduce the wave climate provided the framework to assess the future changes in wave climate. The future conditions of wave climate were considered at the end of the 21st century, through numerical simulations of future events (2070-2100). These results were compared to those obtained by simulating the present climate events (1975-2005), to assess the wave climate change at the end of the 21st century. Finally, in order to provide an assessment of the impact of climate change on the design of onshore and offshore structures, the SWH for different return periods using the present (1975-2005) and the future (2070-2100) climates was determined.

2.3. Results and discussion

2.3.1. Assessment of synthetic events

The use of synthetic events as a means to replace the short records of TC available is exemplified by Emanuel and Jagger (2010) where such an approach provides good results in low frequency areas such as New England. This is also shown by the estimation

of storm surges derived from synthetic events in New York City (Lin et al. 2010, 2012), from which Hurricane Sandy (2012) storm surge corresponds to a return period between 500 and 1000 years. The latter study provides estimates of storm surge based on climate change scenarios, establishing the rate of change between the present and future climate results, independent of uncertainty imposed by the models. To provide a more accurate interpretation of the future climate, it is important to assess the bias of the models to reproduce the present climate. This will indicate if the foreseen changes are a result of the model bias or the climate change scenario.

To provide a sense of the uncertainty imposed by the GCMs on the generated synthetic events, those events were compared to the historical data (HURDAT2) and the events derived from NCEP. Figure 2 shows the comparison of the wind speeds and minimum central pressure intensity and annual cycle for all synthetic events in the present climate. The annual cycle in these plots refer to the month when the maximum wind speed occur for each synthetic event, discriminating by category. The intensity histograms (Figure 2a,b) show a good agreement between all databases, while the annual cycle (Figure 2c) show the same tendencies despite differences between the databases frequencies. The most relevant discrepancy is the presence of more intense events during August for the NCEP events, in contrast to HADGEM, which has more intense events in September. It is also noticeable that the HADGEM model overestimates the number of events in October and underestimates them in July and August. Therefore, the GFDL model has a better representation of both the NCEP and historical events. This is consistent with Sheffield et al. (2013b), where the authors, using a different storm track methodology, find that HADGEM tends to produce too few hurricanes and to overestimate the number of events in October.

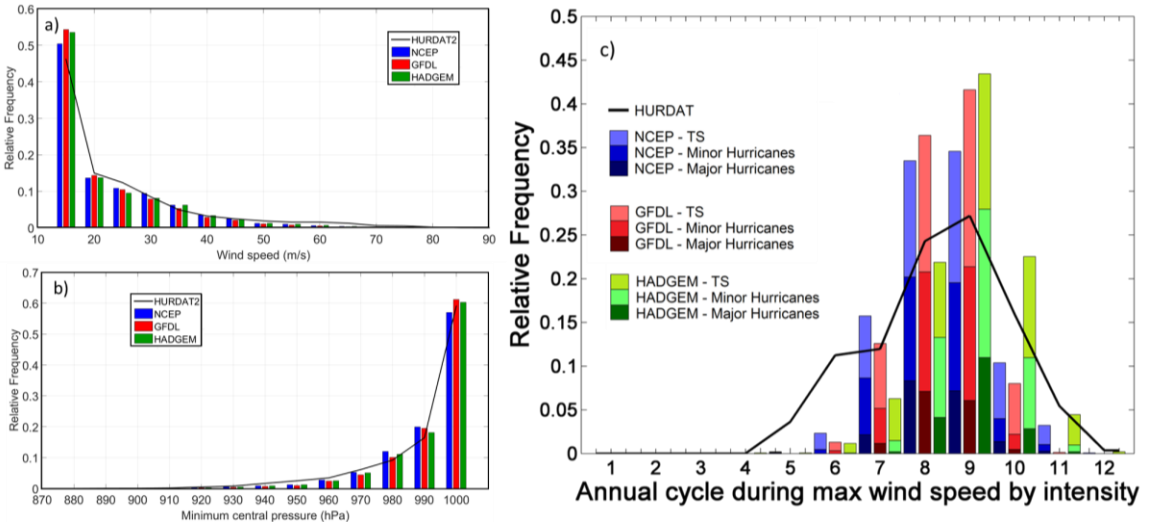

Figure 2. Relative frequency histograms for a) maximum wind speed, b) minimum central pressure and c) annual cycle based on maximum lifetime wind speed.

While the histograms provide an assessment of the characteristics for all events together in the GoM, it is important to assess the geographical distribution of such events. Figure 3 shows the kernel density map for all TCs, hurricanes and major hurricanes (categories 3 to 5) derived from NCEP, GFDL and HADGEM. Based on all TC, the GFDL events provides a better agreement to the NCEP events, with a slight underestimation near the Yucatan Channel and the Florida coast, as well as an overestimation near the US-Mexican border (south of Texas). HADGEM events do represent the concentration of events in Florida, but underestimates the density of events in most of the GoM. A similar pattern was found for all hurricanes, while for major hurricanes the GFDL events overestimate the density of events south of the Mississippi delta and the HADGEM events underrepresent all the events in the Mexican part of the GoM. (Sheffield et al. 2013a,b) found that none of the GCMs used for the CMIP5 is able to reproduce well the Western Hemisphere Warm Pool during the summer over the GoM, showing a negative bias over this region. They also found that not even the GCMs with higher resolution can properly solve the frequency of hurricanes over the North Atlantic.

The study by Camargo (2013) can explain the underestimation of the events by the HADGEM model based on the genesis potential index (GPI, Emanuel and Nolan

2004), which measures the potential of TC formation. The study shows that the HADGEM model has lower GPI values over the main development region (MDR) compared to the NCEP reanalysis and the GFDL model. The GPI index is based on vorticity, wind shear, midlevel relative humidity and potential intensity, which are variables from the GMCs used by the intensity model of the synthetic events.

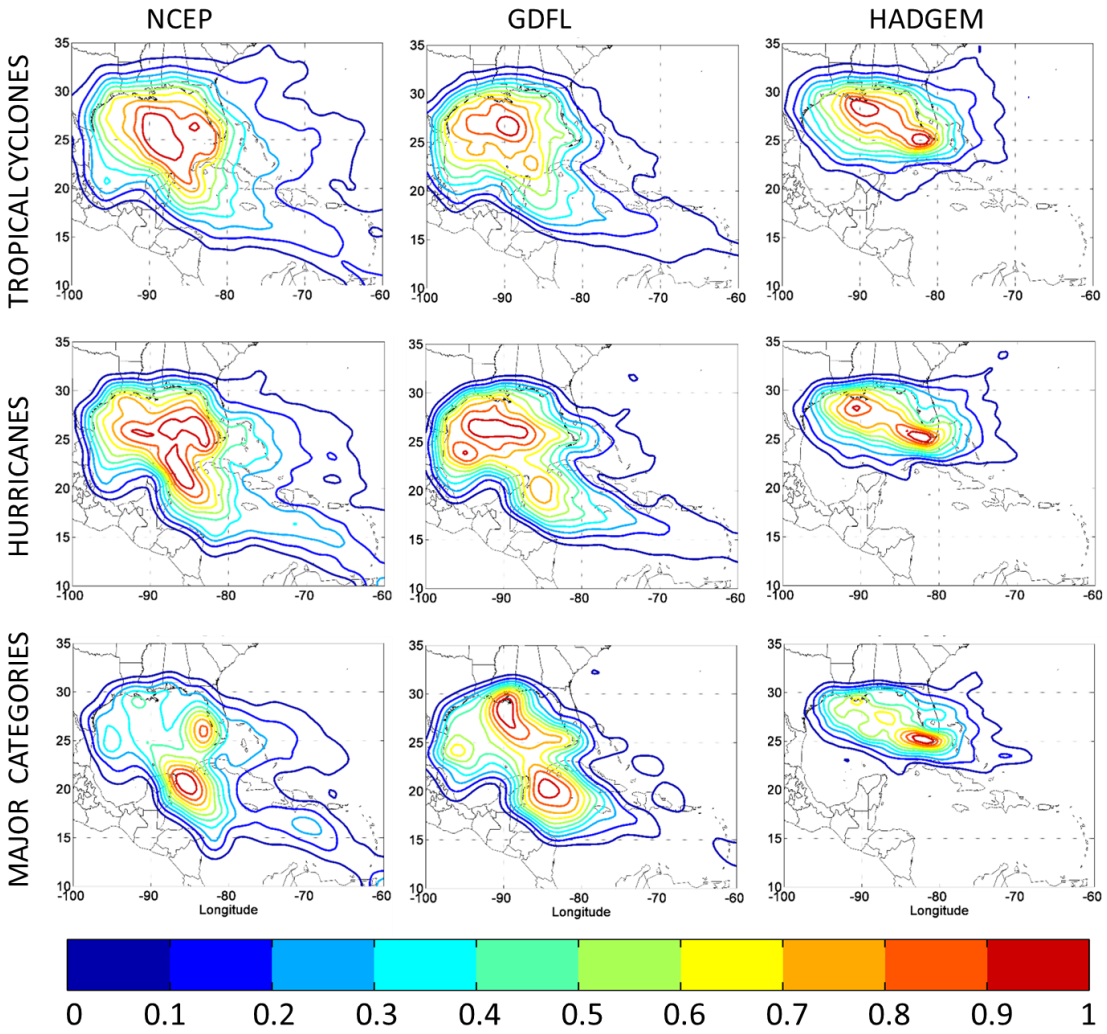

Figure 3. Normalized kernel density (each event scaled to have the unit maximum) for synthetic events in the present climate 1975-2005 for different databases (left: NCEP; center: GFDL; right: HADGEM) corresponding to TC (upper panels), hurricanes (middle panels), and major categories (lower panels).

For a more straightforward assessment of the bias from the synthetic events, the associated waves for each track in the databases were computed. The derived extreme wave climate can be regarded as a low-pass filter that shows only the information about the events that have a relevant impact on the extreme waves. We calculated the bias from the GFDL and HADGEM wave model results by subtracting the wave results from the NCEP events. Figure 4 shows the bias for different wave parameters derived from the GFDL results and Figure 5 from HADGEM. The mean and 99%-ile values for SWH as well as their associated PWP and mean PWP are derived from the maximum envelope maps. These parameters were later used to characterize the present and future wave climates.

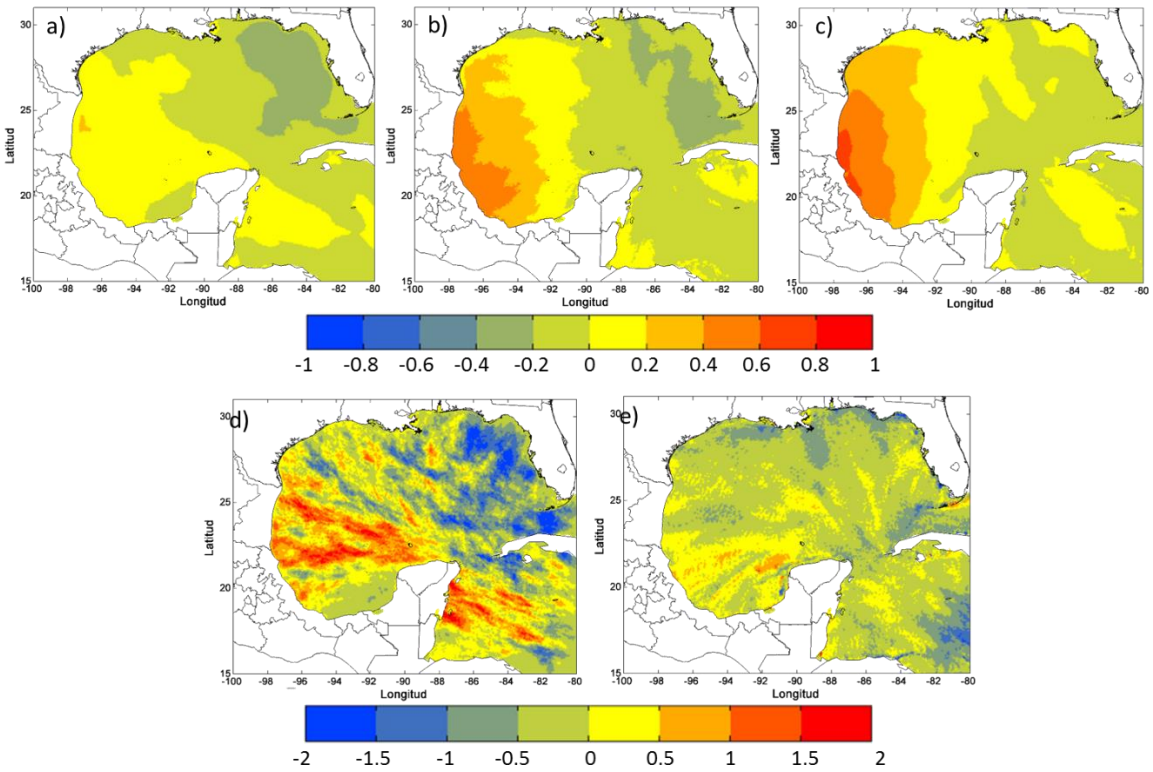

Figure 4. GFDL model bias for a) mean maximum SWH and b) associated PWP, c) mean maximum PWP, d) 99%-ile maximum SWH and e) 99%-ile maximum PWP. The scale corresponds to meters for SWH and seconds for PWP.

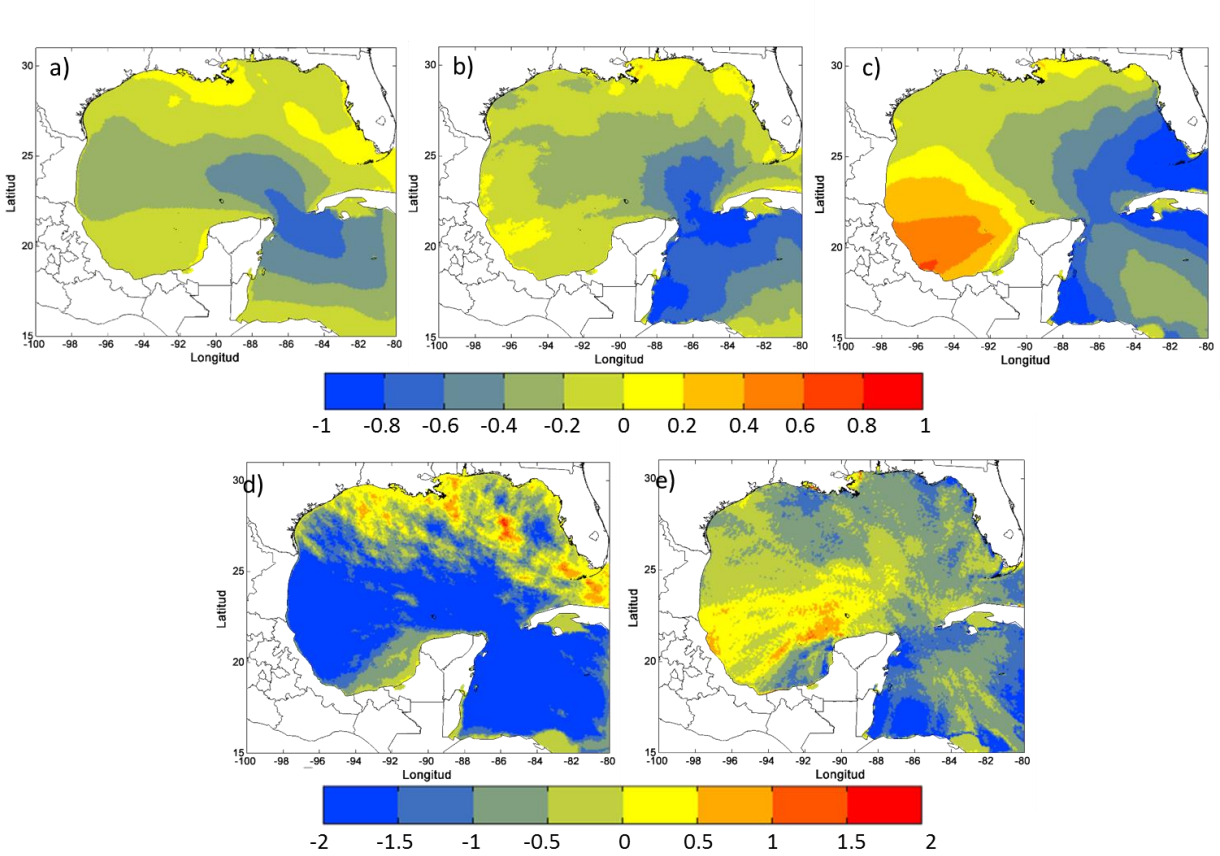

Figure 5. HADGEM model bias for a) mean maximum SWH and b) associated PWP, c) mean maximum PWP, d) 99%-ile maximum SWH and e) 99%-ile maximum PWP. The scale corresponds to meters for SWH and seconds for PWP.

In general, the GFDL derived waves have a smaller bias than HADGEM. The mean maximum SWH (Figure 4a) and associated PWP (Figure 4b) from the GFDL events are slightly overestimated in the eastern GoM and slightly underestimated in the western GoM. Similar results were obtained for the 99%-ile of maximum SWH (Figure 4d), associated PWP (Figure 4e) and mean maximum PWP (Figure 4c) for GFDL events, although the bias is larger and the associated PWP shows negative bias in the northern GoM.

The HADGEM derived waves show larger biases. The mean maximum SWH (Figure 5a) is underestimated in most of the domain, with the highest negative bias at the Yucatan channel, extending into the Caribbean Sea and along the central GoM towards the west. A similar pattern is observed for the associated PWP (Figure 5b), although the mean PWP (Figure 5c) shows large negative bias in the eastern GoM (more pronounced

near southern Florida and Cuba) and large positive bias in the western GoM, particularly the southwestern area (Campeche sound). The largest negative biases were found for the 99%-ile of the maximum SWH (Figure 5d) along most of the GoM and the western Caribbean Sea, with positive biases in the northern GoM from Texas to Florida. The associated PWP for the 99%ile of maximum SWH (Figure 5) only shows positive biases in the southwestern GoM, with the largest negative biases in the western Caribbean Sea.

An analysis of the genesis location and tracks of the synthetics events derived from NCEP and the GCMs (Figure 6), shows that the GFDL has a better representation of the NCEP events than HADGEM. For instance, Figure 6a shows that the genesis of most events under the NCEP model are distributed over the GoM, Caribbean Sea and the Atlantic, with the genesis of hurricanes distributed along the MDR (Vecchi and Soden 2007). This is also the case for the GFDL derived events (Figure 6b), but is not the case for the HADGEM derived events, where the genesis of hurricanes is mainly concentrated northwest of the MDR, in the area north of Cuba and around Florida (Figure 6c). This has an effect on the intensity during the tracks of the TC, so that the distribution of the intensity of the events is similar for the NCEP and GFDL models (Figure 6d,e) and different from the HADGEM events (Figure 6f). The major hurricanes for the HADGEM events are mostly concentrated in the northeast portion of the GoM, making landfall in Louisiana and Florida (Figure 6f). This explains the largest negative (positive) bias of the maximum SWH (particularly the most extreme waves characterized by the 99%-ile), on the Yucatan Channel and the Caribbean (northern GoM).

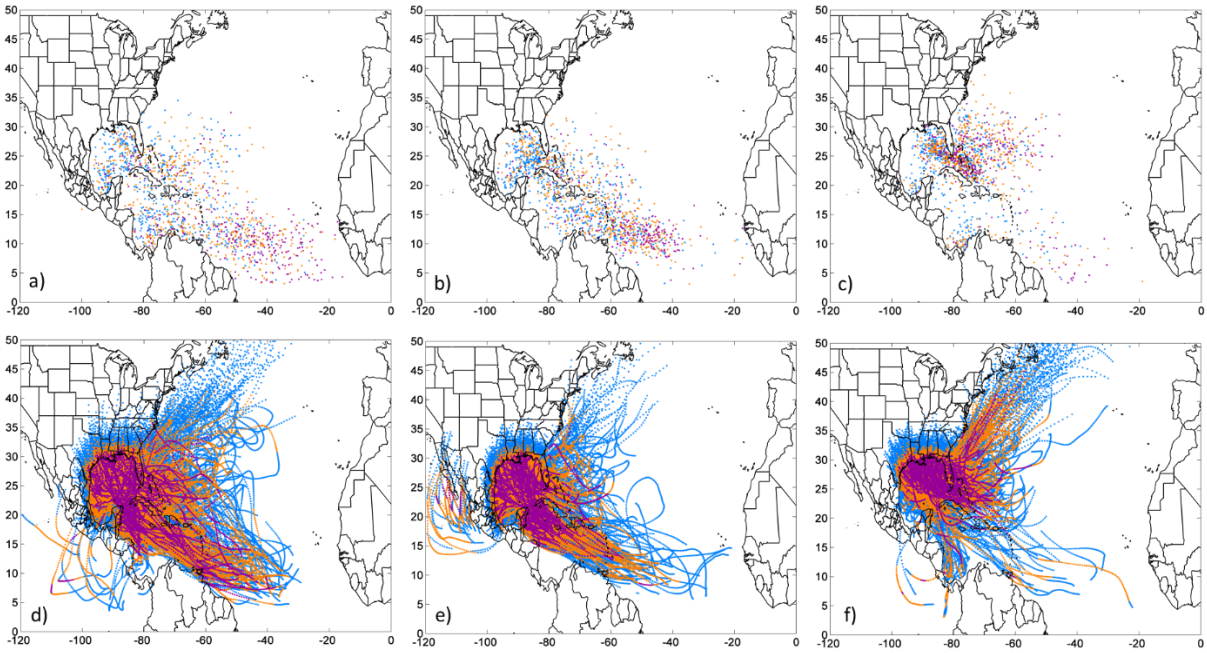

Figure 6. Synthetic events distribution of genesis locations for a) NCEP, b) GFDL, c) HADGEM and track distribution d) NCEP, e) GFDL, f) HADGEM, where blue indicates genesis of an event achieving a maximum intensity of tropical storm, orange indicates maximum intensity of minor hurricane and purple of major hurricane for distribution. Similarly, the color for each track point indicates the intensity achieved at that track location (blue for tropical storm, orange minor hurricane and purple major hurricane).

2.3.2. Tropical cyclone-generated waves

To provide an assessment of the future conditions, the present wave climate from both the GFDL and HADGEM models was used as a reference for the future climate. We show the implications of wave climate change by calculating the design waves for different return periods under present and future climate.

Wave climate at the end of the 21st century

The maximum envelop maps for SWH and PWP (Figure 7-Figure 11) were used to characterize the extreme wave climate derived from TCs in the future (2070-2100). This ensures that the extreme waves are considered, with the mean values as a representation of extreme events, and the 99%-ile the “upper tail” from those events, which are the most

extreme events to occur at a particular location. Also, an average from both models is shown, with blank areas where the projections of the models (i.e. increase or decrease) are in opposite direction.

Considering the mean maximum SWH (Figure 7), the RCP 8.5 scenario (Figure 7b,d) increases the mean, although the HADGEM model (Figure 7d) shows a decrease in the coastal area of Texas. It is important to consider the model biased presented earlier when interpreting the projection obtained by in each model. For instance, the HADGEM projection of an increased mean SWH (Figure 7c,d) occurs in an area where the model underestimates, so that the actual values are biased by the underestimation by the model (Figure 5a). In the case of the GFDL model (Figure 7a,b), the positive bias is small while the negative is larger in the area south of Florida (Figure 4a), so that the actual values of the projected increase are more reliable in the eastern GoM. The increases are greater for the RCP 8.5 scenario than in RCP 4.5 in the GFDL model, but not for HADGEM where the increases cover a larger area in the RCP 4.5, and the RCP 8.5 scenarios even show areas of decreased mean maximum SWH. Both models show an increase of the mean maximum SWH for RCP 4.5, while HADGEM shows a small decrease around Texas and northern Tamaulipas for the RCP 8.5 scenario. As a result, the models average show a general increase of the mean maximum SWH (Figure 7c).

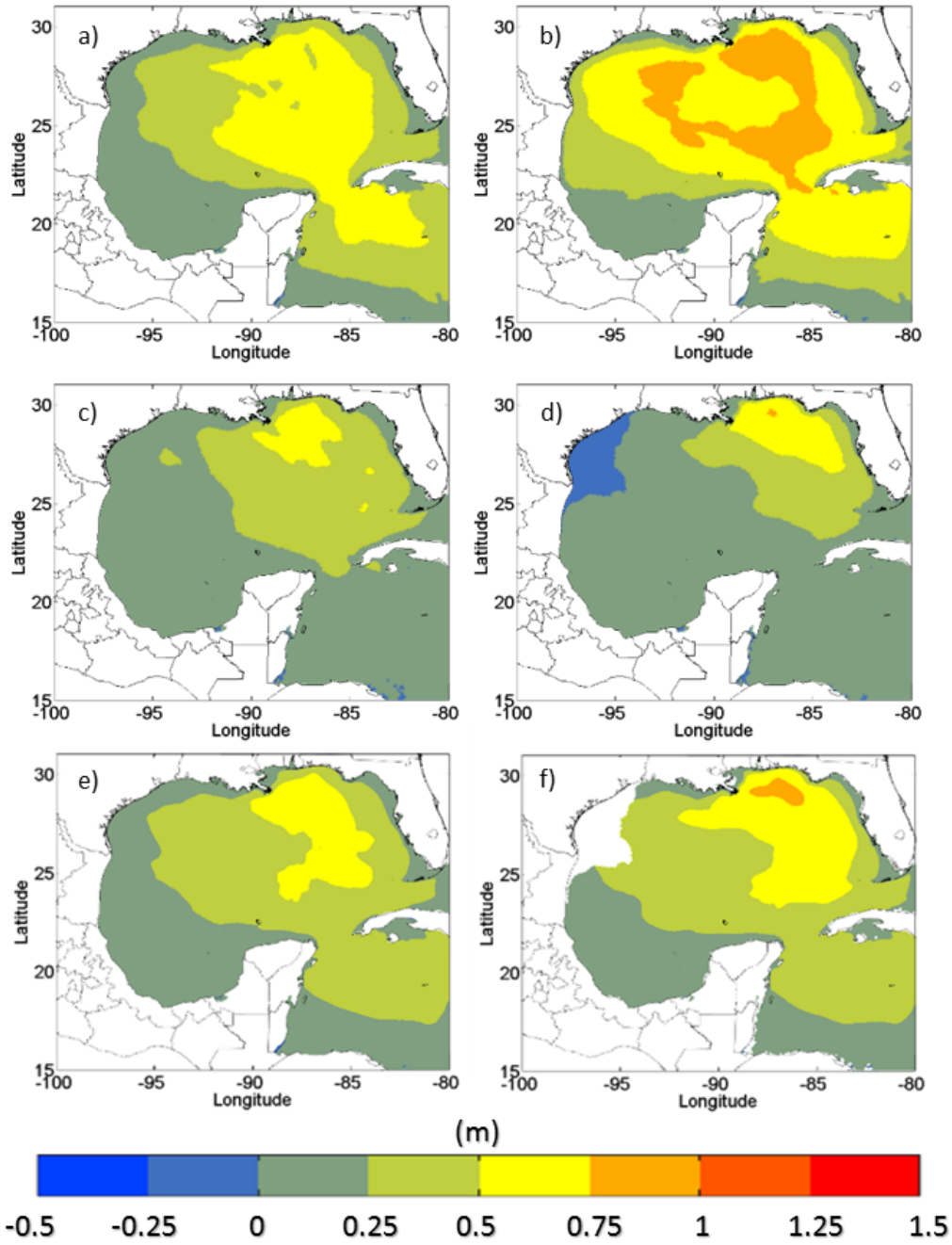

Figure 7. Mean maximum SWH projection for the future climate (2070-2100) based on a,b) GFDL, c,d) HADGEM, and e,f) models average, under the RCP a,c,e) 4.5 and b,d,f) 8.5 scenarios. The color bar represents the difference of SWH in meters between the future climate (2100-2070) minus the present climate (1975-2005).

Figure 8 shows the future change in the PWP associated with the mean maximum SWH. The GFDL model projects an increase in the associated PWP (Figure 8a,b), which is higher for the RCP 8.5 scenario, particularly in the western and northern GoM (Figure 8b). The highest increase is found in the RCP 8.5 scenario and for the GFDL model in the northeastern GoM between Louisiana and Florida (Figure 8b), where there is a slight negative bias (Figure 4b). The HADGEM model projects less increase in associated PWP than the GFDL model and more increase for the RCP 4.5 than the RCP 8.5 scenario (Figure 8c,d) as a result of a slight higher increase of the mean maximum SWH (Figure 7c,d). The average of both models show an overall increase in the PWP associated with the mean maximum SWH, with only a small area showing and opposite trend in the projection, which corresponds to a small area offshore Texas (Figure 8e,f). The northeastern GoM increase of both SWH and the associated PWP is likely to affect the offshore oil extraction areas, but it is important to consider that areas such as the Campeche Sound and offshore of Tamaulipas, are likely to experience an increase in the PWP although there is no apparent increase in the SWH. The higher increase found in the RCP 4.5 scenario compared to the RCP 8.5 for both mean maximum SWH and associated PWP in the HADGEM model, is result of the TC genesis location, particularly the major hurricane events, as well as the concentration of the higher intensities in the northeast GoM near Florida. Please note that these results may be biased by the garden sprinkler effect.

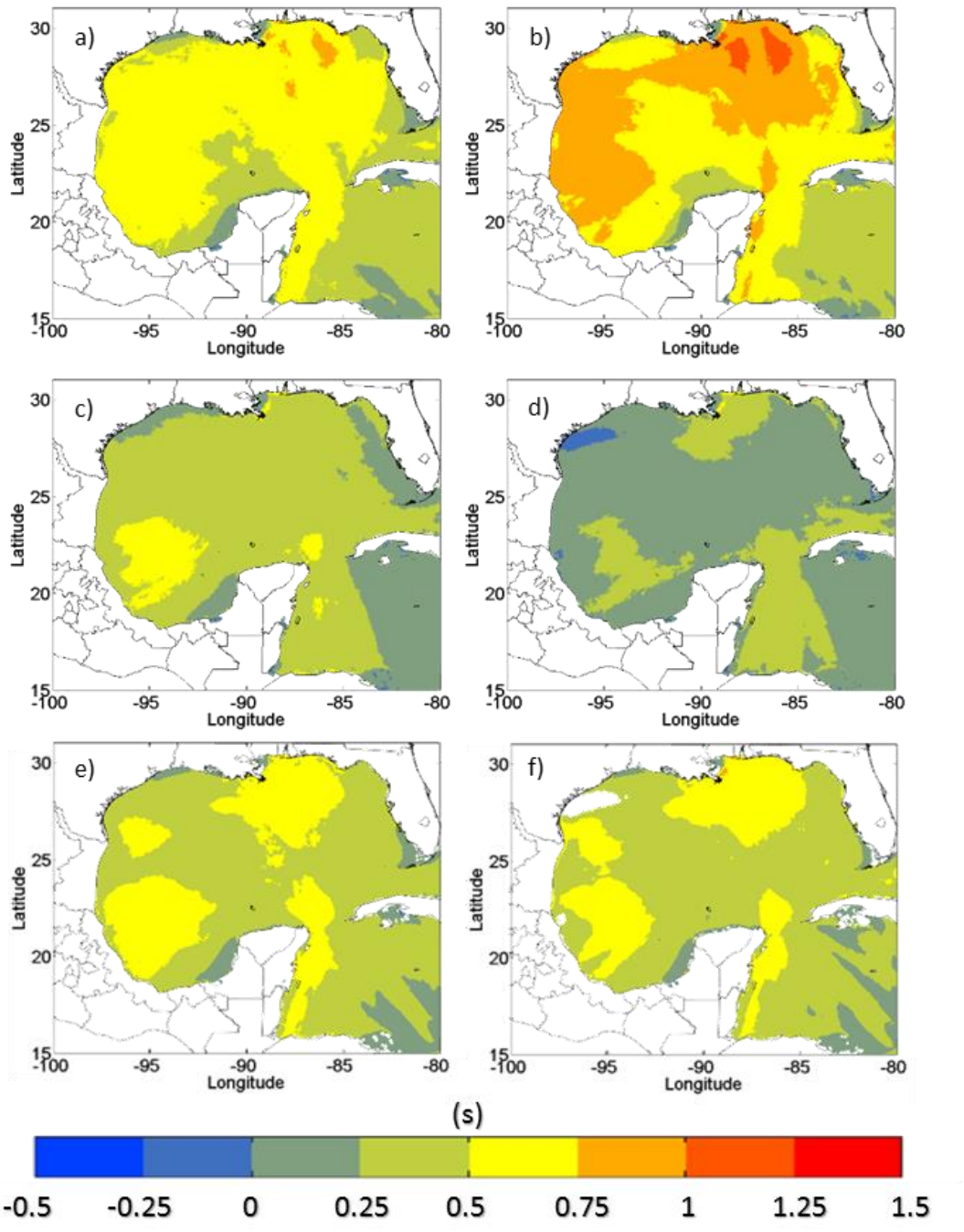

Figure 8. PWP associated with the mean maximum SWH projection for the future climate (2070-2100) based on a,b) GFDL, c,d) HADGEM, and e,f) models average, under the RCP a,c,e) 4.5 and b,d,f) 8.5 scenarios. The color bar represents the difference of PWP in seconds between the future climate (2100-2070) minus the present climate (1975-2005).

The mean maximum PWP is shown as an indication of the reach of the TC driven swell. This swell can affect creating erosion and/or flooding in areas located far from the TC track, despite smaller SWH. Figure 9 shows the change in the maximum PWP in the future climate in relation to the present climate. For the RCP 4.5 scenario there is a slight increase of PWP for both models (Figure 9a,c), although the GFDL model projects a larger increase particularly in the northwestern GoM (Figure 9a). The HADGEM model does project an increase for the RCP 4.5 escenario but smaller than the GFDL model (Figure 9c). For the RCP 8.5 scenario in the GFDL model, there is a slight increase in the eastern GoM with respect the RCP 4.5 scenario, although the increase is almost entirely in the GoM (Figure 9b). This does not occurs for the HADGEM model under the RCP 8.5 scenario, where the western GoM show a decrease in the mean maximum PWP and a slight increase for the rest of the GoM (Figure 9d). The average of both models show an overall increase in the mean maximum PWP and in similar intensity for both the RCP 4.5 and 8.5 scenarios. While the tendency of the projection is an increase for both HADGEM and GFDL under the 4.5 scenario, this is not the case for the RCP 8.5 scenario, where most of the western GoM show a projection in opposite directions. It is important to notice that the western coast of the Yucatan Peninsula shows a decrease in the mean maximum PWP in both scenarios.

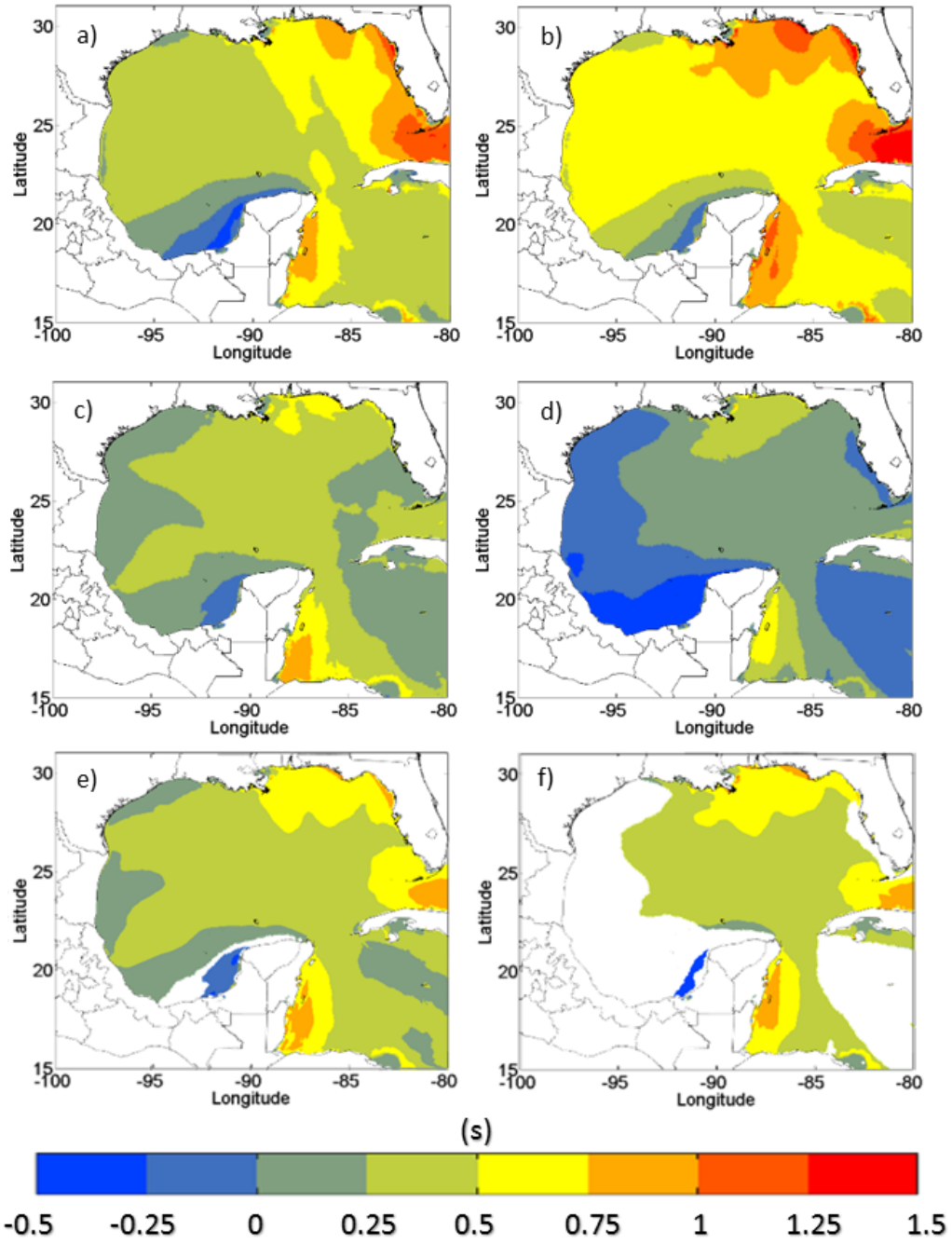

Figure 9. Mean maximum PWP projection for the future climate (2070-2100) based on a,b) GFDL, c,d) HADGEM, and e,f) models average, under the RCP a,c,e) 4.5 and b,d,f) 8.5 scenarios. The color bar represents the difference of PWP in seconds between the future climate (2100-2070) minus the present climate (1975-2005).

The 99%-ile of the maximum SWH (Figure 10) and associated PWP (Figure 11), represent the highest end of the extreme waves derived from the synthetic TCs. Figure 10 show that the 99%-ile of maximum SWH increases for both models and scenarios except for a thin strip from northern Yucatan to southern Texas in HADGEM under RCP 8.5 scenario (Figure 10d). The increase for all models is larger at the northern and eastern GoM, with the largest increase for the GFDL model under RCP 8.5 (Figure 10b). The average between the two models show a similar increase than the individual models for the RCP 4.5 scenario, while the HADGEM models results in a smaller increase in the average than that of the GFDL model for the RCP 8.5 (Figure 10e,f). Still, the increase in the northeastern GoM is expected to be of larger intensity than the expected mild increase of the 99%-ile of maximum SWH in the Campeche Sound.

The associated PWP of the 99%-ile of maximum SWH shows a larger increase for the HADGEM model (Figure 11c,d) in the Campeche sound but larger in other areas for the GFDL model (Figure 11a,b) particularly for the RCP 8.5 scenario. The average of both models show a higher increase in the RCP 8.5 than RCP 4.5 (Figure 11e,f), although there is a discrepancy around Florida and the northern Yucatan Peninsula. Considering that these results correspond to the most intense events, the garden sprinkler effect is most likely to be influencing the results, so that the conclusions should be taken with caution.

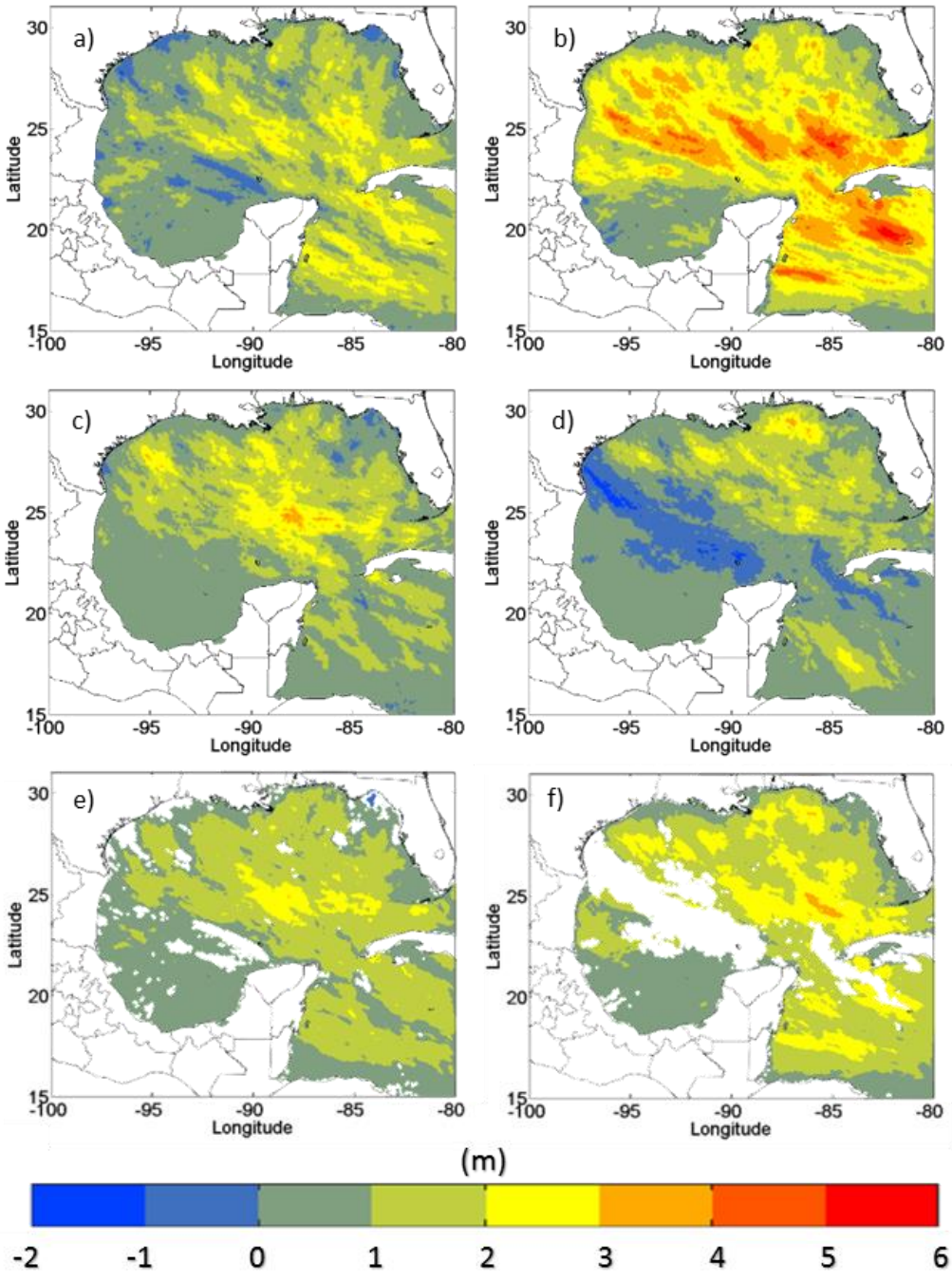

Figure 10. 99%-ile of maximum SWH projection for the future climate (2070-2100) based on a,b) GFDL, c,d) HADGEM, and e,f) models average, under the RCP a,c,e) 4.5 and b,d,f) 8.5 scenarios. The color bar represents the difference of SWH in meters between the future climate (2100-2070) minus the present climate (1975-2005).

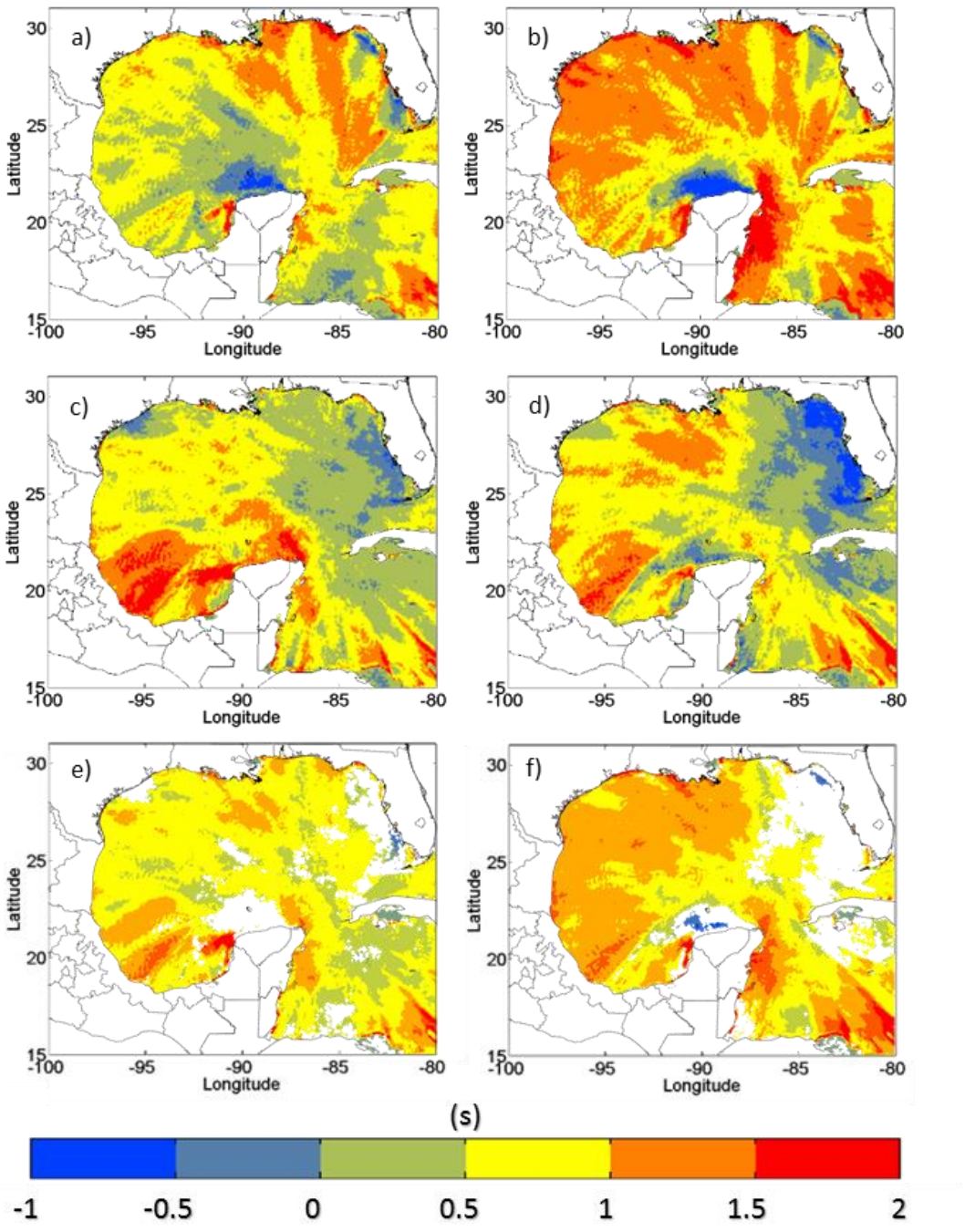

Figure 11. PWP associated to 99%-ile maximum SWH projection for the future climate (2070-2100) based on a,b) GFDL, c,d) HADGEM, and e,f) models average, under the RCP a,c,e) 4.5 and b,d,f) 8.5 scenarios. The color bar represents the difference of PWP in seconds between the future climate (2100-2070) minus the present climate (1975-2005).

The future changes in wave climate were further analyzed by means of the wave power. The maximum wave power was calculated from each synthetic event by adding the maximum wave power at each grid point. Figure 12 show the wave power for the present and future climates, where each box represent the 25%-ile (bottom) and 75%-ile (top) bounding the median (middle line); the whiskers extend to the outmost points not considered outliers (based on 1.5 times the 25-75%-iles), and the wider dash lines represent the 10%-ile (bottom) and 90%-ile (top). The GFDL results show a good representation of the present climate based on the comparison to the NCEP derived results. While the GFDL model slightly underestimates the higher percentiles in the present climate, the HADGEM shows a larger bias, underestimating the most energetic storms. The GFDL model shows a clear tendency to more energetic storms in the future climate based on the median and upper percentiles. This tendency is increased in the RCP 8.5 scenario. Considering that the GFDL slightly underestimates the higher percentiles, it is more likely that they will be increased in the future. The HADGEM model does show an increase in the upper percentiles but in this case the increase is small and it is slightly higher for the RCP 4.5 scenario. Considering that the HADGEM model underestimates the higher percentiles, it is also expected that the future climate will bring more wave power in the GoM.

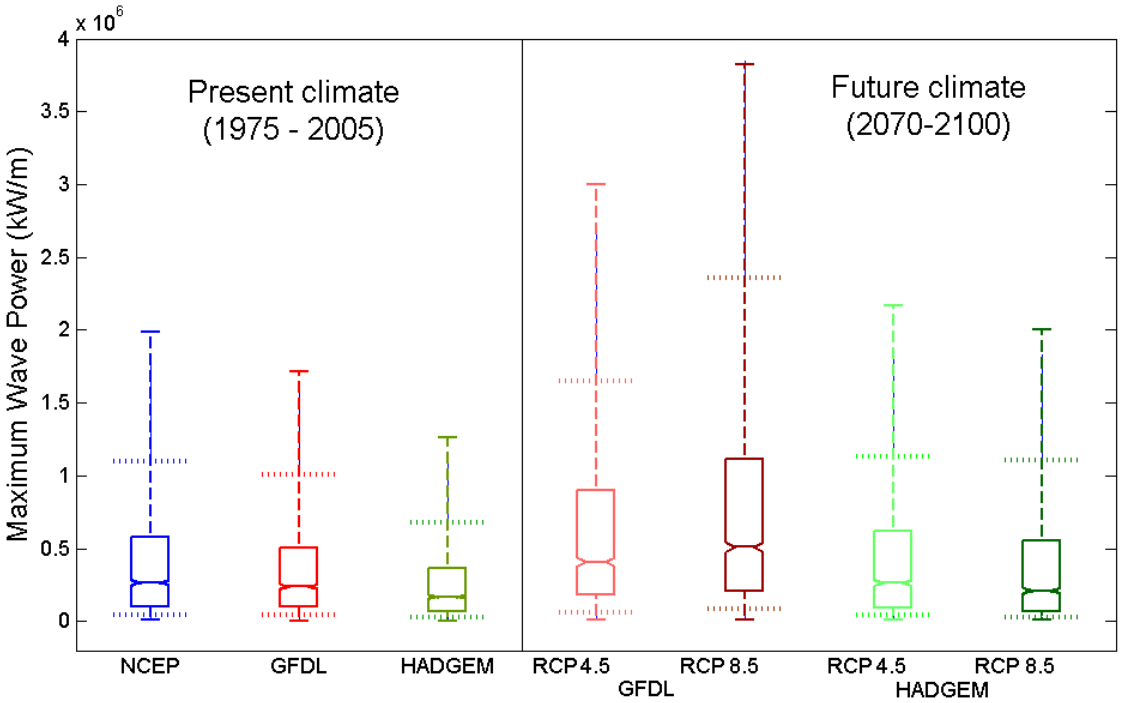

Figure 12. Wave power (kW/m) in the Gulf of Mexico from TCs in the present and future climate.

The results clearly show an increase in the intensity of the TC-derived waves in the GoM, regardless of the GCMs biases. The GFDL increase in intensity is more pronounced under the RCP 8.5 scenario, while the HADGEM model shows a decrease in the RCP 8.5 scenario when compared to the RCP 4.5. This is because the HADGEM bias towards a concentration of high intensity events in the area near Cuba and Florida. A similar result was found by Fan et al. (2013) where four CMIP3 models projected a decrease of more than 20% in the SWH, due to the seldom penetration into the GoM by hurricanes in the future climate under the A1B scenario.

Considering the work by Camargo (2013), the HADGEM model shows no significant change in the GPI for the future climate, while the GFDL model shows a considerable increase in the MDR, the GoM and the northwestern Atlantic. The same study shows a slight decrease or change in the Potential Index in the MDR for the

HADGEM and a considerable increase for the GFDL model. Finally, Camargo (2013) shows an increase in the wind shear for the future climate in the Caribbean and the Mexican part of the GoM, while the GFDL model shows a decrease in those areas as well as the northwestern Atlantic. These three parameters provide a physical explanation for the results discussed above.

Design SWH under different RCP scenarios

The SWH for the design of onshore and offshore structures is based on the degree of damage that could be allowed to a certain installation. Considering a 100-year return period as the design wave, a structure design under such parameter and for a lifespan of 100 years, has a 63% probability of experiencing a design wave event. A caveat of using a fixed design wave is that it assumes that the wave climate is stationary, so that the statistical characteristics of the wave climate will remain unchanged during the structure lifetime. Our previous results show that is not the case under a warming climate. The 100-year SWH based on the present climate (e.g. 1975-2005) will differ from the 100-year SWH based on the future climate (e.g. 2070-2100). In some areas, the SWH is expected to increase (decrease), so that a structure designed under present climate conditions will have an increased (decrease) probability of experiencing the design wave during its lifetime, so that it would be more (less) prone to damage by the end of the 21st century.

To illustrate how using a present climate to determine the design wave could result in inadequate design, I determine the 100-year SWH using the Peak Over Threshold (POT) approach (Coles 2001) to select the maximum values for which a Generalized Pareto (GP) distribution was fitted at each computational node. A threshold value of 6 m was used whenever the POT series was above 30 values, and reduced the threshold in increments of 1 m until the series provided a minimum of 30 values. Areas with less than 30 values for a threshold value of 1 m where not considered.

Figure 13 shows the 100 year SWH maps for the present and future climates, based on the GFDL and HADGEM models. The present climate difference between

models is a result of the model biases as explained in section 4.2. The 100-year SWH in the future climate shows an increase of 5 m in some areas between the future (Figure 13c) and the present (Figure 13a) climates. In some cases there is decrease in the future climate (Figure 13f) with respect to the present climate (Figure 13d). The GFDL models shows a gradual increase in the 100-year SWH from the present climate (Figure 13a) to the RCP 4.5 scenarios (Figure 13b) and then to the RCP 8.5 (Figure 13c), so that the present wave climate design wave will underestimate the conditions a structure may experience at a later stage during it lifespan. While the HADGEM model shows a similar behavior for the most northern and eastern part of the GoM, for the western and southern part there is a decrease in the 100-year SWH for the RCP 8.5 than the RCP 4.5 and present climate.

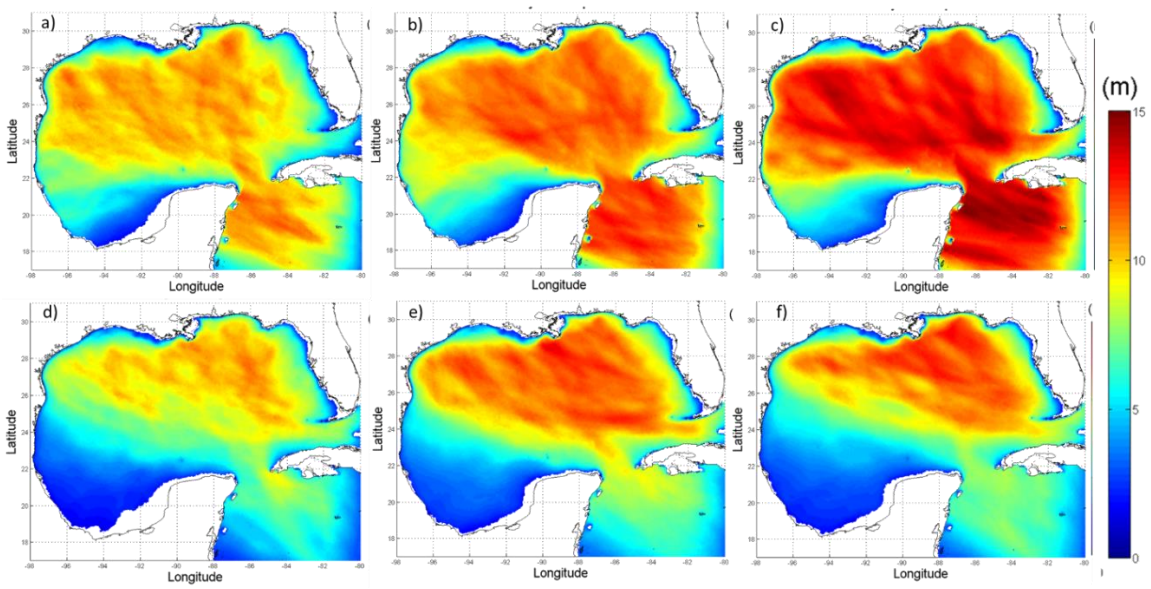

Figure 13. 100-year SWH for GFDL under a) present climate, and future climate under b) RCP 4.5 and c) RCP 8.5 scenarios, and for HADGEM under d) present climate, and future climate under e) RCP 4.5 and f) RCP 8.5 scenarios

The 100-year SWH results for the present and future climates indicate that using the present wave climate may result in under/over design of offshore and coastal

structures. Please note that extreme value analysis is very sensitive to data and the probability distribution function, so that the above results may vary considerably when applying other criteria. As such, these results are only to illustrate the effect of a warming climate in the selection of design criteria (e.g. 100-year SWH).

2.4. Conclusions

This study presents a new method to estimate the wave climate derived from TCs using synthetic events. The method overcomes the limitations imposed by historical records (short time series of events), as well as the limited number of events in GCMs and their underestimation of maximum wind speeds. Furthermore, the method reproduces the basin wide statistical features of TCs (wind speed and minimum pressure intensity and annual cycle) when the NCEP-derived events are compared to historical events. The GCM-derived events (GFDL and HADGEM) show biases when the present climate-derived events are compared to those from NCEP. In particular, the genesis of the major category events derived from HADGEM show a higher concentration near Florida and Cuba, compared to the NCEP and GFDL events which are mostly generated in the Atlantic and eastern Caribbean Sea. In turn, the major category events from HADGEM events are concentrated in the northeastern part of the GoM, while the NCEP and GFDL are more evenly distributed in the GoM.

Numerical results show that global warming leads to an increased SWH, although such an increase may only be limited to certain areas. In the case of the GFDL model, the increase is generalized and it is higher in the RCP 8.5 scenario compared to the RCP 4.5. In the HADGEM derived climate, the increase is higher for the RCP 4.5 scenario since there is a tendency for the events to shift towards the northeast when global warming is increased (i.e. RCP 8.5 scenario). The result is that in the southwestern part of the GoM, the HADGEM model projects a decrease in SWH with increasing warming.

An assessment of the overall wave power in the GoM from the synthetic events showed that global warming will most likely cause a higher wave power. This wave power

increases considerably for the GFDL model and is higher for the RCP 8.5 scenario than for RCP 4.5. For the HADGEM model the increase in wave power is less for the RCP 8.5 scenario compared to the RCP 4.5 for the same reasons discussed above.

Considering that the GFDL present wave climate shows less bias than HADGEM when compared to the NCEP derived climate, there is more likely to be an increase in the TC-derived wave activity of the GoM with a warming climate. Still, the uncertainty imposed by GCMs unable us to provide definite conclusions. This work only deals with 2 GCMs so it is advised to perform a similar study involving other models in order to reduce uncertainty.

To show the importance of determining the future wave climate for practical applications, the 100-year SWH was determined for the GoM. The results show that the design wave can change considerably when considering the present or the future climate. The relevance of this conclusion is that the structures that are designed nowadays based on the 100-year return period will still be under its expected lifespan into the 22nd century. This should raise questions about the suitability of using present climate statistics for design of onshore/offshore structures, and whether future climate statistics should be considered.

Chapter 3.

Extreme ocean waves from *Nortes*

3.1. Introduction

Ocean waves generated by *Nortes* are an important design parameter and operational issue in the GoM. Unlike waves generated by TCs, which have devastating consequences mainly confined to an area surrounding the track of the event, *Norte*-derived waves are more frequent and with a more regional impact across the GoM. Both the high occurrence and regional effect of *Nortes* have yearly consequences for oil and gas industry, shipping, and fisheries of the GoM, Their presence usually imposes operational downtime so that *Norte*-derived waves are important parameters for the design of onshore and offshore facilities and activities.

Despite the yearly economic and social impacts from *Norte*-derived waves, their study is limited and mainly implicit in the characterization of the GoM wave climate. For instance, Ramírez-Elías (2007) characterized the wave climate at the northwestern Mexican Gulf and attributes the highest winter waves to *Nortes*; while (Mendoza et al. 2013) characterize the northern Yucatan storm waves, attributing the winter storms to *Nortes*. In the wave climate characterization by Appendini et al. (2014), it is shown that *Norte*-derived waves modulate the winter wave climate, rising the mean SWH and dominating the extreme wave climate. They also show that the design wave heights in the western Mexican Gulf are similar to those of the eastern Gulf for up to a 30-year return period, where the former are derived from *Nortes* and the latter from hurricanes. This clearly denotes the relevance of studying the *Norte* derived waves, in particular for Mexico.

Although there are only a few studies of *Norte*-derived ocean waves, there are several studies regarding the origin of *Nortes* and their consequences as they pass through North America. Such studies refer to polar outbreaks, cold surges or Central American Cold Surges as the source of *Nortes*. These events are related to synoptic

scale waves from mid latitudes, associated with high pressure systems, frequently originated at the Rocky Mountains in the USA and moving into the GoM generating strong northerly winds and important temperature decreases (Schultz et al. 1997). Considering the effect of the polar outbreaks over the North American weather, the characterization of the air masses has been prioritized over the location of the low and high pressure systems (Willett 1934). Those polar masses descending towards the GoM are the continuation of the blizzards in the northwestern US states that become milder when entering along the northwestern Texas boundary (Taylor 1888; Schultz et al. 1997), and are responsible for the sudden drops of temperature affecting crops (Rogers and Rohli 1991), humans (Ruiz 1892) and even aircrafts (Hansman 1984). Thus, the importance of their study in the US is usually related to continental weather rather than to the derived ocean waves.

Considering the weather impact of cold surges over North America, Willett (1934) provides an air mass classification. As part of their studies to understand cold surges passing through North America, Dallavalle and Bosart (1975) describe their anticyclogenesis and propagation. They propose two types of events based on their trajectories over the US and until they reach the GoM, but they leave out any description of their trajectories over the Gulf. Mecikalski and Tilley (1992) provide another classification scheme based on the path of the anticyclone and the minimum latitude reached both by the anticyclone and surge line. While this study does not focus on the GoM, the surge line of the events do enter the Gulf. Also, considering the different paths of the events, we can inferred that the influence on the sea state over the GoM can differ between event types.

The study from Reding (1992) provides an analysis of the incursion of North American polar air mases into the tropics, which he refers to as “Central American Cold Surges”. He identifies the events using satellite imagery (GOES) and comparing with weather measurements in Merida, Yucatan. He looks for a temperature decrease of 4°C or more in 48 hours and sustained winds between 300° and 30° for more than 24 hours after the cold front passage, in order to consider the onset of the event (incursion into Central America). Reding (1992) provides a complete list of events between 1979 and 1990, including onset date, duration, latitude of southern most intrusion, and the drop of

temperature at the Merida weather station. While Klaus (1973) provides a list of events starting in 1899, he does not provide the methodology he used to identify events. Hence, Reding (1992) provides the first comprehensive database of *Nortes* that cross the GoM, were the methodology for identification of events is provided.

The identification criteria based on temperature had been used earlier by Hill (1969) for studying cold fronts affecting Mexico. In this study, Hill (1969) identifies the events based on an inter-diurnal temperature drop of at least 3°C at selected weather stations in Northern Mexico. As with the works by Dallavalle and Bosart (1975) and Mecikalski and Tilley (1992), he characterizes the cold fronts into two types based on their trajectories, but according to their point of entrance into Mexico and their general direction of advance. His findings are that the Northern type mainly accounts for 60 to 80% of temperature drops in eastern Mexico and seldom affects the Pacific. The exception for the influence on the Pacific side of Mexico is the area of the Isthmus of Tehuantepec, where the Northern type generates strong gap winds known as *Tehuanos* (Alvarez et al. 1989) or *Tehuantepecers* (Hurd 1929). Such winds have been associated with *Norte* events (Romero-Centeno et al. 2003), and can even generate waves that propagate offshore into the Pacific ocean (García-Nava et al. 2009).

Schultz et al. (1998) provide a classification of the events identified by Reding (1992) and group them into 3 categories, based on their temperature and duration. This is similar to the classifications provided by Hill (1969), Mecikalski and Tilley (1992), Konrad (1996) and Crisp and Lewis (1992), where the effect over the GoM is not considered. Klaus (1973) had already provided a classification of *Nortes* into 8 types according to their meridional penetration, although the method is not described.

As none of the above classification studies is related to the sea state, it is then interesting and relevant to read the work by Frankenfield (1917) who provides a classification of *Nortes* based on the location of the high and low pressure systems. The location of pressure systems is critical in determining the wave conditions, as has been shown in more recent studies (Camus et al. 2014; Perez et al. 2015; Izaguirre et al. 2012), where mean sea level pressure (MSLP) is used as the predictor for wave conditions. Since

the *Norte*-derived waves affect mostly the Mexican Gulf coast and have no relevant marine impact on the US Gulf coast, research following Frankenfield (1917) was reoriented by studies focused on air masses. The work by Willett (1934) leaves no doubt about this shift, with his statement that the pressure systems are not relevant to determine the weather.

It is also interesting that during the end of the 18th century and early 19th century there are several documents describing *Nortes* or *Northers* and their effect over the sea state. This studies thrive when the U.S. was exploring the coastal waters of the Mexican Gulf, as well as during the Panama Canal planning, construction and early operations. The text by Commander Baker (Baker 1874) showed that *Nortes* affected shipping, since sea travel was delayed by such events. The editor of the *Monthly Weather Review* (Notes by the Editor 1893) provided an account about the effects of some *Nortes* and the damages infringed on vessels and houses in Tampico and Veracruz; there was even one fatal incident. Further south, the work by Boucard (1883) described the Yucatan coastal flooding during *Nortes*, leaving a short strip of land between the sea and the lagoons, while the work by Ruiz (1892) mentioned the public health effects resulting from the temperature drops. It is clear from these early works that *Nortes* may impose in Mexico a set of negative effects, in contrast to the US Gulf coast. Over a broader area, the Monthly Weather Review (Notes by the Editor 1898) equates *Northers* to TCs regarding their importance for commercial vessels, thus the importance to predict them in Panama as accurately as in Veracruz, Tampico and La Habana. Frankenfield (1917) cites several memoranda related to the Panama Canal, describing *Northers* and how they are the main storms affecting the area between the months of November and April. Indeed, this work provides the first classification of *Nortes*, based on the description of four events in Panama. The classification corresponds to the location of the pressure systems, where one of the events created tropical storm strength winds. Clearly, *Nortes* are an important meteorological phenomena that has a significant effect on the state of the sea, making its study relevant for the GoM and particularly for Mexico.

Considering that previous studies focused on the continental effect of cold surges, in June 2014 the Engineering Institute of UNAM launched a project (#4340) entitled “Clasificación de Nortes en función del oleaje asociado en el Golfo de México y variación

ante el cambio climático", which linked the atmospheric events to the derived sea state (i.e. ocean waves). As the Principal Investigator of this Project, I set the overall strategy to develop an identification method for *Nortes* and their classification based on the derived wave power from each event. The partial results of the project are described by Hernández-Lasheras (2015), who analyzed the winter seasons from 1986-1987 and 2008-2010 to derive an index for identification of *Norte* events based on the testing of different procedures, as well as first classification of events by using Principal Component Analysis (PCA) and a subsequent clustering of events using k-means, following Sáenz and Durán-Quesada (2015). While those results provide the methodological procedure for analysis, they do not fully characterize the *Nortes* climatology due to the short time frame analyzed. Here I expand the work to assess a longer time frame and also the effects of global warming on the future *Nortes* climate, which is the main goal of this Chapter.

3.2. Methodology

In order to determine the effect of global warming over the *Norte*-derived ocean waves in the GoM, I established three main goals: 1) First to identify *Norte* events, 2) Second, to model the ocean waves in the interest of obtaining the wave power maps for each identified event, and 3) Third, to classify events by performing a PCA of the wave power maps followed by a cluster analysis using k-means. The methodology followed is summarized in Figure 14.

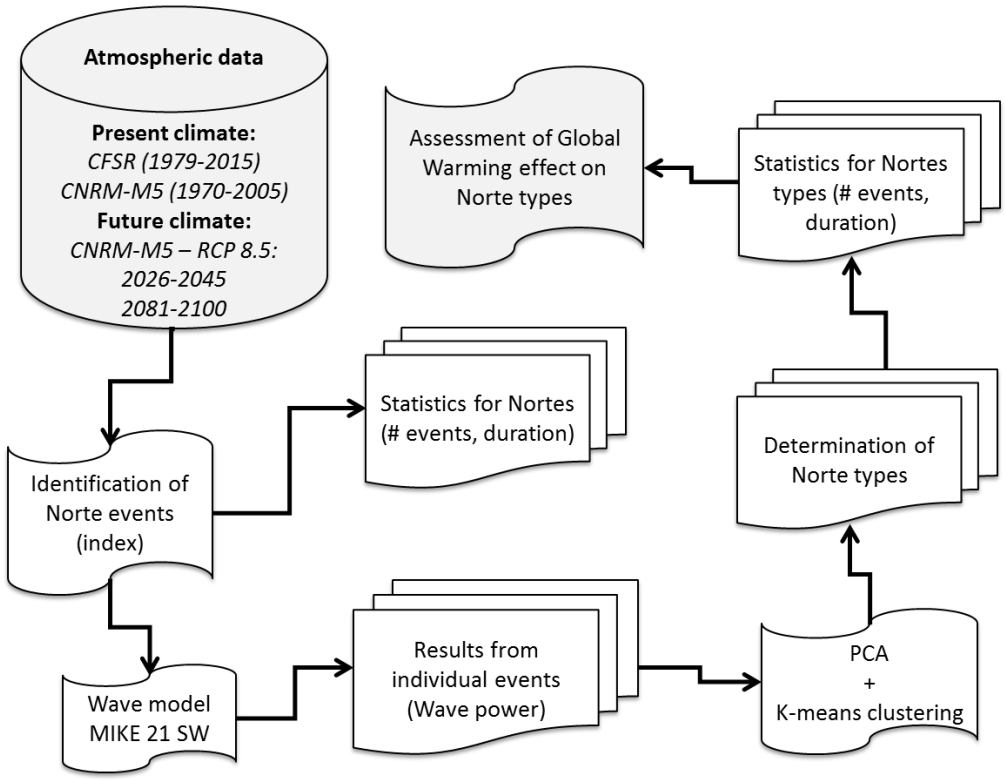

Figure 14. Flux diagram for the assessment of *Norte*-derived waves and effect of global warming.

The above activities were based on two different databases, the CFSR reanalysis (Saha et al. 2010) and the CMIP5 model CNRM-M5.1 (Voldoire et al. 2013), referred hereafter as CNRM and developed by the Centre National de Recherches Météorologiques (National Centre for Meteorological Research) in France. The CFSR data was used as the baseline to assess the CNRM model performance to reproduce the present climate. The selection of the CNRM model was based on the assessment of 15 CMIP5 GCMs where the CNRM showed the best performance for the meridional wind component over the southeastern region of Mexico (Salinas et al. 2016). Considering that a strong the meridional wind component is a characteristic of *Nortes*, the CNRM model was then used to assess the present (1970-2005), near future (2026-2045) and far future (2081-2100) climates.

The CFSR reanalysis is composed of coupled ocean, atmosphere, land and sea ice models, including data assimilation. The atmospheric model has an increased vertical and horizontal resolution (~38 km) in comparison to other reanalyses shown, to accurately reproduce *Norte* wind fields to be used as forcing to wave models (Appendini et al. 2013). Also, the CFSR has been successfully used for wave modeling in studies (Cox et al. 2011; Chawla et al. 2013; Stopa and Cheung 2014). A detailed description of the CFSR reanalysis and the models that conform it is found in Saha et al. (2010).

The CNRM is a coupled ocean and atmosphere model including an ice model and land cover scheme and fully described in Voldoire et al. (2013). The works by Sheffield et al. (2013a,b) found that the CNRM model performs well in reproducing the historical atmospheric conditions. For Mexico, the CNRM was found to be one of the best models to reproduce historical surface wind conditions (J.A. Salinas-Prieto, personal communication, September 26, 2016).

3.2.1. Identification of *Nortes*: MSA index

Previous studies have identified historical *Nortes* or cold surges using satellite imagery and weather charts (Reding 1992; Schultz et al. 1997; Mecikalski and Tilley 1992; Dimego et al. 1976; Dallavalle and Bosart 1975; Henry 1979). Such a procedure is subjective, time-consuming and not applicable to future events. Particularly, since the identification of events in the future climate is only possible by using numerical model results. One identification method is based on the sudden decrease in surface temperature at different locations, as previously done by different authors, either from measurements (Vazquez-Aguirre 2000; Hill 1969) or model data (Perez et al. 2015). Including the wind direction component is a complementary method which has been also applied (Reding 1992; Schultz et al. 1998; López-Méndez 2009), as well as the surface pressure associated with anticyclones over central Nebraska and the 12-hour isollabaric rise in north-central Texas (Colle and Mass 1995). Those methods can identify the arrival of a *Norte* at a particular location, and the stronger cold surges affecting the U.S. (Colle and Mass 1995), but in this study the goal is to identify the events that cross the GoM. To do so, a new method is proposed based on the difference in reduced MSLP and wind

speed, as obtained from numerical models, and the work from Hernández-Lasheras (2015), who made several test to develop the Merida – San Antonio index (MSA), given by

Equation 5

$$MSA = \frac{RSLP_{SAT} - RSLP_{MID}}{1013} \cdot WS_{42055} \qquad (1)$$

where $RSLP_{SAT}$ is the reduced MSLP in San Antonio, Texas; $RSLP_{MID}$ is the reduced MSLP in Merida, Yucatan; and WS_{42055} is the wind intensity at the location of NOAA's National Buoy Data Center buoy 42055, which is located in the Campeche Sound at 214 nautical miles Northeast of Veracruz, at 22.203°N latitude and 94.00°W longitude.

The parameters and locations for the index were determined from a series of analysis of MSLP, meridional wind velocity, temperature and moisture flux convergence, including Hövmoller diagrams, spatio-temporal maps and analysis of different weather stations. Such graphical analyses are feasible for a few seasons, but it would be subjective, time consuming, and prone to errors for an extended database as is the case of the present study. Still, those analyses allowed to identify the parameters needed to develop the MSA index. Such work is summarized in Hernández-Lasheras (2015).

In this study, the MSA index was used to identify *Nortes* for an extended database using the CFSR reanalysis from 1979-2015. A *Norte* event was considered when MSA was equal or higher to 5, indicating a positive MSLP gradient between San Antonio and Merida, as well as strong winds in the Campeche Sound. While the index captured the *Norte* events, it also included other type of events, in particular low pressure events over the Yucatan Peninsula without necessarily having the presence of a high pressure over North America (e.g. TC). Subsequently, the index was modified to include the strong negative meridional wind velocity that characterize *Norte* events. The new index includes a second term to discriminate for low pressure events creating a strong gradient on MSLP between Texas and Yucatan. The new index is referred to as MSA_i and is given by

Equation 6

$$MSA_i = MSA \cdot SIGN\left(\frac{RSLP_{SAT} - RSLP_{MID}}{-V_{42035}}\right) \qquad (2)$$

where V_{42035} is the NDBC buoy located offshore Galveston, Texas, at 29.232°N latitude and 94.413°W longitude.

The MSA_i value was also calculated considering the reduced MSLP at the location of the weather station from San Angelo, Texas instead of San Antonio. This was done considering the work of Davis and Kalkstein (1990) where they include such a station as one of the locations to classify the surface weather regimes over US, including cold fronts. San Antonio still produced better results when compared to the events identified in other studies.

Another important parameter was the minimum duration of a *Norte* event, as well as the time between events to consider them to be independent one from the other. Figure 15 shows the mean monthly number of events as found by other authors and the MSA_i considering different minimum durations. The comparison is not straightforward since the MSA_i is intended to locate only *Nortes*, that is, anticyclone events, while DiMego et al. (1976) and Henry (1979) report on all cold fronts, regardless of being low or high pressure systems. This explains why there are more events found by such authors in comparison to the MSA_i. Reding (1992) provides an underestimation when compared to the MSA_i values using 12 hours, which is explained by the fact that Reding (1992) only consider events that penetrate into Central America and the events that dissipate over the GoM are not considered. The overestimation of events by Vazquez-Aguirre (2000) could be due to their criteria to consider only a temperature decrease of 2°C in 24 hours instead of 4°C in 48 hours as done by Reding (1992).

The MSA_i index based on a minimum duration of 18 hours identifies most of the events identified by Reding (1992) and shows a similar occurrence. Since the work of Reding (1992) provides the most comprehensive database for events crossing the entire GoM, the index is found to be adequate in identifying *Norte* events. While the minimum

duration of 18 hours is considered optimal, a study by Pérez et al. (2014) suggests that the future climate will present more *Norte* events but of shorter duration. It was then decided to use the minimum duration of 12 hours, in order to capture short duration events.

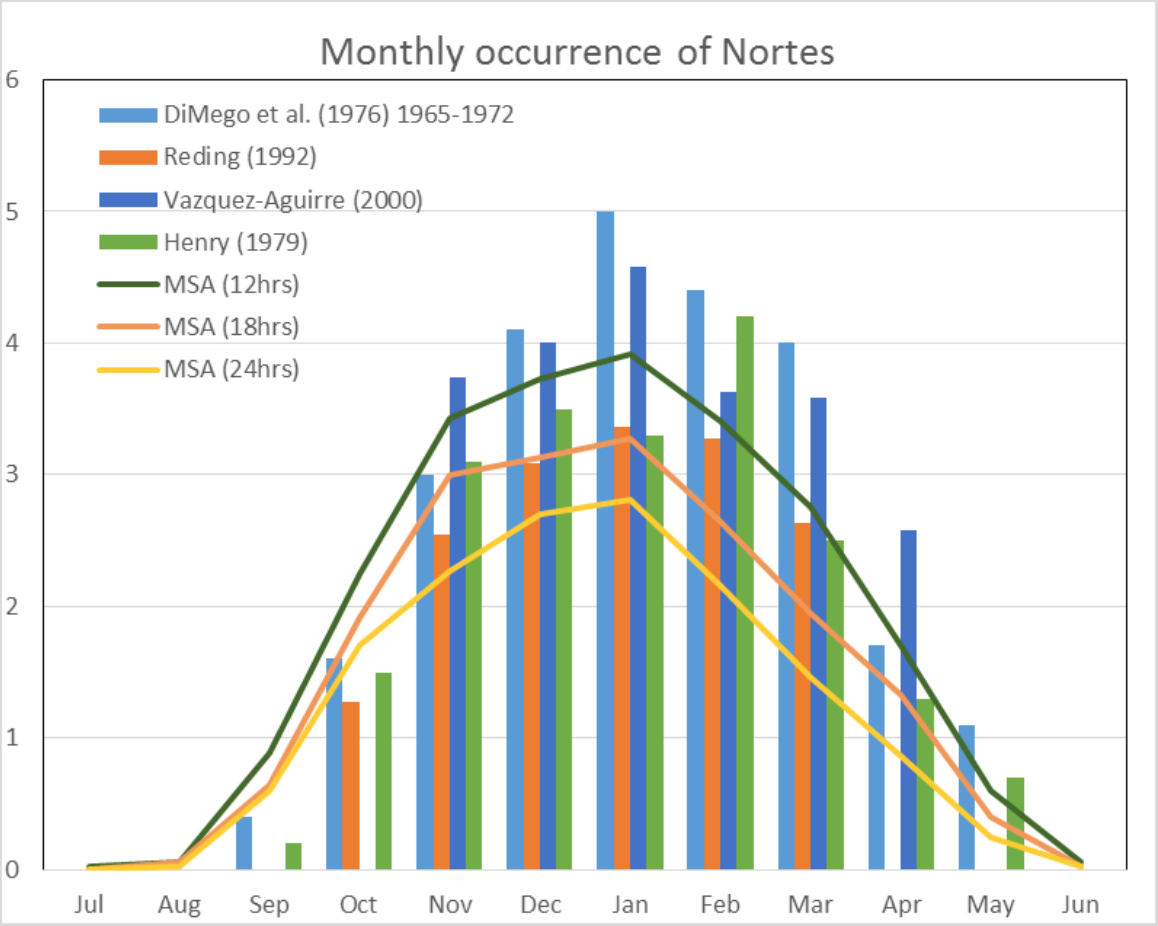

Figure 15. Monthly occurrence of *Nortes* as identified by different authors and the MSA index using different time thresholds.

3.2.2. Wave modeling

To obtain the wave conditions from each identified *Norte* event, the third-generation wave model MIKE 21 SW (Sørensen et al. 2004) was forced using the wind

fields from the CFSR reanalysis and the CNRM model. The use of wind reanalysis for wave modeling of *Nortes* has been assessed by Appendini et al. (2013), for the North American Regional Reanalysis (Mesinger et al. 2006), NCEP (Kalnay et al. 1996) and ERA-Interim (Dee et al. 2011) reanalyses, concluding that the coarser NCEP reanalysis can accurately reproduce *Norte* events to be used for wave modeling. The CFSR reanalysis has already been used to characterize the worlds wave climate (Chawla et al. 2013) and particularly for the GoM by Ruiz-Salcines (2013). The CFSR has an approximate resolution of 38 km and should accurately reproduced *Nortes* for wave modelling (Appendini et al. 2013).

The MIKE 21 SW model description has already been provided in section 2.2.3 as well as the model setup, which is also used to model the *Norte*-derived waves. The wave power results for each *Norte* event was saved to be latter used for the classification of events. The wave power was used since it summarize the information from the wind system that generated the ocean waves for a particular time, where the waves are a result of the wind intensity, duration of the storm and the fetch. This last parameter refers to the area over which the wind is transferring energy to the ocean surface, which is a result of the storm path. The storm duration determines the time that the wind is blowing over a particular fetch, so that the storm duration and translation speed becomes relevant for the resulting waves.

3.2.3. Classification of *Nortes*

As mentioned before, the wave power derived from each *Norte* was used to classify the events. The methodology followed is similar to the one applied by Sáenz and Durán-Quesada (2015), where a weather type classification was done for Central America, based on a Principal Component Analysis (PCA) applied to wind reanalysis data and a subsequent k-means cluster analysis to identify weather types.

The PCA was performed for the mean wave power obtained for each *Norte* event found in the CFSR reanalysis and CNRM datasets (present and future climates). The idea of performing the PCA analysis over all the events is to be able to characterize all the

events available, independently of the database, so that we can assess the occurrence of each type of event on each of the databases. As a sensitivity analysis, the PCA was performed independently over the CFSR and the CNRM present climate datasets; this allows us to assess if the CNRM is accurately reproducing the type of events found in the CFSR dataset.

A k-means cluster analysis was then performed over the principal components (PCs) obtained for each event in each dataset. The frequency of the different types of *Norte* events was then obtained to assess the accuracy of the CNRM model to reproduce the present climate (in reference to the CFSR results), as well as the effect of climate change over the frequency of the different types of *Nortes*.

3.3. Results and discussion

3.3.1. Occurrence of *Norte* events

The results for the identification of *Nortes* is analyzed for both the present and future climates. The present climate assessment is based on the CFSR reanalysis data and the CNRM model, in order to determine if the CMIP5 model can accurately reproduce *Norte* events. Based on such assessment, it is possible to evaluate the future climate considering the possible model bias from the CNRM.

Present climate assessment

The MSA_i index was first applied to the CFSR data and compared to other studies (Figure 15), proving to be adequate for identifying *Norte* events. The number of *Norte* events and their duration when applying the MSA index to the CFSR and CNRM models is shown in Table 3. The present climate events show that the CNRM (19.5 events/yr) underestimates the mean number of annual events by 5 events, when compared to the CFSR data (24.5 events/yr). Also, the duration of the events is approximately 37.5 hours in the CNRM, when the CFSR data shows a mean duration of approximately 44.4 hours, although the latter has a higher standard deviation. The number of events found is higher

than what was found by Reding (1992), which was 16.1 events per year. The discrepancy in the number of events is most likely due to the fact that (Reding 1992) only considers the events that cross the entire GoM to enter the Caribbean Sea, while the MSA_i index considers all the events entering the GoM when the high pressure is present in North America. This underestimation of events is inferred in the work by Schultz et al. (1997) where he pinpoints the events studied by Colle and Mass (1995) which never reach Merida and thus not registered in the work by Reding (1992).

Table 3. Norte events and duration based on CFSR and CNRM in the present climate

Statistic measure	Present climate	
	CFSR	CNRM-M5
	1979-2005	1979-2005
Total events	636	507
Mean annual events	24.5	19.5
Mean duration (hrs)	44.4	37.5
Duration STD (hrs)	25	19.5

The monthly occurrence of events (Figure 16) shows a similar distribution of the events during the year, although the CNRM underestimates the number of events during the first months (September through November) and end (April) of the *Nortes* season, as well as February. When the relative frequency is considered, the CNRM mainly overestimates the *Nortes* during the months of highest occurrence (December and January).

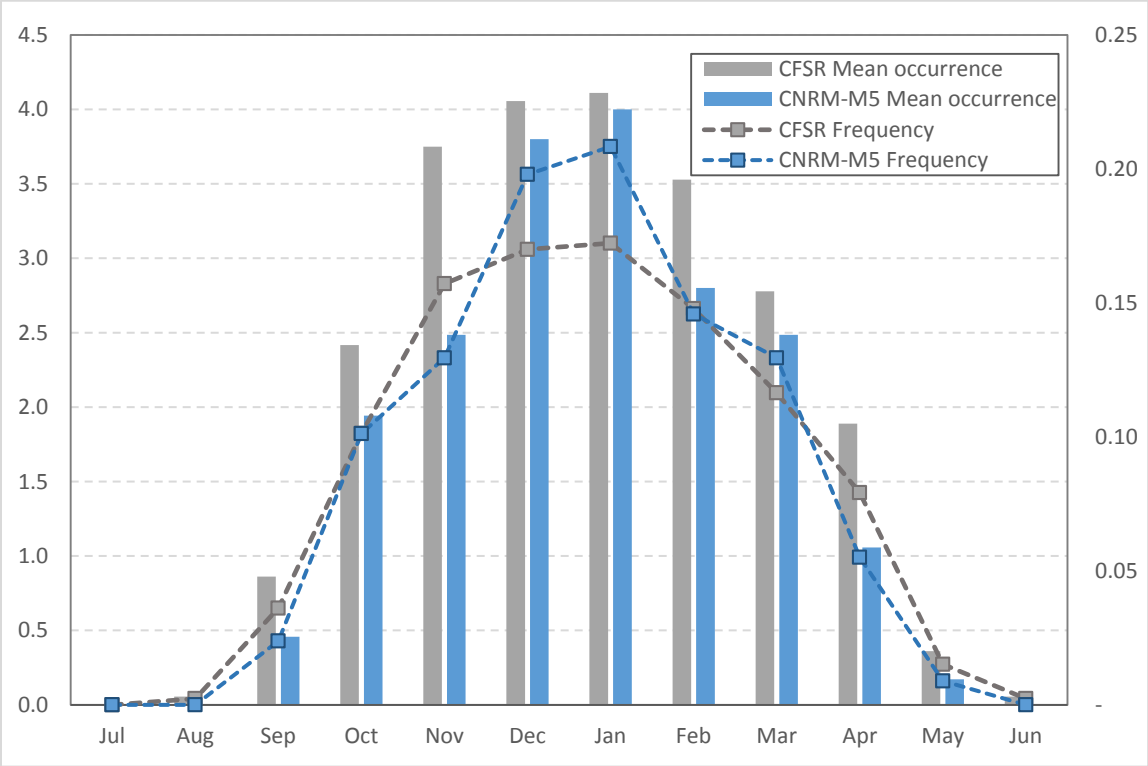

Figure 16. Mean monthly *Norte* events and frequency for the present climate based on CFSR and CNRM, as determined by the MSA_i index.

The monthly duration of events is summarized in Table 4 and shown in Figure 17. In general, CNRM events underestimate the duration, although the standard deviation is smaller (except in May). The highest underestimation of the duration by the CNRM occurs in at the beginning of the season (September through November). This is an important results considering the work of Pérez et al. (2014) who finds that in the future climate the *Norte* events will be more intense but of shorter durations, which could be due to a model bias not discussed in their work.

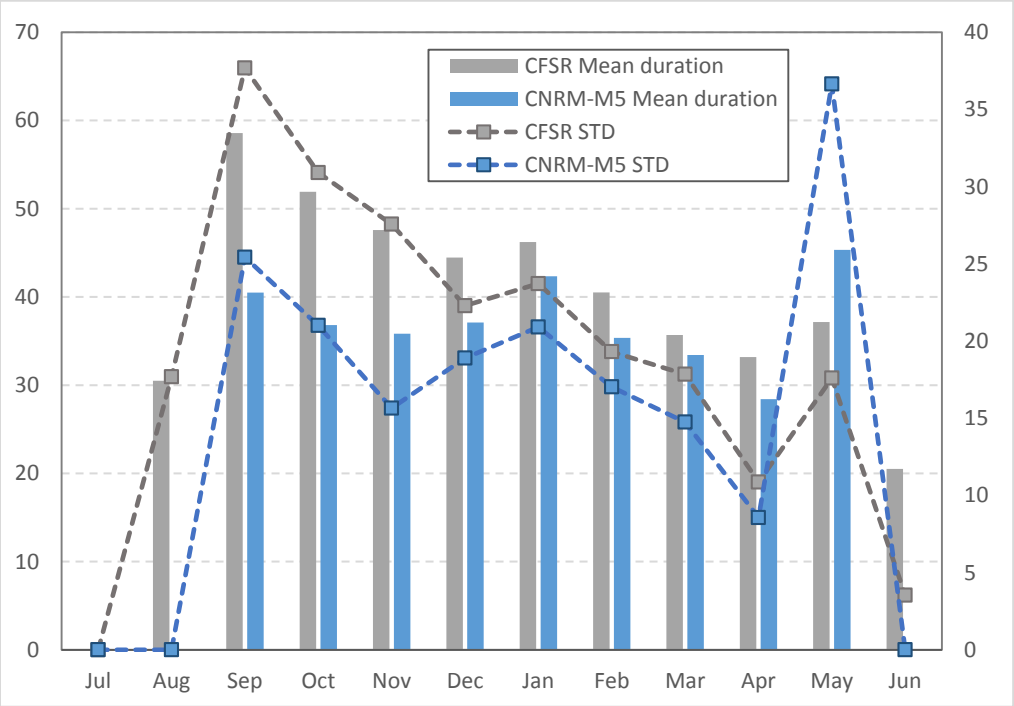

Figure 17. Mean monthly *Norte* events and frequency for the present climate based on CFSR and CNRM, as determined by the MSA_i index.

Table 4. Occurrence of *Norte* events by month and corresponding mean duration and standard deviation

Month/ model	Mean occurrence		Mean duration		STD of duration	
	CFSR 1979-2015	CNRM 1970-2005	CFSR 1979-2015	CNRM 1970-2005	CFSR 1979-2015	CNRM 1970-2005
Jul	0.0	0.0	-	-	-	-
Aug	0.1	0.0	30.5	-	17.7	-
Sep	0.9	0.5	58.6	40.5	37.7	25.4
Oct	2.4	1.9	51.9	36.8	30.9	21.0
Nov	3.8	2.5	47.6	35.8	27.6	15.7
Dec	4.1	3.8	44.5	37.1	22.3	18.9
Jan	4.1	4.0	46.2	42.4	23.7	20.9
Feb	3.5	2.8	40.5	35.4	19.3	17.0
Mar	2.8	2.5	35.7	33.4	17.8	14.7
Apr	1.9	1.1	33.2	28.4	10.9	8.6
May	0.4	0.2	37.2	45.3	17.6	36.6
Jun	0.1	0.0	20.5	-	3.5	-
Yearly	23.9	19.2	43.8	36.9	24.3	18.6

3.3.2. Types of *Norte* events

The following is a description of the different types of *Norte* events, describing the PCA and k-means cluster analysis, following the assessment of *Nortes* in the present and future climates.

Principal Component Analysis

The PCA was applied to all the *Norte* events found in the databases, including the CFSR and the CNRM for the present and future climates. This allows us to classify *Nortes* accounting for all possible configurations and then to assess the occurrences in each of the databases. Figure 18 shows that 95% of the variance is explained by the first 7 Principal Components (PCs).

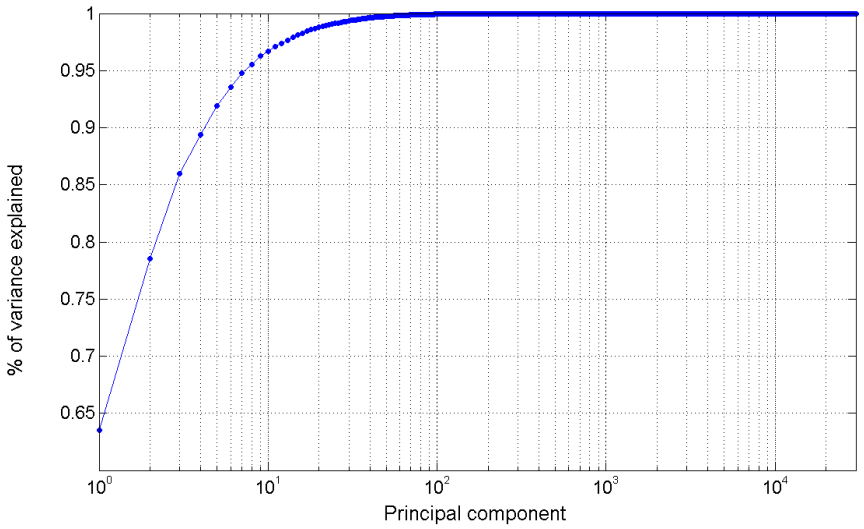

Figure 18. Percentage of variance explained by the Principal Components.

The mean wave power for all the *Norte* events (Figure 19) shows how the *Nortes* influence the waves propagating over most parts of the GoM, with more intense waves

along the western Mexican Gulf coast. The first three principal component coefficients are shown in Figure 20, which explain 86% of the variance. The first mode explains 63.5% of the variance and is related to how *Nortes* affect most of the GoM, concentrating the wave energy in the southern coast of Veracruz. The second mode explains 15.1% of the variance, which is related to the most intense events, concentrated again in the southern part of Veracruz. While the second mode is also a result of the longest fetch, the intensity of the winds is higher and/or the winds last longer with the same direction, resulting in the most intense events. The third mode explains 7.41% of the variance and is related to the effect of *Nortes* over the northern part of the GoM.

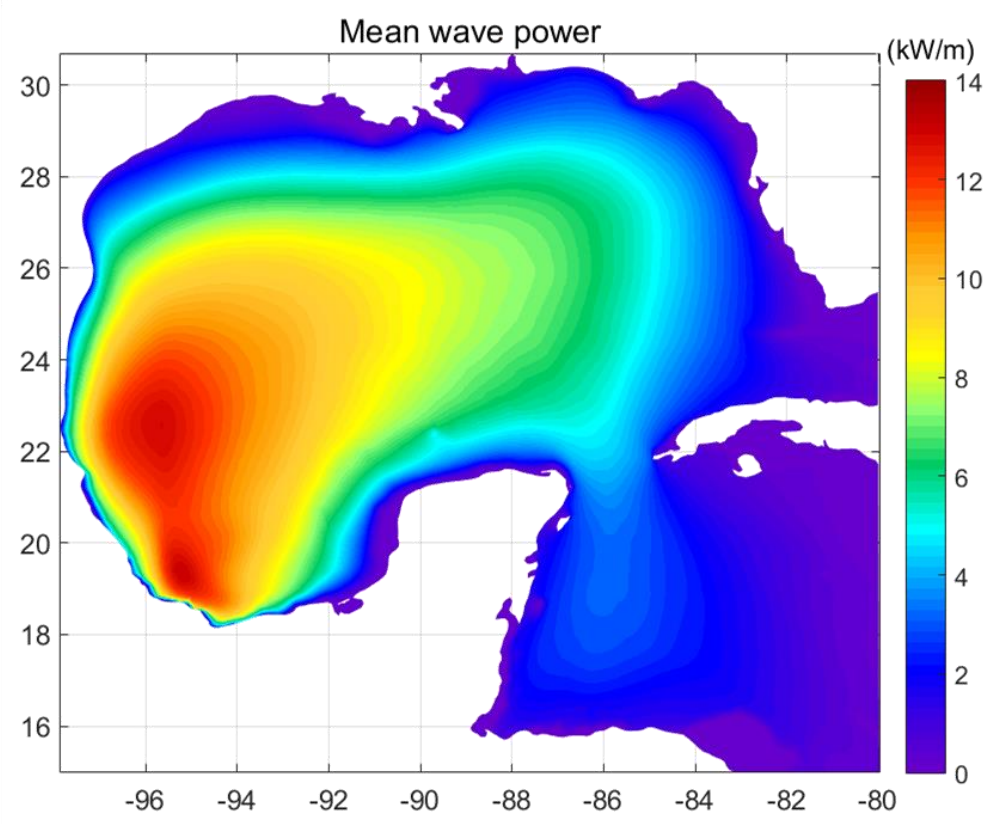

Figure 19. Mean wave power from all *Norte* events.

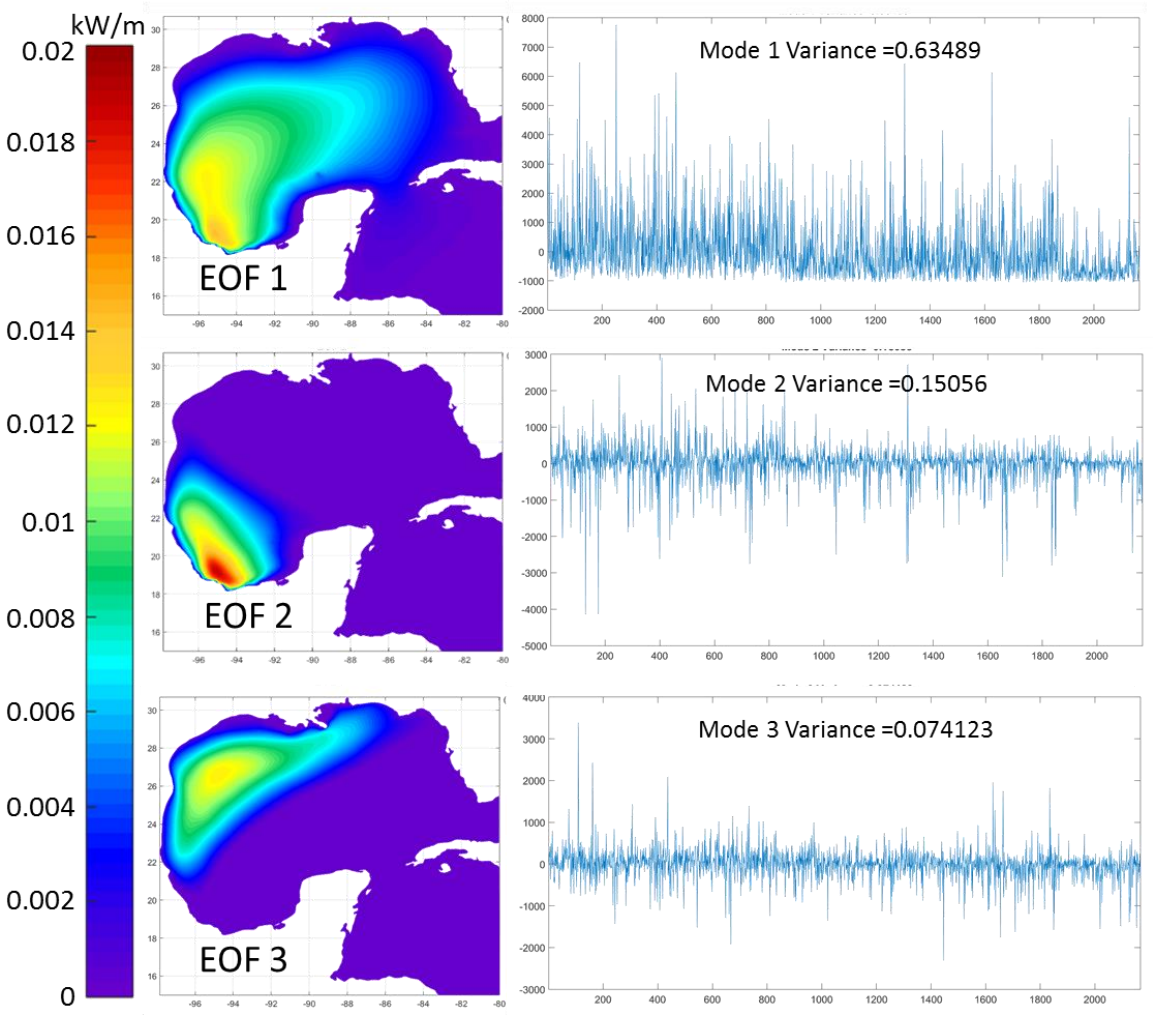

Figure 20. First 3 empirical orthogonal functions (left) and modes (right) for each of the *Norte* events.

As an example to describe the contributions of the different PC in an important event in Mexico, Figure 21 shows the *Norte* event that generated extreme flooding in Tabasco in early November of 2007. The *Norte* entered the GoM on October 30th and during its travel along the Gulf until November 2nd generated extreme precipitation that led to flooding in the state of Tabasco. For this event, the first two PCs have a very important contribution, were PC1 characterizes most *Nortes* and PC2 characterizes the most intense events. PC3 is negative, denoting that contribution in the northern GoM is low.

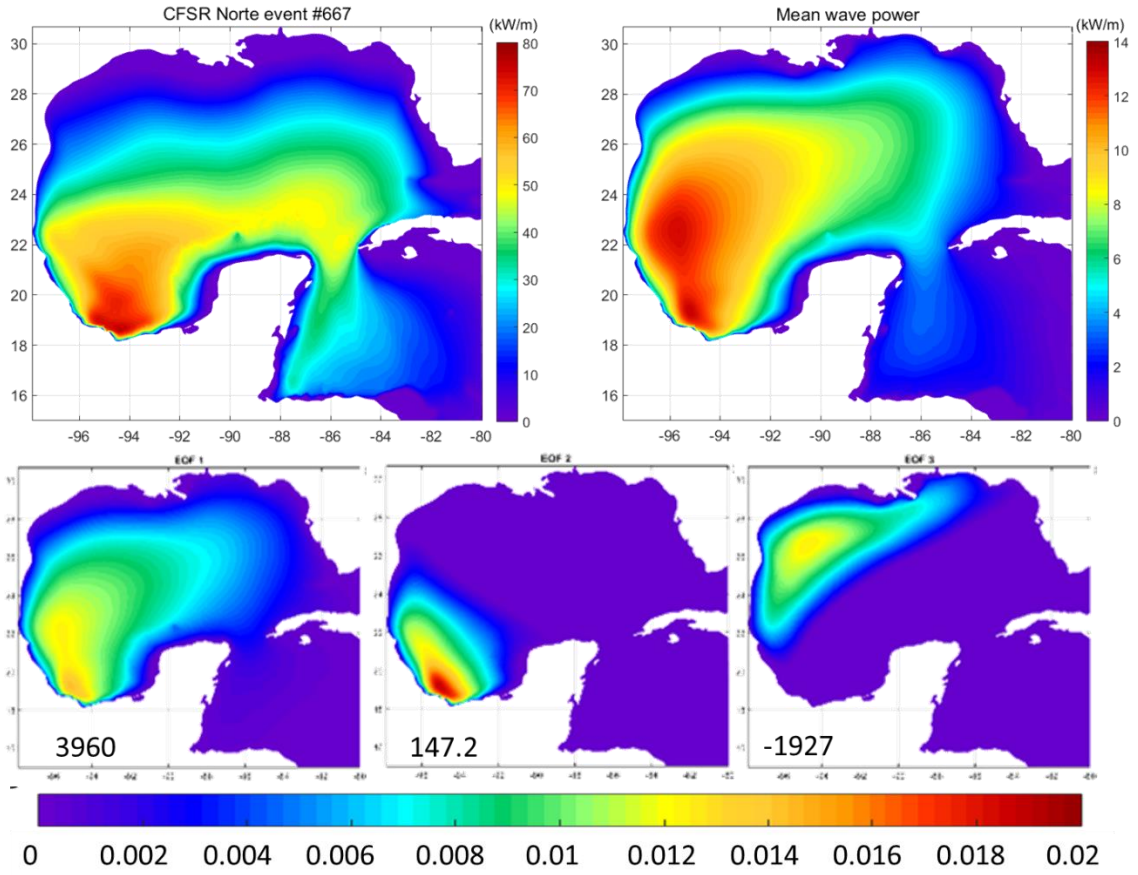

Figure 21. October 30 through November 1, 2007 *Norte* event, the values in the lower panels indicate the score value for the corresponding empirical orthogonal function.

One of the important characteristics of the PCA is that the events can be reconstructed without losing much information. Figure 22 shows the wave power for the October-November 2007 event (CFSR event #667) and the reconstructed wave power maps using 3, 6 and 67 PCs. When using the first 67 PCs, the reconstruction barely loses any information from the original event; using 6 components leads to an overestimation of the wave power, and using 3 PCs results in a somehow dissimilar spatial distribution of the

wave power. Still, even when using 3 PCs there is an acceptable reconstruction of the events, which shows how powerful the PCA can be.

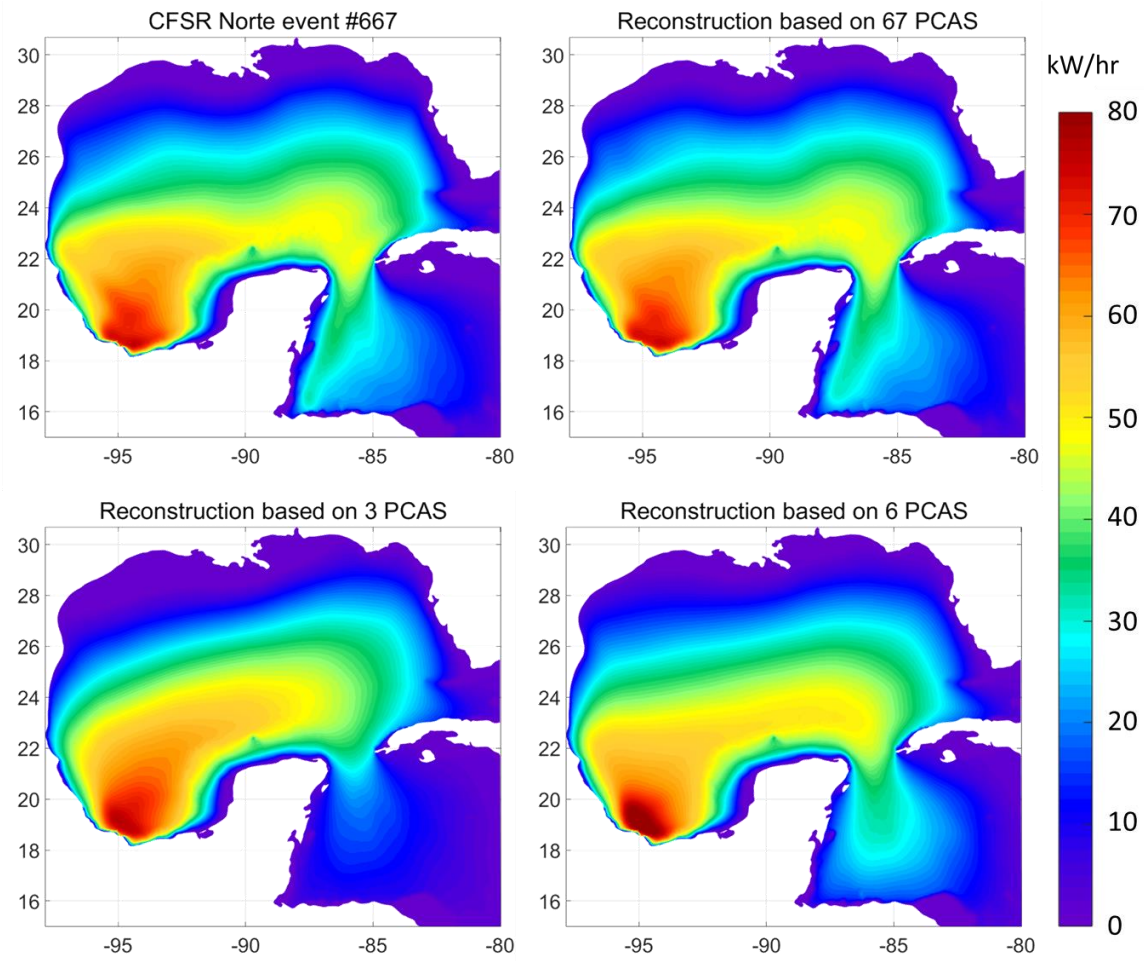

Figure 22. Reconstruction of the October 30 - November 1, 2007 *Norte* event, based on different number of PCAs.

K-means clustering

The classification of *Norte* events was done based on the PCs instead of the events. This is possible if we consider that the PCs reduce the dimensionality of the events and that such events can be accurately reconstructed from a limited number of PCs. It

was found that the types of *Nortes* obtained by the k-means clustering was dependent on the number of PCs, particularly when using a limited number of PCs. It was found that starting from a minimum number of 44 PCs, the *Norte* types show minimum changes when increasing the number of PCs, and above 67 PCs there where barely any changes when including more PCs. Thus, it was decided to use 67 PCs, which explain 99.86% of the variance. The example from Figure 22, shows how the first 67 PCs provided an excellent reconstruction of the original event.

Since the k-means clustering requires that the number of classifications is predefined, several tests were performed to determine the optimal number of classifications. The tests suggested that a large number of classifications would generate types of *Nortes* with very low occurrences and with no distinct characteristics of a *Norte*. During the testing it was also found that some classifications were composed by a low number of events, most likely a result from an incorrect selection of events by the MSA_i, In order to confirm that those events would not “contaminate” the resulting clusters, tests were performed with and without those events. The results were slightly different, but the main features of the clusters remain constant. In any case, for the final processing, those events (15 out of 2181 events, less than 0.7%), were removed from the PCA before doing the k-means classification. After several tests with a different predefined number of classifications, it was decided that 5 clusters provided the most optimal classifications of the events. Figure 23 show the final classification of the *Norte* types.

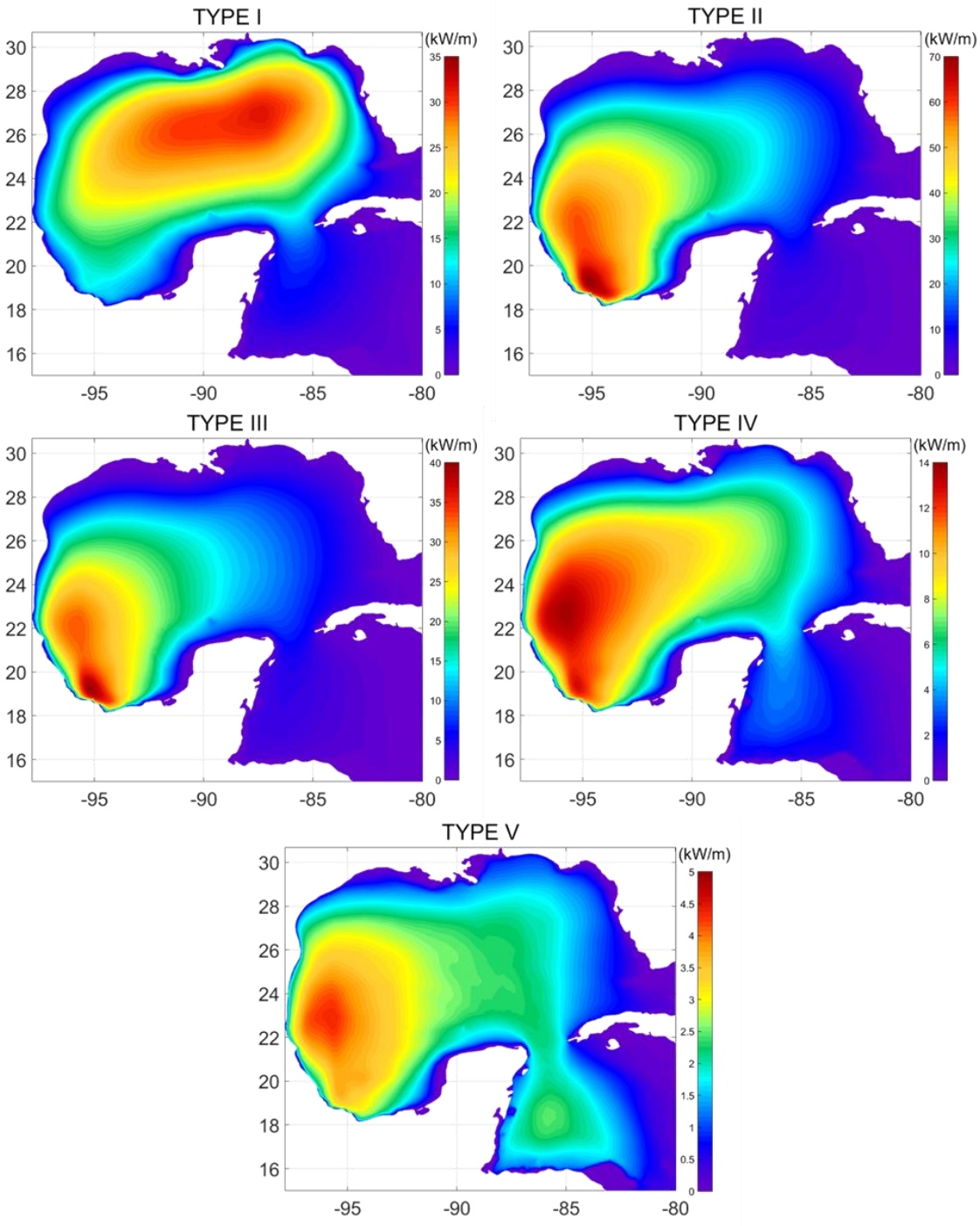

Figure 23. Types of *Nortes* based on k-means clustering applied on the wave power principal components.

Type I represent *Nortes* that mainly affect the northern GoM, while types II, III, IV and V present a more common pattern for *Nortes* with differences in the highest wave power areas, as well as the wave power intensity. For instance, Type II has a low occurrence but the most extreme events doubling the wave power for the Type III events and more than 10 times the Type V, which is the most common *Norte* type. Type III has a similar pattern as type II but the intensity of the events is half the wave power from type II events. The highest wave power in both cases is located south of Veracruz in the areas of the Tuxtlas, between Alvarado and Coatzacoalcos south of Veracruz. This area has been cited since the end of the 19th century as being “subject to the full force of the northers” (Ruiz 1892).

The frequency of occurrence for each type of *Norte* is shown in Figure 24 together for all databases (CFSR and CNRM present and future climates) and in Figure 25 only for the present climate, differentiating between CFSR and CRNM (values shown in Table 5). Figure 24 shows that the highest occurrence is the Type V events, although this is a result of the CNRM data, since the CFSR shows a higher occurrence of the Type IV events (Figure 25). In the CNRM database, the type V events represent more than half of the events corresponding to this type, in contrast to 1/3 in the CFSR events. This is an important discrepancy, since the mildest events (type V) are in fact overestimated in the CNRM events, which are further used to determine the future climate.

Regardless to the difference between CFSR and CNRM for the Type V and IV events, both events have the highest occurrences. For the rest of the events the distribution is similar for the two databases, with the most extreme events (type II) with the lowest occurrence, while the milder events (types IV and V) have the highest occurrence rates.

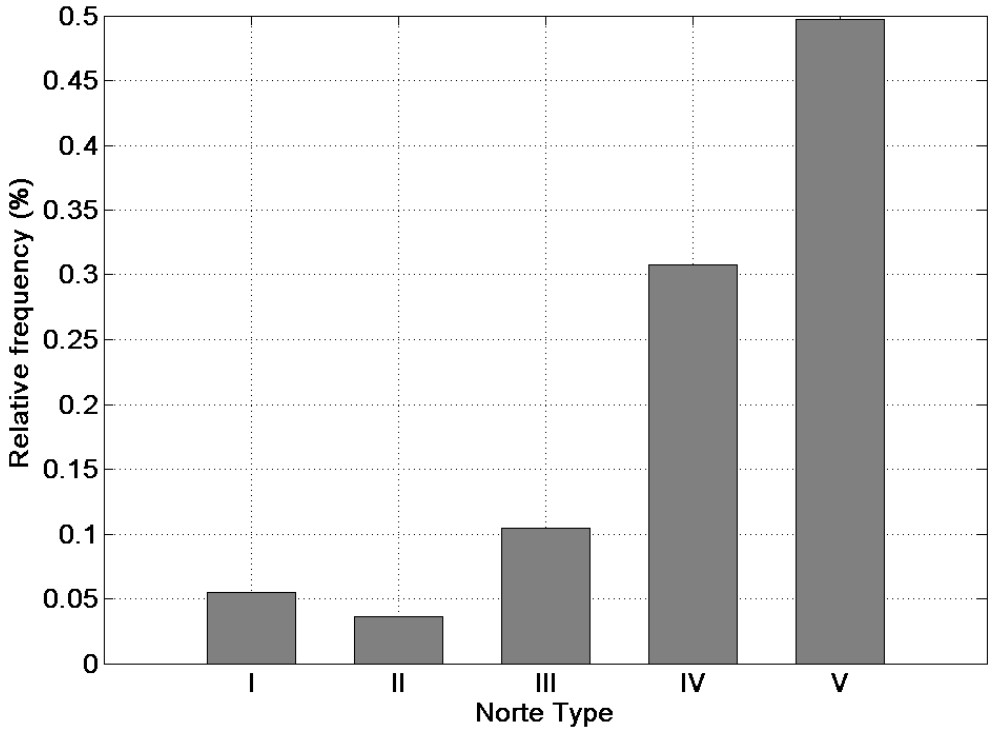

Figure 24. *Norte* type histogram for all events, including present climate: CFSR (1979-2015) and CNRM (1970-2005); and future climate: CNRM (2026-2045, 2081-2100).

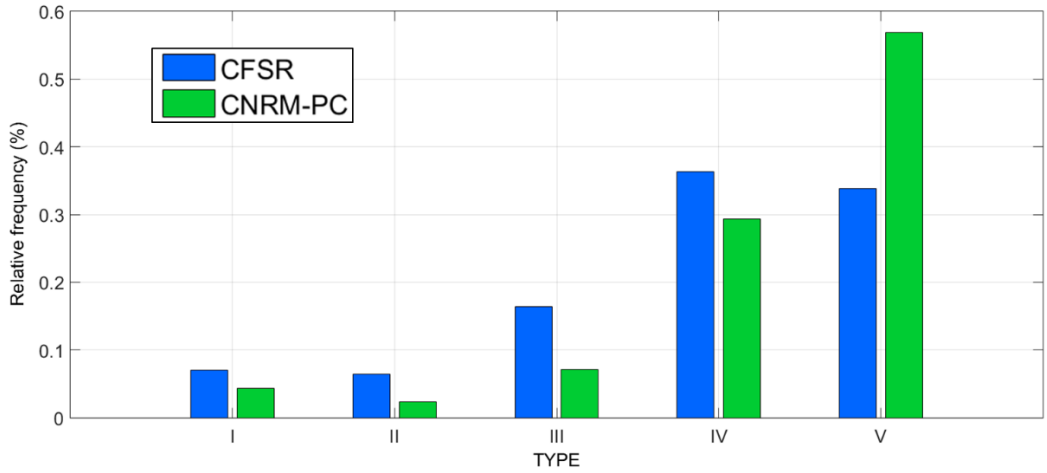

Figure 25. *Norte* type histogram for CFSR (1979-2015) and CNRM (1970-2005).

It is relevant to notice that Types I through IV have the most influence over the Caribbean Sea. If we only consider Types I, II, III and IV, the annual occurrence of *Nortes* is 15.8 events (Table 5), which is similar to the annual number of 16 events per year established by Reding (1992) for events registered in Merida and entering the Caribbean Sea. Also, an early description of *Nortes,* based on their presence at the northwestern part of the GoM, reported a yearly occurrence of 5 to 10 events (Hunt 1863). Those event would be analogous to Types I, II and III, which have the largest influence in this area, and which occurrence is 7 events per year (Table 5). Both cases add to the validation of the MSA_i.

Table 5. Occurrence of Norte events by type for the present climate based on CFSR and CNRM.

Norte Type	% of occurrence		No. of occurrences	
	CFSR	CNRM-M5	CFSR	CNRM-M5
	1979-2015	1970-2005	1970-2006	1970-2007
I	7.00%	4.30%	1.7	0.8
II	6.40%	2.40%	1.5	0.5
III	16.40%	7.10%	3.9	1.4
IV	36.30%	29.30%	8.7	5.6
V	33.90%	56.80%	8.1	10.9

3.3.3. Effect of climate change on *Nortes*

To assess the effect of climate change on the *Nortes* affecting the GoM, two time frames were used: near future (NF) climate (2026-2045) and far future (FF) climate (2081-2100). The annual number of events, monthly distribution and corresponding duration of *Nortes* in the present and future climates are summarized in Table 6. The future climate shows a decrease in the number of events, with fewer events in for the FF but barely any change in the NF. The duration is slightly reduced for the FF but basically the same for

the NF. This results are in disagreement with Pérez et al. (2014), who find that a warmer climate will result in an increased number of *Nortes* but with shorter lifespans.

Table 6. *Norte* events and duration based on CNRM for the present and future climates

Statistic measure	Present climate	Future climate	
	CNRM-M5	CNRM-M5	
	1970-2005	2026-2045	2081-2100
Total events	675	348	288
Mean annual events	19.3	18.3	16
Mean duration (hrs)	36.9	37.3	36
Duration STD (hrs)	19	20	18

Figure 26 shows the monthly mean number of events and Figure 27 shows the monthly mean duration and standard deviation. Table 7 shows such information.

Table 7. Monthly and yearly mean occurrence, duration and standard deviation of *Norte* for the present and future climates based on CNRM.

Month	Mean occurrence			Mean duration			STD		
	1970-2005	2026-2045	2081-2100	1970-2005	2026-2045	2081-2100	1970-2005	2026-2045	2081-2100
Jul	0	0	0	-	-	-	-	-	-
Aug	0	0.1	0	-	18	-	-	0	-
Sep	0.5	0.4	0.3	41	56	31	25	34	10
Oct	1.9	2	1.8	37	47	41	21	27	20
Nov	2.5	2.4	2.3	36	36	42	16	16	24
Dec	3.8	3.4	3.1	37	37	36	19	20	19
Jan	4	3.8	2.8	42	38	35	21	19	16
Feb	2.8	3	2.6	35	36	32	17	18	13
Mar	2.5	1.9	1.6	33	32	33	15	18	11
Apr	1.1	1.1	0.5	28	28	27	9	8	7
May	0.2	0.2	0.1	45	30	44	37	7	0
Jun	0	0.1	0	-	32	-	-	0	-

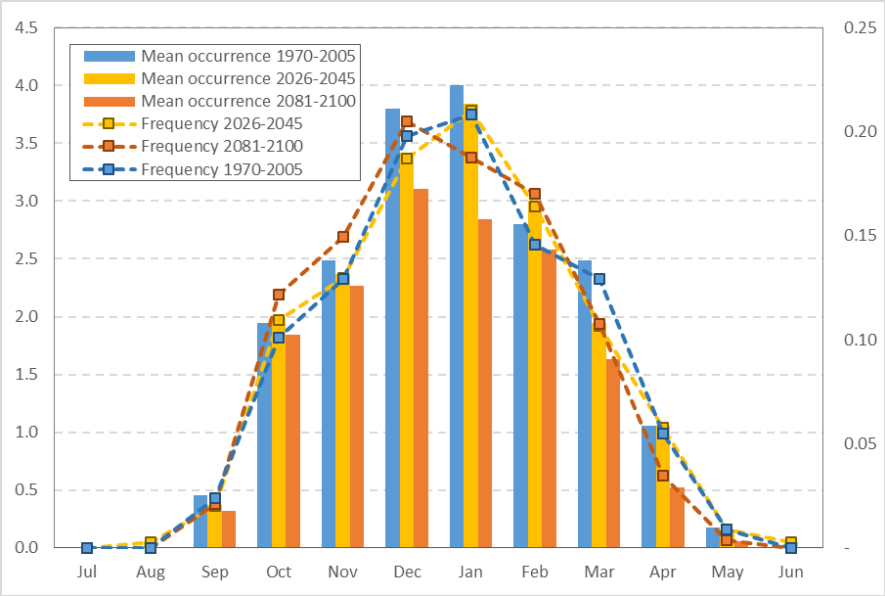

Figure 26. Mean monthly *Norte* events and frequency for the present and future climates based on CNRM, as determined by the MSA_i index.

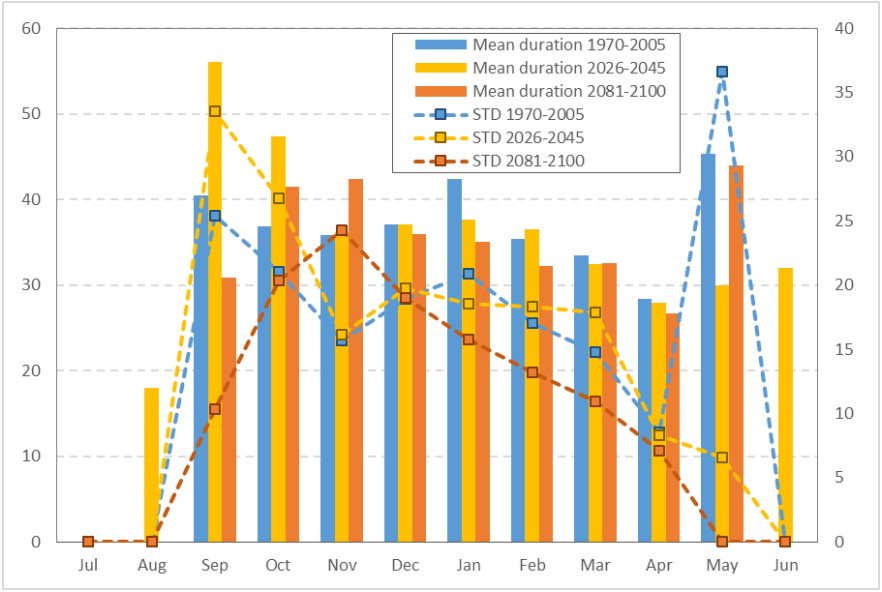

Figure 27. Mean monthly *Norte* events and frequency for the present climate based on CFSR and CNRM, as determined by the MSA_i index.

The distribution for the frequency of the different *Norte* types in the future climate is maintained, although there is an increase/decrease relative to the present climate (Figure 28 and Table 8). The main changes are summarized below:

- For *Nortes* affecting the northern part of the GoM (Types I, II and III) there is a decrease in frequency in the future climate, with the exception of the NF climate, where there is an increase of the events with more influence in the eastern side of the GoM (Type I), as well as the second most intense events (Type III).

- The *Nortes* with a largest influence on the northeastern GoM (Type I) show an increase in the NF but a decrease in the FF, with only one event occurring every 4.8 years.

- The most intense *Norte* events (Type II) show a decrease in the future climate. For the FF climate the frequency indicates the presence of 1 event every 19 years.

- The least intense events (Type V) show a decrease in the NF, but present the largest increase in the FF from all event types.

- The most frequent event type according to CFSR (Type IV), show a slight increase in NF but large decrease in FF.

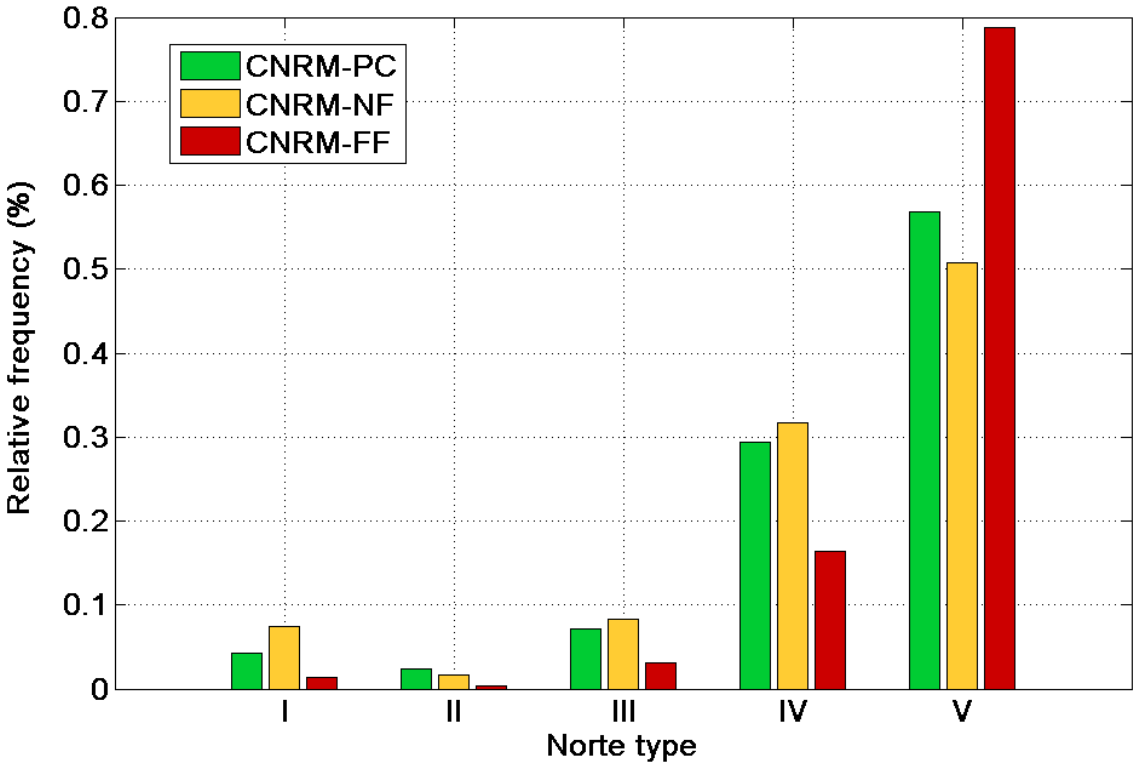

Figure 28. *Norte* type histogram for present (1970-2005), near future (2026-2045) and far future (2081-2100) climate, based on CNRM.

Table 8. Occurrence of Norte events by type for the present (1970-2005), near future (2026-2045) and far future (2081-2100) climate, based on CNRM.

Norte Type	% of occurrence			No. of occurrences			Year until occurrence		
	CNRM-M5			CNRM-M5			CNRM-M5		
	1970-2005	1970-2006	1970-2007	1970-2005	1970-2006	1970-2007	1970-2005	1970-2006	1970-2007
I	4.3%	7.5%	1.4%	0.8	1.4	0.2	1.2	0.7	4.8
II	2.4%	1.7%	0.3%	0.5	0.3	0.1	2.2	3.2	19.0
III	7.1%	8.4%	3.1%	1.4	1.5	0.5	0.7	0.7	2.1
IV	29.3%	31.7%	16.3%	5.6	5.8	2.5	0.2	0.2	0.4
V	56.8%	50.7%	78.8%	10.9	9.3	11.9	0.1	0.1	0.1

Table 9 shows the percentage change in the occurrence of the different *Norte* types in the future climates based on the present climate and also the near future for the

fat future climate. Those values clearly show a decrease in the number of *Nortes* at the end of the century, except for the increase in the mildest events (Type V).

Table 9. Occurrence increase of Norte events by type for the present (1970-2005), near future (2026-2045) and far future (2081-2100) climate, based on CNRM.

Norte Type	Increase in future climate		
	CNRM-M5		
	NF(PC)	FF(PC)	FF(NF)
I	65%	-75%	-85%
II	-31%	-88%	-83%
III	11%	-65%	-69%
IV	3%	-56%	-57%
V	-15%	9%	29%

The yearly occurrences of *Nortes* is shown in Figure 29 for a graphic visualization of the changes from the present climate and the near and far future climates. The basic statistics for each climate are shown in Table 10.

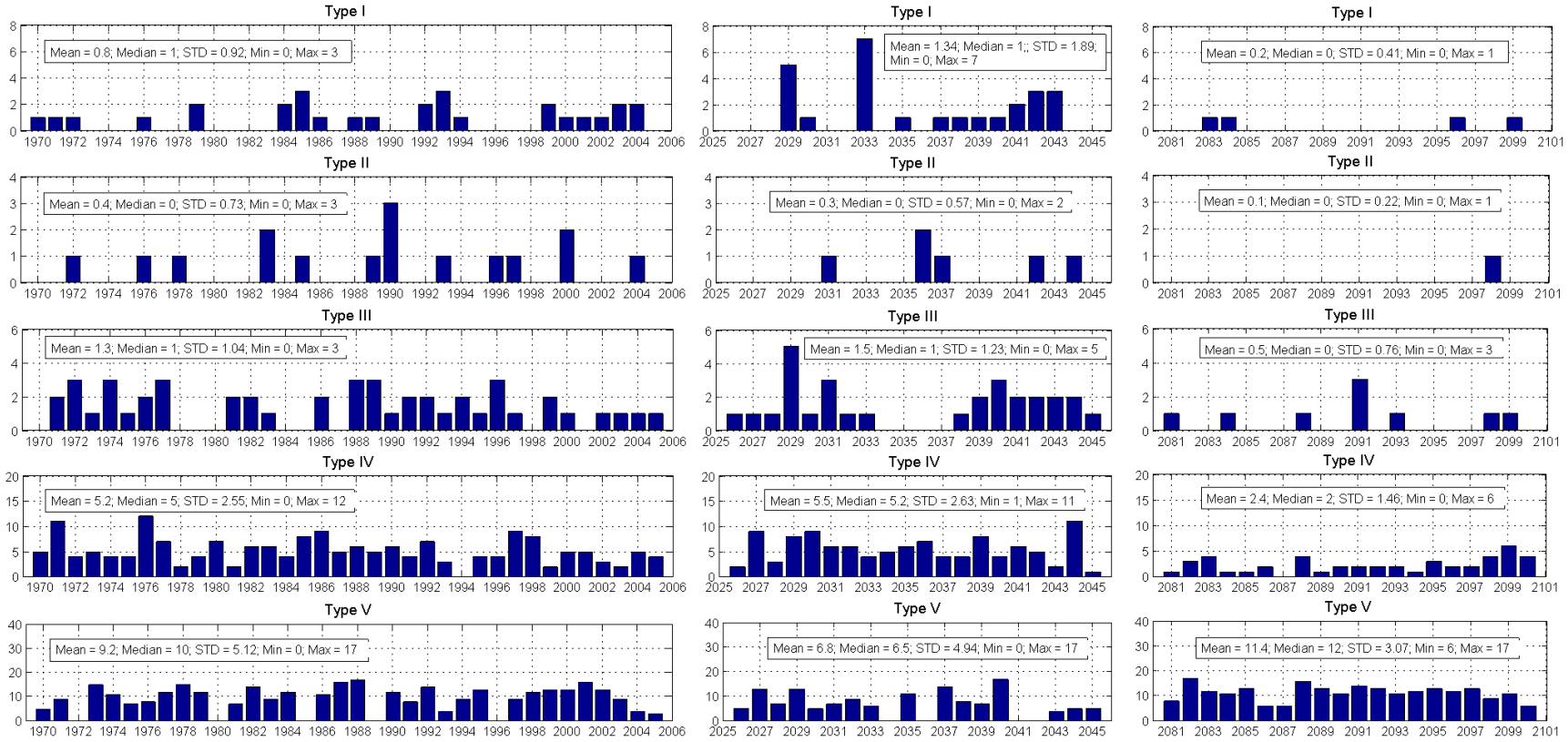

Figure 29. Yearly occurrences by *Norte* type for present (1970-2005), near future (2026-2045) and far future (2081-2100) climate, based on CNRM.

Table 10. Basic statistics for the different *Norte* types in the present (1970-2005), near future (2026-2045) and far future (2081-2100) climate, based on CNRM.

Norte Type	Average			Standard deviation		
	1970-2005	2026-2045	2081-2100	1970-2005	2026-2045	2081-2100
Type I	0.8	1.3	0.2	0.92	1.89	0.41
Type II	0.4	0.3	0.1	0.73	0.57	0.22
Type III	1.3	1.5	0.5	1.04	1.23	0.76
Type IV	5.2	5.5	2.4	2.55	2.63	1.46
Type V	9.2	6.8	11.4	5.12	4.94	3.07
Total events	17.0	15.4	14.4			

Norte Type	Median			Minimum		
	1970-2005	2026-2045	2081-2100	1970-2005	2026-2045	2081-2100
Type I	1	1	0	0	0	0
Type II	0	0	0	0	0	0
Type III	1	1	0	0	0	0
Type IV	5	5.5	2	0	1	0
Type V	10	6.5	12	**0**	0	6

Norte Type	Maximum		
	1970-2005	2026-2045	2081-2100
Type I	3	7	1
Type II	3	2	1
Type III	3	5	3
Type IV	12	11	6
Type V	17	17	17

3.4. Conclusions

Despite the impact of ocean waves on activities in the GoM (e.g. maritime transport, oil extraction and tourism), the study of cold surges, *Nortes*, have been focused on their impacts on surface temperature and precipitation. This study has then focused on the effect of *Nortes* over the sea state of the GoM as well as the effect of climate change. To do so, this work provides a new method to identify *Nortes* that generate waves in the GoM, as well as a first classification of *Norte* events in relation to the ocean waves.

To identify *Norte* events, the MSA index was developed on the basis of the work by Hernández-Lasheras (2015), accounting for the strongly northerly wind component of *Nortes* in the northwestern part of the GoM. The improved MSA_i index was obtained from the CFSR to identify *Nortes* and validated against events identified by previous works. The identification of events was also performed over CNRM for both the present and future climates. The present climate events were compared to those obtained using the CFSR, which resulted in an underestimation of events by CNRM, and slightly shorter durations. The number of events is reduced in the future climate, particularly at the end of the 21st century, while the duration is maintained. Considering the bias of CNRM to generate less *Norte* events, it is considered that the reduced number of *Nortes* will not occur in the near future, but most likely in the far future, with the events maintaining the same duration. This is not in agreement with Pérez et al. (2014), who find that the warming climate will bring shorter but longer events. It should be mentioned that Pérez et al. (2014) did not provide an assessment of accuracy of the model (TL959L60 AGCM from the Earth Simulator of the Meteorological Research Institute of Japan) used to reproduce the present climate, so that their conclusions could be the result of a model bias.

A principal component analysis was done over the resulting mean wave power from each individual *Norte* event. The first 2 PCs represent the most common characteristics of the events, which have a main effect on the western coast of the Mexican Gulf. Together with the 3rd PC they explain 67% of the variance. The PCs were used to classify the events by using clustering by k-means, to provide 5 types of *Nortes*. Most of the types shows the wave power concentrated in the western GoM, with varying degree of intensity as well as the location of the most intense areas, while one of the types represent the events affecting the northern area of the GoM. The occurrence between the types of *Nortes* in the CFSR and CNRM databases are similar, with highest occurrence for Type V (events with lowest wave power) and Type IV (second to lowest wave power), although the highest occurrence type is inverted for the CFSR and the CNRM. Both types represent more than half of the events in both CFSR and CNRM. The future climate shows a decrease in most of the *Norte* types, except for the mildest events (Type V).

Based on the analysis of *Norte* types and their frequency under a warming climate it is concluded that the CNRM model indicates that the GoM will present fewer intense events and more mild events in relation to the wave power generated. If we consider that the CNRM provides accurate results, the warming climate will most likely result in less damage to infrastructure and less down-time in marine facilities due to less frequent intense *Nortes* and more frequent mild *Nortes* in the GoM.

Chapter 4.

Conclusions and future work

The present work analyses the extreme ocean waves in the GoM, which are generated by TCs and *Nortes*. While tropical cyclone generated waves are more intense and result in larger damage, *Norte*-derived waves have a larger occurrence and create constant disruptions of coastal/marine activities during the winter. Based on the analysis presented in this work, it is concluded that the warming climate will most likely result in more intense waves derived from TCs but more frequent mild *Norte* events. This results have two important implications: 1) the structural design of coastal and marine facilities should be revised to include the effect of increased wave heights for the most extreme events, i.e. from TCs, and 2) planning of operation of coastal and marine facilities could include the effect of the most frequent extreme events, i.e. *Nortes*, although it is more likely that the frequency of such events is reduced, except for the mildest events which are expected to increase.

The above conclusions are based on a limited set of data derived from the CMIP5 experiments (GFDL and HADGEM for TCs and CNRM for *Nortes*). Considering the uncertainty imposed by the GCMs, the results cannot be consider conclusive, but provide a first approximation in the assessment of the extreme wave conditions in the GoM. It is important to consider also that the uncertainty is not only a result of the GCMs, since there is uncertainty inherit to the wave model, the generation of synthetic events and most important, the climate change scenarios themselves. There are different ways to reduce uncertainty; for instance, the wave model is calibrated to measured data and the synthetic events to basin wide frequency of events. The uncertainty imposed by the RCP scenarios are part of the uncertainty inherent to climate change studies, but the uncertainty of the CMIP5 models is commonly dealt with by the use of many of the models. In this study I only used a limited number of CMIP5 models, so that the actual effect of climate change on the extreme ocean waves of the GoM cannot be conclusive.

Despite the uncertainty, this work provides insight into what we can expect for extreme ocean waves in the GoM. Nevertheless, future work should be oriented towards reducing such uncertainty. For instance, the use of more CMIP models from previous and coming phases could reduce uncertainty by providing an ensemble of the results, both for TC and *Nortes*. The use of more models will allow for a more robust statistical assessment and would provide a measure for the uncertainty.

With regards to *Nortes*, this work uses the wave power as a proxy to classify those events, since it condenses information related to wind duration, intensity and direction. A further step will be to analyze the *Nortes* pertaining to each type considering their MSLP spatial distribution and duration. This may provide a conceptual model for each type of event, although this is unclear since a short duration but intense wind speed may create similar wave power than weaker winds with longer duration, as long as the direction of the winds is similar. Still, it is worth analyzing the atmospheric component to further understand *Norte* events affecting the GoM.

Another important aspect associated with *Nortes* in Mexico is precipitation. The methodology used in this work could be applied to precipitation instead of wave power to classify *Nortes* and to assess the effect of climate change. The results provided in this work suggested less intense *Nortes* in the future climate and more mild events; how could this result be related to precipitation? This is a critical issue in Mexico, since *Nortes* can lead to water availability issues, either scarcity or flooding.

References

Allan, J. C., and P. D. Komar, 2006: Climate Controls on US West Coast Erosion Processes. *J. Coast. Res.*, **223**, 511–529, doi:10.2112/03-0108.1. http://www.bioone.org/doi/abs/10.2112/03-0108.1 (Accessed June 6, 2014).

Alvarez, L. G., A. Badan-Dangon, and A. Valle, 1989: On coastal currents off Tehuantepec. *Estuar. Coast. Shelf Sci.*, **29**, 89–96, doi:10.1016/0272-7714(89)90075-9.

American Petroleum Institute (API), 2007: *Interim Guidance on Hurricane Conditions in the Gulf of Mexico*. Washington, DC., 54 pp.

Appendini, C. M., A. Torres-Freyermuth, F. Oropeza, P. Salles, J. López, and E. T. Mendoza, 2013: Wave modeling performance in the Gulf of Mexico and Western Caribbean: Wind reanalyses assessment. *Appl. Ocean Res.*, **39**, 20–30, doi:10.1016/j.apor.2012.09.004. http://linkinghub.elsevier.com/retrieve/pii/S0141118712000788 (Accessed March 5, 2013).

——, A. Torres-Freyermuth, P. Salles, J. Lopez-Gonzalez, and E. T. Mendoza, 2014: Wave climate and trends for the Gulf of Mexico: A 30 year wave hindcast. *J. Clim.*, **27**, 1619–1632, doi:dx.doi.org/10.1175/JCLI-D-13-00206.1.

Arrhenius, S., 1896: in the Air upon the Temperature of the Ground. *Philos. Mag. J. Sci.*, **41**, 237–276.

Baker, F. H., 1874: Survey of a portion of the Mexican-Gulf Coast. *Am. Geogr. Soc.*, **5**, 237–242.

Battjes, J. A. A., and J. P. F. M. P. F. M. Janssen, 1978: Energy loss and set-up due to breaking of random waves. *Proceedings of the 16th international conference on coastal engineering*, Vol. 1 of, 569–587 http://journals.tdl.org/icce/index.php/icce/article/view/3294 (Accessed August 23, 2013).

Boucard, A., 1883: On a Collection of Birds from Yucatan. *J. Zool.*, **51**, 434–513, doi:doi:10.1111/j.1469-7998.1883.tb06660.x.

Caires, S., V. R. Swail, and X. L. Wang, 2006: Projection and Analysis of Extreme Wave Climate. *J. Clim.*, **19**, 5581–5605, doi:10.1175/JCLI3918.1. http://journals.ametsoc.org/doi/full/10.1175/JCLI3918.1 (Accessed June 30, 2014).

Camargo, S. J., 2013: Global and regional aspects of tropical cyclone activity in the CMIP5 models. *J. Clim.*, **26**, 9880–9902, doi:10.1175/JCLI-D-12-00549.1.

Camus, P., F. J. Méndez, I. J. Losada, M. Menéndez, A. Espejo, J. Pérez, A. Rueda, and Y. Guanche, 2014: A method for finding the optimal predictor indices for local wave climate conditions. *Ocean Dyn.*, **64**, 1025–1038, doi:10.1007/s10236-014-0737-2.

Chao, Y.-Y., J.-H. G. M. Alves, and H. L. Tolman, 2005: An Operational System for Predicting Hurricane-Generated Wind Waves in the North Atlantic Ocean. **20**, 652–671.

Chawla, A., D. M. Spindler, and H. L. Tolman, 2013: Validation of a thirty year wave hindcast using the Climate Forecast System Reanalysis winds. *Ocean Model.*, **70**, 189–206, doi:10.1016/j.ocemod.2012.07.005. http://linkinghub.elsevier.com/retrieve/pii/S1463500312001047 (Accessed April 9, 2013).

CIRIA, CUR, and CETMEF, 2007: *The Rock Manual. The use of rock in hydraulic engineering*. 2nd editio. London, UK., 1267 pp.

Coles, S., 2001: *An Introduction to Statistical Modeling of Extreme Values*. Springer UK, 208 pp.

Colle, B. A., and C. F. Mass, 1995: The structure and evolution of cold surges east of the Rocky Mountains. *Mon. Weather Rev.*, **123**.

Cox, a T., V. J. Cardone, and V. R. Swail, 2011: On the use of the climate forecast system reanalysis wind forcing in ocean response modeling. *12th Int. Work. Wave Hindcasting Forcasting 3rd Coast. Hazards Symp.*, 20, Paper G3.

Cruz, A. M., and E. Krausmann, 2008: Damage to offshore oil and gas facilities following hurricanes Katrina and Rita: An overview. *J. Loss Prev. Process Ind.*, **21**, 620–626, doi:10.1016/j.jlp.2008.04.008.

Dallavalle, J. P., and L. F. Bosart, 1975: A synoptic investigation of anticyclogenesis

accompanying North American polar air outbreaks.pdf. *Mon. Weather Rev.*, **103**, 941–957.

Davis, R. E., and L. S. Kalkstein, 1990: Development of an automated spatial synoptic climatological classification. *Int. J. Climatol.*, **10**, 769–794, doi:10.1002/joc.3370100802. http://doi.wiley.com/10.1002/joc.3370100802.

Dee, D. P., and Coauthors, 2011: The ERA-Interim reanalysis: configuration and performance of the data assimilation system. *Q. J. R. Meteorol. Soc.*, **137**, 553–597, doi:10.1002/qj.828. http://doi.wiley.com/10.1002/qj.828 (Accessed February 28, 2013).

Dietrich, J. C., and Coauthors, 2011: Modeling hurricane waves and storm surge using integrally-coupled, scalable computations. *Coast. Eng.*, **58**, 45–65, doi:10.1016/j.coastaleng.2010.08.001. http://linkinghub.elsevier.com/retrieve/pii/S0378383910001250 (Accessed July 13, 2012).

Dimego, G. J., L. F. Bosart, and G. W. Endersen, 1976: An examination of the frequency and mean conditions sourrounding frontal incursions into the Gulf of Mexico and Caribbean Sea. *Mon. Weather Rev.*, **104**, 709–717.

DiMego, G. J., L. F. Bosart, and G. W. Endersen, 1976: An Examination of the Frequency and Mean Conditions Surrounding Frontal Incursions into the Gulf of Mexico and Caribbean Sea. *Mon. Weather Rev.*, **104**, 709–718, doi:10.1175/1520-0493(1976)104<0709:AEOTFA>2.0.CO;2.

Dodet, G., X. Bertin, and R. Taborda, 2010: Wave climate variability in the North-East Atlantic Ocean over the last six decades. *Ocean Model.*, **31**, 120–131.

Eldeberky, Y., and J. A. Battjes, 1996: Spectral modeling of wave breaking: Application to Boussinesq equations. *J. Geophys. Res.*, **101**, 1253, doi:10.1029/95JC03219. http://doi.wiley.com/10.1029/95JC03219 (Accessed August 23, 2013).

Emanuel, K., 2010: Tropical cyclone activity downscaled from NOAA-CIRES Reanalysis, 1908–1958. *J. Adv. Model. Earth Syst.*, **2**, doi:10.3894/JAMES.2010.2.1.

——, 2011: Global Warming Effects on U.S. Hurricane Damage. *Weather. Clim. Soc.*, **3**, 261–268, doi:10.1175/WCAS-D-11-00007.1.

http://journals.ametsoc.org/doi/abs/10.1175/WCAS-D-11-00007.1 (Accessed February 27, 2013).

——, 2015: Effect of upper-ocean evolution on projected trends in tropical cyclone activity. *J. Clim.*, **28**, 8165–8170, doi:10.1175/JCLI-D-15-0401.1.

——, and D. S. Nolan, 2004: Tropical cyclone activity and the global climate system. *26th Conf. on Hurricanes andTropical Meteorology*, Miami, FL, Amer. Meteor. Soc. [Available online at http://ams.confex.com/ams/pdfpapers/75463.pdf.], 10A.2.

——, and T. Jagger, 2010: On Estimating Hurricane Return Periods. *J. Appl. Meteorol. Climatol.*, **49**, 837–844, doi:10.1175/2009JAMC2236.1. http://journals.ametsoc.org/doi/abs/10.1175/2009JAMC2236.1 (Accessed April 9, 2013).

——, and R. Rotunno, 2011: Self-Stratification of Tropical Cyclone Outflow. Part I: Implications for Storm Structure. *J. Atmos. Sci.*, **68**, 2236–2249, doi:10.1175/JAS-D-10-05024.1. http://journals.ametsoc.org/doi/abs/10.1175/JAS-D-10-05024.1 (Accessed May 21, 2013).

——, S. Ravela, E. Vivant, and C. Risi, 2006: A statistical deterministic approach to hurricane risk assessment. *Bull. Am. Meteorol. Soc.*, **87**, 299–314, doi:10.1175/BAMS-87-3-299. http://journals.ametsoc.org/doi/abs/10.1175/BAMS-87-3-299 (Accessed March 14, 2013).

——, R. Sundararajan, and J. Williams, 2008: Hurricanes and Global Warming: Results from Downscaling IPCC AR4 Simulations. *Bull. Am. Meteorol. Soc.*, **89**, 347–367, doi:10.1175/BAMS-89-3-347. http://journals.ametsoc.org/doi/abs/10.1175/BAMS-89-3-347 (Accessed May 21, 2013).

Emanuel, K. A., 2013: Downscaling CMIP5 climate models shows increased tropical cyclone activity over the 21st century. *Proc. Natl. Acad. Sci. U. S. A.*, **110**, 12219–12224, doi:10.1073/pnas.1301293110. http://www.pnas.org/content/110/30/12219.full (Accessed September 6, 2014).

Fan, Y., I. M. Held, S.-J. Lin, and X. L. Wang, 2013: Ocean Warming Effect on Surface Gravity Wave Climate Change for the End of the Twenty-First Century. *J. Clim.*, **26**, 6046–6066, doi:10.1175/JCLI-D-12-00410.1. http://journals.ametsoc.org/doi/abs/10.1175/JCLI-D-12-00410.1 (Accessed June 30,

2014).

——, S.-J. Lin, S. M. Griffies, and M. a. Hemer, 2014: Simulated Global Swell and Wind-Sea Climate and Their Responses to Anthropogenic Climate Change at the End of the Twenty-First Century. *J. Clim.*, **27**, 3516–3536, doi:10.1175/JCLI-D-13-00198.1. http://journals.ametsoc.org/doi/abs/10.1175/JCLI-D-13-00198.1 (Accessed May 24, 2014).

Frankenfield, H. C., 1917: "Northers" of the Canal Zone. *Mon. Weather Rev.*, **45**, 546–550.

García-Nava, H., F. J. Ocampo-Torres, P. Osuna, and M. a. Donelan, 2009: Wind stress in the presence of swell under moderate to strong wind conditions. *J. Geophys. Res.*, **114**, C12008, doi:10.1029/2009JC005389. http://doi.wiley.com/10.1029/2009JC005389 (Accessed April 9, 2013).

Griffies, S. M., and Coauthors, 2011: The GFDL CM3 coupled climate model: Characteristics of the ocean and sea ice simulations. *J. Clim.*, **24**, 3520–3544, doi:10.1175/2011JCLI3964.1.

Gulev, S. K., and V. Grigorieva, 2004: Last century changes in ocean wind wave height from global visual wave data. *Geophys. Res. Lett.*, **31**, L24302, doi:10.1029/2004GL021040. http://doi.wiley.com/10.1029/2004GL021040 (Accessed July 2, 2014).

Gulev, S. K., V. Grigorieva, A. Sterl, and D. Woolf, 2003: Assessment of the reliability of wave observations from voluntary observing ships: Insights from the validation of a global wind wave climatology based on voluntary observing ship data. *J. Geophys. Res.*, **108**, 3236. http://www.knmi.nl/publications/fulltexts/gulev_voswaves_jgr_2003.pdf.

Hallegatte, S., 2007: The Use of Synthetic Hurricane Tracks in Risk Analysis and Climate Change Damage Assessment. *J. Appl. Meteorol. Climatol.*, **46**, 1956–1966, doi:10.1175/2007JAMC1532.1. http://journals.ametsoc.org/doi/abs/10.1175/2007JAMC1532.1 (Accessed March 26, 2013).

Hansman, H., 1984: The effect of the atmospheric droplet size distribution on aircraft ice accretion. *J. Aircr.*, **22**, 503–508.

Hasselmann, S., and K. Hasselmann, 1985: Computations and parameterizations of the nonlinear energy transfer in a gravity-wave spectrum. Part I: A new method for efficient computations of the exact nonlinear transfer integral. *J. Phys. Oceanogr.*, **15**, 1369–1377.

——, ——, J. H. Allender, and T. P. Barnett, 1985: Computations and parameterizations of the nonlinear energy transfer in a gravity-wave spectrum. Part II: Parameterizations of the nonlinear energy transfer for application in wave models. *J. Phys. Oceanogr.*, **15**, 1378–1391.

Hemer, M. a., Y. Fan, N. Mori, A. Semedo, and X. L. Wang, 2013a: Projected changes in wave climate from a multi-model ensemble. *Nat. Clim. Chang.*, **3**, 471–476, doi:10.1038/nclimate1791. http://www.nature.com/nclimate/journal/v3/n5/full/nclimate1791.html%5Cnhttp://dx.doi.org/10.1038/nclimate1791 (Accessed March 22, 2013).

——, J. Katzfey, and C. E. Trenham, 2013b: Global dynamical projections of surface ocean wave climate for a future high greenhouse gas emission scenario. *Ocean Model.*, **70**, 221–245, doi:10.1016/j.ocemod.2012.09.008. http://linkinghub.elsevier.com/retrieve/pii/S1463500312001321 (Accessed May 30, 2014).

Henry, W. K., 1979: Some aspects of the fate of cold fronts in the Gulf of Mexico. *Mon. Weather Rev.*, **107**, 1078–1082.

Hernández-Lasheras, J., 2015: Identificación y clasificación de Nortes en función del oleaje asociado en el Golfo de México. Universidad de Cantabria, 52 pp.

Hill, J. B., 1969: Temperature variability and synoptic cold fronts in the winter climate of Mexico. McGill University, 108 pp.

Hill, K. A., and G. M. Lackmann, 2011: The impact of future climate change on TC intensity and structure: A downscaling approach. *J. Clim.*, **24**, 4644–4661, doi:10.1175/2011JCLI3761.1.

Hope, M. E., and Coauthors, 2013: Hindcast and validation of Hurricane Ike (2008) waves, forerunner, and storm surge. *J. Geophys. Res. Ocean.*, **118**, 4424–4460, doi:10.1002/jgrc.20314.

Hunt, E. B., 1863: Key West physical notes; zodiacal light; atmospheric transparency; Gulf Stream cloud bank; ray bands; northers; hurricanes; ventilation; yellow fever; a water moonrise. *Am. J. Sci.*, **35**, 388–396, doi:doi: 10.2475/ajs.s2-35.105.388.

Hurd, W. E., 1929: Northers of the Gulf of Tehuantepec. *Mon. Weather Rev.*, **57**, 192–194, doi:10.1126/science.27.693.594. http://www.sciencemag.org/cgi/doi/10.1126/science.27.693.594.

IPCC, 2014a: *Climate Change 2014 Synthesis Report Summary Chapter for Policymakers*. Geneva, Switzerland, 151 pp pp.

——, 2014b: *Climate Change 2014: Impacts, Adaptation, and Vulnerability. Part B: Regional Aspects. Contribution of Working Group II to the Fifth Assessment Report of the Intergovernmental Panel on Climate Change*. B. V.R. et al., Eds. Cambridge University Press, Cambridge, United Kingdom and New York, NY, USA, 688 pp.

Izaguirre, C., M. Menéndez, P. Camus, F. J. Méndez, R. Mínguez, and I. J. Losada, 2012: Exploring the interannual variability of extreme wave climate in the Northeast Atlantic Ocean. *Ocean Model.*, **59**, 31–40. http://www.sciencedirect.com/science/article/pii/S146350031200131X (Accessed October 23, 2013).

Jeong, C. K., V. Panchang, and Z. Demirbilek, 2012: Parametric Adjustments to the Rankine Vortex Wind Model for Gulf of Mexico Hurricanes. *J. Offshore Mech. Arct. Eng.*, **134**, 41102, doi:10.1115/1.4006148. http://offshoremechanics.asmedigitalcollection.asme.org/article.aspx?articleid=1484971 (Accessed October 28, 2013).

Johnson, H. K., and H. Kofoed-Hansen, 2000: Influence of bottom friction on sea surface roughness and its impact on shallow water wind wave modeling. *J. Phys. Ocean.*, **30**, 1743–1756.

Jones, C. D., and Coauthors, 2011: The HadGEM2-ES implementation of CMIP5 centennial simulations. *Geosci. Model Dev.*, **4**, 543–570, doi:10.5194/gmd-4-543-2011.

Kaiser, M. J., and Y. Yu, 2010: The impact of Hurricanes Gustav and Ike on offshore oil and gas production in the Gulf of Mexico. *Appl. Energy*, **87**, 284–297, doi:10.1016/j.apenergy.2009.07.014.

http://dx.doi.org/10.1016/j.apenergy.2009.07.014.

Kalnay, E., and Coauthors, 1996: The NCEP/NCAR 40-year reanalysis project. *Bull. Am. Meteorol. Soc.*, **77**, 437–471, doi:10.1175/1520-0477(1996)077<0437:TNYRP>2.0.CO;2.

Keeling, C. D., R. B. Bacastow, A. E. Bainbridge, C. A. Ekdahl, P. R. Guenther, and L. S. Waterman, 1976: Atmospheric carbon dioxide variations at Mauna Loa Observatory , Hawaii. *Tellus*, **28**, 538–551, doi:10.1111/j.2153-3490.1976.tb00701.x.

Klaus, D., 1973: Las invasiones de aire frio en los tropicos a sotavento de las montañas rocallosas. *Geofis. Int.*, **13**, 99–143.

Klotzbach, P., W. Gray, and C. Fogarty, 2015: Active Atlantic hurricane era at its end ? *Nat. Publ. Gr.*, **8**, 737–738, doi:10.1038/ngeo2529. http://dx.doi.org/10.1038/ngeo2529.

Komar, P. D., and J. C. Allan, 2008: Increasing Hurricane-Generated Wave Heights along the U.S. East Coast and Their Climate Controls. *J. Coast. Res.*, **242**, 479–488, doi:10.2112/07-0894.1. http://www.bioone.org/doi/abs/10.2112/07-0894.1 (Accessed March 21, 2013).

Komen, G. J., L. Cavaleri, M. Donelan, K. Hasselmann, S. Hasselmann, and P. A. E. M. Janssen, 1994: *Dynamics and modelling of ocean waves*. Cambridge University Press, Cambridge, 554 pp.

Konrad, C. E., 1996: Relationships between the intensity of cold-air outbreaks and the evolution of synoptic and planetary-scale features over North America. *Monthl*, 1067–1083.

Landsea, C. W., 2007: Counting Atlantic Tropical Cyclones Back to 1900. *Eos, Trans. Am. Geophys. Union*, **88**, 197, doi:10.1029/2007EO180001.

Lin, N., and D. Chavas, 2012: On hurricane parametric wind and applications in storm surge modeling. *J. Geophys. Res.*, **117**, D09120, doi:10.1029/2011JD017126. http://doi.wiley.com/10.1029/2011JD017126 (Accessed May 21, 2013).

——, and K. Emanuel, 2015: Grey swan tropical cyclones. *Nat. Clim. Chang.*, **advance on**, 1–8, doi:10.1038/NCLIMATE2777.

http://dx.doi.org/10.1038/nclimate2777%5Cn10.1038/nclimate2777%5Cnhttp://www.nature.com/nclimate/journal/vaop/ncurrent/abs/nclimate2777.html#supplementary-information.

Lin, N., K. a. Emanuel, J. a. Smith, and E. Vanmarcke, 2010: Risk assessment of hurricane storm surge for New York City. *J. Geophys. Res.*, **115**, D18121, doi:10.1029/2009JD013630. http://doi.wiley.com/10.1029/2009JD013630 (Accessed April 9, 2013).

Lin, N., K. Emanuel, M. Oppenheimer, E. Vanmarcke, and P. Sciences, 2012: Physically based assessment of hurricane surge threat under climate change. *Nat. Clim. Chang.*, **2**, 462–467, doi:10.1038/nclimate1389. http://www.nature.com/doifinder/10.1038/nclimate1389 (Accessed March 19, 2013).

Lionello, P., S. Cogo, M. B. Galati, and a. Sanna, 2008: The Mediterranean surface wave climate inferred from future scenario simulations. *Glob. Planet. Change*, **63**, 152–162, doi:10.1016/j.gloplacha.2008.03.004. http://linkinghub.elsevier.com/retrieve/pii/S0921818108000349 (Accessed June 17, 2014).

Liu, H., L. Xie, L. J. Pietrafesa, and S. Bao, 2007: Sensitivity of wind waves to hurricane wind characteristics. *Ocean Model.*, **18**, 37–52, doi:10.1016/j.ocemod.2007.03.004. http://linkinghub.elsevier.com/retrieve/pii/S1463500307000388 (Accessed April 9, 2013).

López-Méndez, J. V., 2009: Análisis del evento meteorológico del 2007 relacionado con la inundación de Tabasco. Poosgrado en Ciencias de la Tierra, Universidad Nacional Autónoma de México, 117 pp.

Manabe, S., and R. T. Wetherald, 1967: Thermal Equilibrium of the Atmosphere with a Given Distribution of Relative Humidity. *J. Atmos. Sci.*, **24**, 241–259, doi:10.1175/1520-0469(1967)024<0241:TEOTAW>2.0.CO;2. http://journals.ametsoc.org/doi/abs/10.1175/1520-0469(1967)024%3C0241:TEOTAW%3E2.0.CO;2.

Mecikalski, J. R., and J. S. Tilley, 1992: Meteorology and Atmospheric Physics Cold Surges Along the Front Range of the Rocky Mountains : Development of a Classification Scheme. *Meteorol. Atmos. Phys.*, **271**, 249–271.

Mendelsohn, R., K. Emanuel, S. Chonabayashi, and L. Bakkensen, 2012: The impact of climate change on global tropical cyclone damage. *Nat. Clim. Chang.*, **2**, 205–209, doi:10.1038/nclimate1357. http://www.nature.com/doifinder/10.1038/nclimate1357 (Accessed March 9, 2013).

Mendoza, E. T., M. A. Trejo-rangel, P. Salles, C. M. Appendini, J. Lopez-, and A. Torres-freyermuth, 2013: Storm characterization and coastal hazards in the Yucatan Peninsula. 790–795, doi:10.2112/SI65-134.1.

Menéndez, M., F. J. Méndez, I. J. Losada, and N. E. Graham, 2008: Variability of extreme wave heights in the northeast Pacific Ocean based on buoy measurements. *Geophys. Res. Lett.*, **35**, L22607, doi:10.1029/2008GL035394. http://doi.wiley.com/10.1029/2008GL035394 (Accessed June 4, 2014).

Mesinger, F., and Coauthors, 2006: North American regional reanalysis. *Bull. Am. Meteorol. Soc.*, **87**, 343–360, doi:10.1175/BAMS-87-3-343.

Meza-Padilla, R., C. M. Appendini, and A. Pedrozo-Acuña, 2015: Hurricane induced waves and storm surge modeling for the Mexican coast. *Ocean Dyn.*, **65**, 1199–1211, doi:10.1007/s10236-015-0861-7.

Mori, N., T. Yasuda, H. Mase, T. Tom, and Y. Oku, 2010: Projection of extreme wave climate change under global warming. *Hydrol. Res. Lett.*, **4**, 15–19, doi:10.3178/HRL.4.15. http://jlc.jst.go.jp/JST.JSTAGE/hrl/4.15?from=Google (Accessed June 30, 2014).

Moss, R. H., and Coauthors, 2010: The next generation of scenarios for climate change research and assessment. *Nature*, **463**, 747–756. http://dx.doi.org/10.1038/nature08823.

Nakicenovic, N., and R. Swart, 2000: *Special report on emissions scenarios*. N. Nakicenovic and R. Swart, Eds. Cambridge University, Cambridge, UK, 599 pp.

Notes by the Editor, 1893: The Northers of Tampico and Vera Cruz. *Mon. Weather Rev.*, **21**, 363–364.

——, 1898: Northers in the Caribbean Sea and the Gulf of Mexico. *Mon. Weather Rev.*, **26**, 568–568.

Olume, V., and Coauthors, 2011: Hurricane Gustav (2008) Waves and Storm Surge : Hindcast , Synoptic Analysis , and Validation in Southern Louisiana. 2488–2522, doi:10.1175/2011MWR3611.1.

Panchang, V., C. K. Jeong, and Z. Demirbilek, 2013: Analyses of Extreme Wave Heights in the Gulf of Mexico for Offshore Engineering Applications. *J. Offshore Mech. Arct. Eng.*, **135**, 31104-031104–031115, doi:10.1115/1.4023205. http://offshoremechanics.asmedigitalcollection.asme.org/article.aspx?articleid=1685264 (Accessed October 28, 2013).

Panchang, V. G., and D. Li, 2006: Large waves in the Gulf of Mexico caused by Hurricane Ivan. *Bull. Am. Meteorol. Soc.*, **87**, 481–489, doi:10.1175/BAMS-87-4-481.

Pérez, E. P., V. Magaña, E. Caetano, and S. Kusunoki, 2014: Cold surge activity over the Gulf of Mexico in a warmer climate1. *Front. Earth Sci.*, **2**, 1–10, doi:10.3389/feart.2014.00019. http://journal.frontiersin.org/Journal/10.3389/feart.2014.00019/full.

Perez, J., M. Menendez, P. Camus, F. J. Mendez, and I. J. Losada, 2015: Statistical multi-model climate projections of surface ocean waves in Europe. *Ocean Model.*, **96**, 161–170, doi:10.1016/j.ocemod.2015.06.001.

Pielke, R. a., J. Gratz, C. W. Landsea, D. Collins, M. A. Saunders, and R. Musulin, 2008: Normalized Hurricane Damage in the United States: 1900–2005. *Nat. Hazards Rev.*, **9**, 29–42, doi:10.1061/(ASCE)1527-6988(2008)9:1(29).

Powell, M. D., S. H. Houston, L. R. Amat, and N. Morisseau-Leroy, 1998: The HRD real-time hurricane wind analysis system. *J. Wind Eng. Ind. Aerodyn.*, **77–78**, 53–64, doi:http://dx.doi.org/10.1016/S0167-6105(98)00131-7. http://www.sciencedirect.com/science/article/pii/S0167610598001317.

Powell, M. D., and Coauthors, 2010: Reconstruction of Hurricane Katrina's wind fields for storm surge and wave hindcasting. *Ocean Eng.*, **37**, 26–36, doi:10.1016/j.oceaneng.2009.08.014. http://linkinghub.elsevier.com/retrieve/pii/S0029801809002121 (Accessed April 3, 2013).

Ramírez-Elías, D. A., 2007: Climatología y eventos extremos de oleaje en la costa tamaulipeca. Universidad Autónoma de Tamaulipas, 79 pp.

Reding, P. J., 1992: The Central American cold surge: An observational analysis of the deep southward penetration of North American cold fronts. Texas A&M, 178 pp.

Reed, A. J., M. E. Mann, K. A. Emanuel, and D. W. Titley, 2015: An analysis of long-term relationships among count statistics and metrics of synthetic tropical cyclones downscaled from CMIP5 models. *J. Geophys. Res. Atmos.*, **120**, 7506–7519, doi:10.1002/2015JD023357.

Reguero, B. G., F. J. Méndez, and I. J. Losada, 2013: Variability of multivariate wave climate in Latin America and the Caribbean. *Glob. Planet. Change*, **100**, 70–84, doi:10.1016/j.gloplacha.2012.09.005. http://linkinghub.elsevier.com/retrieve/pii/S0921818112001828 (Accessed June 26, 2014).

Rogers, J. C., and R. V. Rohli, 1991: Florida citrus freezes and polar anticyclones in the Great Plains. *J. Clim.*, **4**, 1103–1113.

Romero-Centeno, R., J. Zavala-Hidalgo, A. Gallegos, and J. J. O'Brien, 2003: Isthmus of Tehuantepec Wind Climatology and ENSO Signal. *J. Clim.*, **16**, 2628–2639, doi:10.1175/1520-0442(2003)016<2628:IOTWCA>2.0.CO;2. http://journals.ametsoc.org/doi/full/10.1175/1520-0442(2003)016%3C2628:IOTWCA%3E2.0.CO;2 (Accessed October 25, 2013).

Rosengaus-Moshinsky, M., M. Jiménez-Espinosa, and M. T. Vázquez-Conde, 2002: *Atlas climatológico de ciclones tropicales en México*. Centro Nacional para la Prevención de Desastres. Instituto Mexicano de Tecnología del Agua., Mexico,.

Ruggiero, P., P. D. Komar, and J. C. Allan, 2010: Increasing wave heights and extreme value projections: The wave climate of the U.S. Pacific Northwest. *Coast. Eng.*, **57**, 539–552, doi:10.1016/j.coastaleng.2009.12.005. http://linkinghub.elsevier.com/retrieve/pii/S0378383909002142 (Accessed March 8, 2013).

Ruiz-Salcines, P., 2013: Campos de viento para hindcast de oleaje: reanálisis, paramétricos y fusión. M.E. thesis, Dept. Ciencias y Técnicas del Agua y del Medio Ambiente. Universidad de Cantabria, 84 pp.

Ruiz, L. E., 1892: Epidemic and endemic diseases observed in the ports of entry of the Mexican Gulf. *Public Health Pap. Rep.*, **18**, 180–188.

Sáenz, F., and A. M. Durán-Quesada, 2015: A climatology of low level wind regimes over Central America using a weather type classification approach. *Front. Earth Sci.*, **3**, 1–18, doi:10.3389/feart.2015.00015. http://journal.frontiersin.org/article/10.3389/feart.2015.00015/abstract.

Saha, S., and Coauthors, 2010: The NCEP Climate Forecast System Reanalysis. *Bull. Am. Meteorol. Soc.*, **91**, 1015–1057, doi:10.1175/2010BAMS3001.1. http://journals.ametsoc.org/doi/abs/10.1175/2010BAMS3001.1 (Accessed October 21, 2013).

Salinas, J. A., G. Colorado, M. E. Maya, and M. J. Montero, 2016: Global Ensamble Models for the tropical area. *The International Conference on Regional Climate CORDEX 2016*, Stockholm, Sweden, World Climate Research Program.

Schultz, D. M., W. E. Bracken, L. F. Bosart, G. J. Hakim, M. A. Bedrick, M. J. Dickinson, and K. R. Tyle, 1997: The 1993 Superstorm Cold Surge: Frontal Structure, Gap Flow, and Tropical Impact. *Mon. Weather Rev.*, **125**, 5–39, doi:10.1175/1520-0493(1997)125<0005:TSCSFS>2.0.CO;2. http://journals.ametsoc.org/doi/abs/10.1175/1520-0493(1997)125%3C0005:TSCSFS%3E2.0.CO;2 (Accessed October 25, 2013).

——, ——, and ——, 1998: Planetary- and Synoptic-Scale Signatures Associated with Central American Cold Surges. *Mon. Weather Rev.*, **126**, 5–27.

Semedo, A., K. Sušelj, A. Rutgersson, and A. Sterl, 2011: A Global View on the Wind Sea and Swell Climate and Variability from ERA-40. *J. Clim.*, **24**, 1461–1479, doi:10.1175/2010JCLI3718.1. http://journals.ametsoc.org/doi/abs/10.1175/2010JCLI3718.1 (Accessed March 21, 2013).

——, R. Weisse, A. Behrens, A. Sterl, L. Bengtsson, and H. Günther, 2013: Projection of Global Wave Climate Change toward the End of the Twenty-First Century. *J. Clim.*, **26**, 8269–8288, doi:10.1175/JCLI-D-12-00658.1. http://journals.ametsoc.org/doi/abs/10.1175/JCLI-D-12-00658.1 (Accessed January 24, 2014).

Sheffield, J., and Coauthors, 2013a: North American Climate in CMIP5 experiments. Part I: Evaluation of historical simulations of continental and regional climatology. *J. Clim.*, **26**, 9209–9245, doi:10.1175/JCLI-D-12-00592.1.

——, and Coauthors, 2013b: North American Climate in CMIP5 Experiments . Part II: Evaluation of Historical Simulations of Intraseasonal to Decadal Variability. *J. Clim.*, **26**, 9247–9290, doi:10.1175/JCLI-D-12-00593.1.

Sørensen, O. R., H. Kofoed-Hansen, M. Rugbjerg, and L. S. Sørensen, 2004: A third-generation spectral wave model using an unstructured finite volume technique. *Proceedings of the 29th International Conference on Coastal Engineering*, ASCE, New York, 894–906.

Sterl, A., and S. Caires, 2005: Climatology, variability and extrema of ocean waves: the Web-based KNMI/ERA-40 wave atlas. *Int. J. Climatol.*, **25**, 963–977, doi:10.1002/joc.1175. http://doi.wiley.com/10.1002/joc.1175 (Accessed July 2, 2014).

Stopa, J. E., and K. F. Cheung, 2014: Intercomparison of wind and wave data from the ECMWF Reanalysis Interim and the NCEP Climate Forecast System Reanalysis. *Ocean Model.*, **75**, 65–83, doi:10.1016/j.ocemod.2013.12.006. http://dx.doi.org/10.1016/j.ocemod.2013.12.006.

Taylor, M. K., 1888: The Climate of Southwestern Texas and its Advantages as a Winter Health Resort. *Trans. Am. Clin. Climatol. Assoc.*, **5**, 209–220.

Tolman, H. L., and J.-H. G. M. Alves, 2005: Numerical modeling of wind waves generated by tropical cyclones using moving grids. *Ocean Model.*, **9**, 305–323.

Vanem, E., B. Natvig, and A. B. Huseby, 2012: Modelling the effect of climate change on the wave climate of the world's oceans. *Ocean Sci. J.*, **47**, 123–145, doi:10.1007/s12601-012-0013-7. http://link.springer.com/10.1007/s12601-012-0013-7.

Vazquez-Aguirre, J. L., 2000: Caracterización objetiva de los Nortes del Golfo de México y su variabilidad interanual. Universidad Veracruzana, .

Vecchi, G. A., and B. J. Soden, 2007: Increased tropical Atlantic wind shear in model projections of global warming. *Geophys. Res. Lett.*, **34**, 1–5, doi:10.1029/2006GL028905.

Vickery, P. J., P. F. Skerlj, and L. A. Twisdale, 2000: Simulation of Hurricane Risk in the U.S. Using Empirical Track Model. *J. Struct. Eng.*, **126**, 1222–1237,

doi:10.1061/(ASCE)0733-9445(2000)126:10(1222). http://ascelibrary.org/doi/abs/10.1061/%2528ASCE%25290733-9445%25282000%2529126%253A10%25281222%2529 (Accessed November 14, 2014).

Voldoire, A., and Coauthors, 2013: The CNRM-CM5.1 global climate model: Description and basic evaluation. *Clim. Dyn.*, **40**, 2091–2121, doi:10.1007/s00382-011-1259-y.

Wang, D.-P., and L.-Y. Oey, 2008: Hindcast of waves and currents in Hurricane Katrina. *Bull. Am. Meteorol. Soc.*, **89**, 487–495.

Wang, D. W., D. A. Mitchell, W. J. Teague, E. Jarosz, and M. S. Hulbert, 2005: Extreme Waves Under Hurricane {Ivan}. *Science (80-.).*, **309**, 896.

Wang, X., F. Zwiers, and V. Swail, 2004: North Atlantic ocean wave climate change scenarios for the twenty-first century. *J. Clim.*, 2368–2383. http://journals.ametsoc.org/doi/abs/10.1175/1520-0442(2004)017%253C2368:NAOWCC%253E2.0.CO%253B2 (Accessed July 3, 2014).

Wang, X. L., and V. R. Swail, 2006: Climate change signal and uncertainty in projections of ocean wave heights. *Clim. Dyn.*, **26**, 109–126, doi:10.1007/s00382-005-0080-x. http://link.springer.com/10.1007/s00382-005-0080-x (Accessed May 26, 2014).

Weisse, R., and Coauthors, 2009: Regional Meteorological–Marine Reanalyses and Climate Change Projections. *Bull. Am. Meteorol. Soc.*, **90**, 849–860, doi:10.1175/2008BAMS2713.1. http://journals.ametsoc.org/doi/abs/10.1175/2008BAMS2713.1 (Accessed June 19, 2014).

Willett, H. C., 1934: North American Air Mass Properties. **1**, 78–87.

Woolf, D. K., P. G. Challenor, and P. D. Cotton, 2002: Variability and predictability of the North Atlantic wave climate. *J. Geophys. Res.*, **107**, 3145, doi:10.1029/2001JC001124. http://doi.wiley.com/10.1029/2001JC001124 (Accessed April 9, 2013).

Young, I. R., 1999: *Wind generated ocean waves*. Elsevier Science, Oxford, 288 pp.

Young, I. R., S. Zieger, and A. V. Babanin, 2011: Global trends in wind speed and wave height. *Science*, **332**, 451–455, doi:10.1126/science.1197219.